Modal Analysis of Large Structures – Multiple Exciter Systems

Brüel & Kjær

Modal Analysis of Large Structures – Multiple Exciter Systems

by

K. Zaveri, M.Phil.

May 1984

1st edition 1st print

ISBN 87 87355 03 5

PREFACE

The increasing interest in the dynamic behaviour of structures in the last couple of decades, has resulted in a proliferation of literature, dealing with what in contemporary language is termed Modal Analysis Techniques. Whilst the dynamic behaviour of a structure is described by analysts in terms of differential equations relating elemental masses and stiffnesses, it can equally well be described by its natural frequencies, principal modes etc. which are modal parameters measurable by the experimentalist. These techniques therefore, not only provide a tool for the analytical description of a structure, but also serve as a common technical language between the analyst and the experimental engineer. Obviously their mutual collaboration is of vital importance, since the accurate measurement of the principal modes of a structure, is a prerequisite for providing data to validate and improve analytical methods, and to verify the dynamic design adequacy of the structure.

This book has therefore been divided into two parts, Theory and Experimental Methods, each with its own introduction (Chapters 1 and 4). However, some overlap is unavoidable, as post-processing of experimental data for automatic Force Appropriation techniques demands mathematical manipulation and interpretation. The main objective is to describe techniques for testing large structures, using multiple exciters to obtain several columns of the frequency response function matrix, and for modal tuning methods to improve the modal parameter estimates. The theoretical chapters have been developed with this in mind, to guide the reader through the basics of modal analysis, and lead to Characteristic Phase Lag Theory — the essence of modal tuning procedures.

The theoretical part starts with Chapter 2, in which a single degree of freedom system is used to introduce viscous and hysteretic (also called structural) damping. To illustrate the differences in the responses, they are plotted as total amplitude and phase against frequency, as real and imaginary part against frequency, and as Nyquist plots.

In Chapter 3, matrix analysis methods are used on a simple two degree of freedom system to illustrate the concept of Eigenvalues and Eigenvectors and their orthogonal properties, generalized mass and stiffness, normalization of mode shapes, and Principal Coordinates. Since matrix methods expedite the transition to the analysis of multiple degree of freedom systems, they are used widely throughout the book. Readers unfamiliar with these techniques are therefore strongly recommended to start with Appendices A and B, which are by no means extensive, but comprehensive enough to facilitate understanding of the main text. The response of forced damped vibration is then dealt with in two sections; one for systems having proportional damping and the other for non-proportionally damped systems. Large structures invariably fall into the latter category, and their response can be obtained using Characteristic Phase Lag Theory, which is described in some depth. To give physical meaning to the above mathematical concepts, each of the sections are clarified by numerical examples.

The experimental part starts with Chapter 5, where the Peak Amplitude and Kennedy and Pancu methods are described, which make use of single exciters to obtain the modal parameters. The limitations of these techniques are pointed out, and sections in this chapter are devoted to emphasizing the problems encountered because of "Close Resonances" and "Contribution from Off-Resonant Modes" — factors which introduce inaccuracies in modal parameter estimates.

Chapter 6 describes the instrumentation necessary for exciting a structure, and for data acquisition and analysis using multiple exciters. Conventional force appropriation techniques (used even today), in which iterative adjustment of forces is carried out manually, are described, together with practical hints and pitfalls to be avoided.

In Chapter 7 Automatic Force Appropriation techniques are described, with particular emphasis on Asher's method. Using his method, the force ratios necessary for tuning the principal modes of vibration can be calculated from the complex admittance matrix, the columns of which are measured experimentally using sinusoidal excitation. By plotting the Nyquist diagrams for narrow band sweeps around the resonance frequencies using the force ratios calculated, the modal parameters can be extracted.

With the advent of dual channel real time analyzers and fast data acquisition equipment, it is now possible to measure a single column or row of a frequency response function (FRF) matrix, using wide band random or transient signal excitation. By curve fitting this data, the rest of the FRF matrix can be synthesized, assuming linearity, and modal parameters determined. As abundant literature can be found on this technique, its basic ideas have only been touched upon here. On the other hand, emphasis has been placed on complementing this technique with Asher's method. Implementation of his method however, requires measurement of several columns of the frequency response function matrix, implying that the structure must be excited at several points successively, using random excitation, and the response measured at various locations. The experimentally measured FRFs are curve fitted using the algorithms available with these techniques, to yield analytically synthesized FRFs. Application of Asher's method to these, has several advantages over using the experimentally measured FRFs which are listed in Chapter 7. Again, narrow band sweeps around the resonance frequencies with the forces calculated, can be used to refine modal parameter estimates. To illustrate the effectiveness of Asher's method, numerical simulation studies carried out on mathematical models are also included.

Chapter 7 furthermore describes briefly topics under current research – among them Ibáñez's suggestion of extending Asher's method using rectangular matrices (number of response measurement locations greater than the number of excitation positions). The method of excitation using dual input random signals, as described by Allemang et al, has also been briefly touched upon. Another promising modal tuning procedure developed by Ensminger and Turner, called the "Minimum Coincident Response" method has been included and some examples illustrated.

Finally the author would like to thank Professor W.L. Hallauer Jr. of Virginia Polytechnic Institute and State University, USA, and Professor R.R. Craig Jr. of the University of Texas at Austin, USA, for granting permission to reproduce some of the analytical and experimental results of their research.

K. Zaveri

CONTENTS

SYMBOL NOTATION

a	Constant
b	Constant
c	Damping coefficient
c_c	Critical damping
e	Base to the Natural Logarithm
f	Frequency
f_0	Undamped natural frequency
j	$\sqrt{-1}$
k	Spring stiffness
l	Length Number of response measurement locations
m	Mass
n	Constant Number of degrees of freedom
p	Number of excitation locations
q	Number of sets of forces
s	Complex frequency
t	Time
u_i	Mode Shape component
w	Energy stored in the system
x	Displacement
$\dot{x}$	Velocity
$\ddot{x}$	Acceleration
A_{ij_r}	Complex residue of r^{th} mode
E	Energy dissipated per cycle at resonance
F	Force
G_{ii}	Autospectrum
G_{ij}	Cross Spectrum
$H_{ij}(f)$	Frequency response function
Im	Imaginary part
K_i	Generalized stiffness
M_i	Generalized mass
Q	Quality factor
Re	Real part
X	Displacement amplitude
$X_i(f)$	Fourier Transform of input
$Y_i(f)$	Fourier Transform of output
α	Constant Angle
β	Constant
γ	Structural (hysteretic) damping factor Square root of Coherence Function
δ	Logarithmic Decrement
ζ	Dimensionless damping ratio
η	Loss factor
η_i	Principal coordinate
θ	Phase angle
λ_i	Roots of characteristic equation (eigenvalue)
π	Constant
σ_r	Decay rate of r^{th} mode
ω	Angular frequency
ω_0	Angular undamped natural frequency
ω_{d_r}	Damped natural frequency of r^{th} mode
ω_*	Test natural frequency
Δ	Difference
Σ	Summation

MATRIX NOTATION

$[c]$ Damping matrix

$[c(\omega)]$ Combined viscous and hysteretic damping matrix

$[d]$ Hysteretic damping matrix

$[k]$ Stiffness matrix

$[m]$ Mass matrix

$\{u\}$ Principal mode shape vector

$\{\bar{u}\}$ Complex displacement vector

$\{x\}$ Displacement vector

$[A]$ System Matrix

$[\bar{A}]$ Complex stiffness matrix

$[\bar{B}]$ Complex admittance matrix

$[B']$ Real part of $[\bar{B}]$

$[B'']$ Imaginary part of $[\bar{B}]$

$[\bar{B}_*]$ Incomplete complex admittance matrix

$[B'_*]$ Real part of $[\bar{B}_*]$

$[B''_*]$ Imaginary part of $[\bar{B}_*]$

$[\tilde{B}_*]$ Incomplete, Rectangular, complex admittance matrix

$[\tilde{B}'_*]$ Real part of $[\tilde{B}_*]$

$[\tilde{B}''_*]$ Imaginary part of $[\tilde{B}_*]$

$[C]$ Diagonalized damping matrix

$\{F\}$ Exciting force vector

$\{F_*\}$ Incomplete exciting force vector

$[\tilde{F}]$ Matrix whose columns are $\{F_*\}$

$[\bar{H}]$ Complex frequency response function matrix

$[H']$ Real part of $[\bar{H}]$

$[H'']$ Imaginary part of $[\bar{H}]$

$[\tilde{H}]$ Rectangular complex frequency response function matrix

$[\tilde{H}']$ Real part of $[\tilde{H}]$

$[\tilde{H}'']$ Imaginary part of $[\tilde{H}]$

$\lfloor \tilde{H}'' \rfloor_i$ i^{th} row of $[\tilde{H}'']$

$[I]$ Identity matrix

$[K]$ Diagonalized stiffness matrix

$[M]$ Diagonalized mass matrix

$\{\bar{U}_*$ Complex displacement amplitude vector

$[\tilde{U}]$ Matrix whose columns are $\{\bar{U}_*\}$

$\{\bar{X}\}$ Fourier Transformed input vector

$\{\bar{Y}\}$ Fourier Transformed output vector

$\{\eta\}$ Principal coordinate vector

$\{\phi\}$ Principal mode shape vector

$[\phi]$ Modal matrix

$[\tilde{\phi}]$ Weighted modal matrix

$\{\psi\}$ Characteristic phase-lag mode shape

$\{\Gamma\}$ Tuning force amplitude vector

$\{\Gamma_*\}$ Incomplete tuning force amplitude vector

$[\Lambda]$ Diagonal matrix with diagonal terms equal to the eigenvalues

THEORY

1. INTRODUCTION

The study of the motion of physical systems resulting from the forces acting on them, is referred to as **dynamics** – the realm of Newton's Laws. One type of dynamic behaviour of physical systems is vibratory motion, in which the system oscillates about a certain equilibrium position. This motion is rendered possible by the ability of materials used in the construction of systems to store potential energy via their elastic properties.

Most physical systems are continuous in character and their parameters are distributed. In many cases the distributed parameters can be replaced by discrete ones by suitable lumping of the continuous system. This should be carried out whenever possible, since lumped parameter systems are described by ordinary differential equations, which are far easier to solve than the partial differential equations describing continuous systems. Having accomplished this, the **number of degrees of freedom** can be established, specifying the number of independent coordinates necessary to define the system.

Oscillatory systems can be classified into two groups according to their behaviour, namely **linear** and **non-linear**. For a linear system, the principle of superposition applies, and the **dependent variables** in the differential equations describing the system appear to the first power only, and also without their cross products. Although only linear systems are dealt with here, some knowledge of non-linear systems is desirable, since all systems tend to become non-linear with increasing amplitudes of oscillation.

The number of degrees of freedom chosen dictates the number of differential equations necessary to characterize the system. As these equations are normally coupled to each other, they must be decoupled before their solution is attempted. To do this, the orthogonal properties of the **Principal Modes** are exploited, enabling the original differential equations to be rewritten in terms of the **Principal Coordinates.**

A physical system generally exhibits two classes of vibration – free and forced. **Free vibration** takes place when a system oscillates under the action of forces inherent in the system itself, and when the external forces are absent. (It is described by the solution of differential equations with their right hand sides set to zero). The system when given an initial disturbance will vibrate at one or more of its **natural frequencies**, which are properties of the dynamical system determined by its mass and stiffness distribution. The resulting motion will be the sum of the Principal Modes in some proportion, and will continue *ad infinitum* in the absence of damping. Thus the mathematical study of free vibration yields information about the dynamic properties of the system, relevant for evaluating the response of the system under forced vibration.

Forced Vibration takes place when a system oscillates under the action of external forces. When the excitation force is oscillatory, the system is forced to vibrate at the excitation frequency. If the frequency of excitation coincides with one of the natural frequencies, **resonance** is encountered, a phenomenon in which the amplitude builds up to dangerously high levels, limited only by the degree of damping.

All physical systems are subject to one or other type of damping, since energy is dissipated through friction and other resistances. These resistances appear in various forms, after which they are named – **viscous**, **hysteretic**, **Coulomb**, **aerodynamic** etc. The properties of the damping mechanisms differ from each other, and not all of them are equally amenable to mathematical formulation. Fortunately, small amounts of damping have very little influence on the natural frequencies, which are therefore normally calculated assuming no damping, as are the principal modes of vibration associated with each of these natural frequencies. However, in calculating the response under forced vibration, not only is it necessary to make assumptions about the **type** of damping, but also the **distribution** of damping – **proportional** or **non-proportional**. This is because the latter type of distribution, generally encountered in complex structures, is considerably more difficult to resolve mathematically, giving what is called **complex modes**, in contrast to **real modes** obtained with proportional damping.

2. SINGLE DEGREE OF FREEDOM SYSTEM

2.1. VISCOUS DAMPING

A complex structure can be considered as a number of masses, interconnected by springs and damping elements to facilitate the analytical solution of the dynamic behaviour of the structure. Since the damping forces in a real structure cannot be estimated with anything like the same accuracy as the elastic and inertia forces, a rigorous mathematical simulation of the damping effects is futile. Nevertheless, to account for the dissipative forces in the structure, assumptions of the form of damping have to be made, that give as good as possible an estimate of the damping forces in practice. Furthermore, the form has to be conducive to easy mathematical manipulation, specifically adaptable to linear equations of motion – implying that the damping forces are harmonic when the excitation is harmonic. Two such suitable forms of damping are viscous and hysteretic and are treated in some depth in Ref. [17–19]. The response of a single degree of freedom system to viscous damping will be described in this section and to hysteretic damping in the next section. Differences in the responses will also be illustrated.

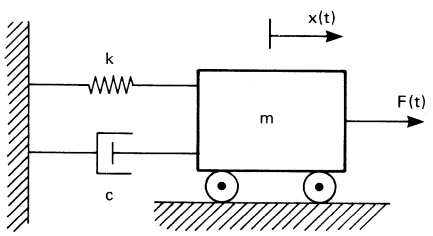

Fig.1. Single degree of freedom system

Fig.1 shows a single degree of freedom system, where a massless dashpot of damping coefficient c and a spring of stiffness k are mounted between the mass m and the fixed wall. The dashpot exerts a damping force $-c\dot{x}$ which is proportional to the instantaneous velocity and is positive in the positive direction of x. The Complex Frequency solution for **free damped** vibration of such a system is given in **Appendix C**. The equation of motion for forced harmonic excitation may be written as

$$m\ddot{x} + c\dot{x} + kx = Fe^{j\omega t} \qquad (1)$$

where x is the displacement
$\dot{x}$ is the velocity
$\ddot{x}$ is the acceleration
F is the excitation force
j is $\sqrt{-1}$
and ω is the excitation frequency.

Dividing equation (1) by m and multiplying the numerator and denominator on the right hand side by k we obtain

$$\ddot{x} + 2\zeta\omega_o\dot{x} + \omega_o{}^2 x = \omega_o{}^2\left(\frac{F}{k}\right)e^{j\omega t} \tag{2}$$

where $\omega_o = \sqrt{\frac{k}{m}}$ undamped natural frequency,

$\zeta = \frac{c}{2m\omega_o} = \frac{c}{c_c}$ dimensionless damping ratio,

c_c critical damping and

$\frac{F}{k}$ extension in the spring caused by F alone.

Using a trial solution of the form

$$x = Xe^{j\omega t}$$

for steady state vibration, it can be shown by differentiation and substitution in equation (2) that

$$X = \frac{\omega_o{}^2\, F/k}{\omega_o{}^2 - \omega^2 + j2\zeta\omega\,\omega_o} = \frac{F/k}{1 - (\omega/\omega_o)^2 + j2\zeta\omega/\omega_o} \tag{3}$$

Thus

$$x = Xe^{j\omega t} = \left[\frac{1}{1 - (\omega/\omega_o)^2 + j2\zeta\omega/\omega_o}\right]\frac{F}{k}e^{j\omega t} \tag{4}$$

It can be seen that the displacement x is proportional to the applied force, the proportionality factor being

$$H(\omega) = \left[\frac{1}{1 - (\omega/\omega_o)^2 + j2\zeta\omega/\omega_o}\right] \tag{5}$$

which is known as the **complex frequency response**. Eq. (4) illustrates that the displacement is a complex quantity which can therefore be broken up into its real and imaginary parts by multiplying the numerator and the denominator of the square brackets by its complex conjugate. Thus

$$x = \left[\frac{1 - (\omega/\omega_o)^2}{\{1 - (\omega/\omega_o)^2\}^2 + (2\zeta\omega/\omega_o)^2} - \frac{j2\zeta\omega/\omega_o}{\{1 - (\omega/\omega_o)^2\}^2 + (2\zeta\omega/\omega_o)^2}\right]\frac{F}{k}e^{j\omega t} \tag{6}$$

This shows that the displacement has one component

$$\mathrm{Re}(x) = \left[\frac{1 - (\omega/\omega_o)^2}{\{1 - (\omega/\omega_o)^2\}^2 + (2\zeta\omega/\omega_o)^2}\right]\frac{F}{k}e^{j\omega t} \tag{7}$$

which is **in-phase** with the applied force and another component

$$\mathrm{Im}(x) = \left[\frac{-2\zeta\omega/\omega_o}{\{1 - (\omega/\omega_o)^2\}^2 + (2\zeta\omega/\omega_o)^2}\right]\frac{F}{k}e^{j\omega t} \tag{8}$$

which has a phase lag of 90° behind the applied force. This component is said to be in **quadrature** with the excitation.

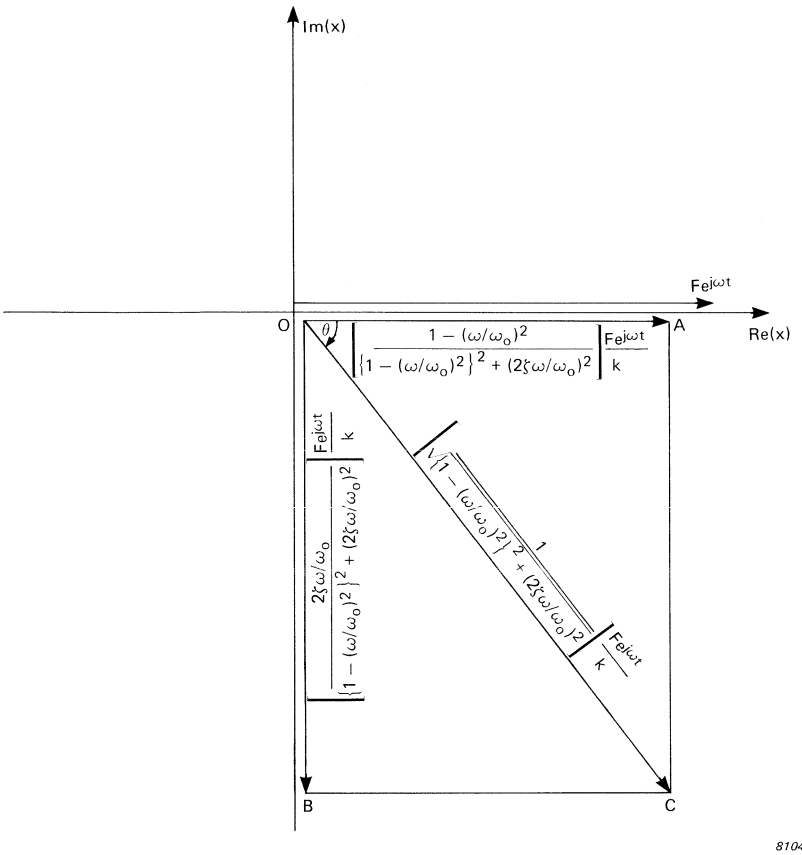

Fig.2. Real and Imaginary Components of displacement relative to the force vector

In Fig.2 the vectors OA and OB show the real and imaginary components of the displacement respectively in the Argand plane. The vector OC is the total displacement, the amplitude of which is given by $\left\{\sqrt{Re^2(x)+Im^2(x)}\right\}$

i.e.
$$\left[\frac{1}{\sqrt{\{1-(\omega/\omega_o)^2\}^2+(2\zeta\omega/\omega_o)^2}}\right]\frac{F}{k}e^{j\omega t} \tag{9}$$

The total displacement lags behind the force vector by an angle θ given by $\left\{\tan^{-1} Im(x)/Re(x)\right\}$

i.e.
$$\theta = \tan^{-1}\frac{2\zeta\omega/\omega_o}{1-(\omega/\omega_o)^2} \tag{10}$$

The steady state solution of eq. 2 can therefore also be written in the form
$$x = \left[\frac{1}{\sqrt{\{1-(\omega/\omega_o)^2\}^2+(2\zeta\omega/\omega_o)^2}}\right]\frac{F}{k}e^{j(\omega t-\theta)} \tag{11}$$
where θ is given by eq. (10).

The quantity in the square brackets of eq. (11) is the absolute value of the complex frequency response, $|H(\omega)|$, see eqs. (4 & 5). It is called the **magnification factor** and is a dimensionless ratio between the amplitude of displacement X and the static displacement F/k.

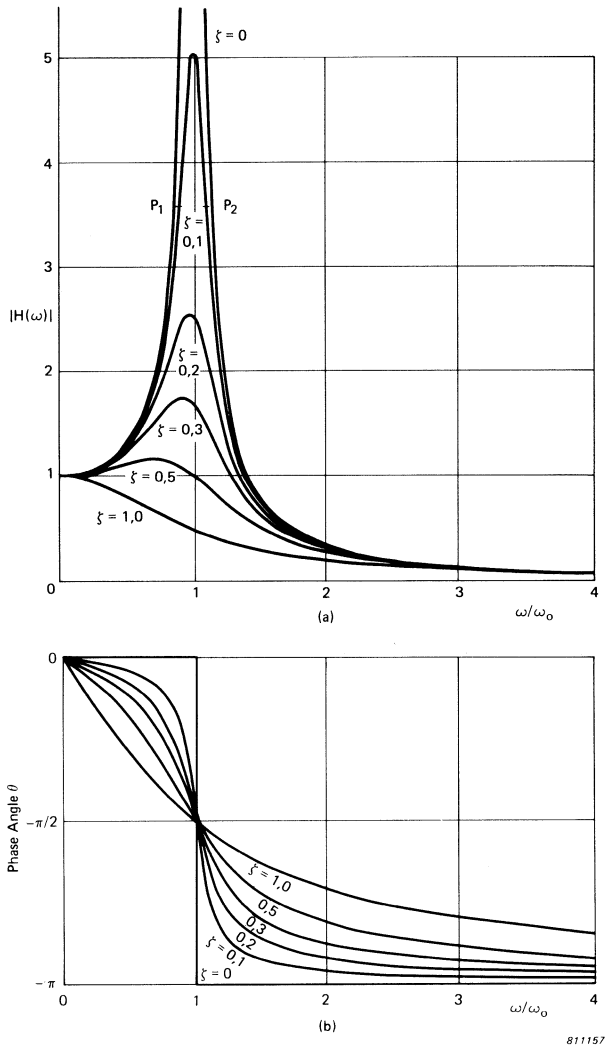

Fig.3.a) Magnification factor $|H(\omega)|$ as a function of the dimensionless frequency ratio ω/ω_0 for various values of the damping ratio ζ

b) Phase lag of displacement behind force as a function of ω/ω_0 for various values of ζ

Fig.3a shows the absolute value of the complex frequency response function $|H(\omega)|$ as a function of the dimensionless frequency ratio ω/ω_0 for various values of the damping ratio ζ. It can be seen that increasing damping ratio ζ tends to diminish the amplitudes and to shift the peaks to the left of the vertical through $\omega/\omega_0 = 1$. The peaks occur at frequencies given by

$$\omega = \omega_0 \sqrt{(1 - 2\zeta^2)} \tag{12}$$

where the peak value of $|H(\omega)|$ is given by

$$|H(\omega)| = \frac{1}{2\zeta\sqrt{1 - \zeta^2}} \tag{13}$$

For light damping ($\zeta < 0{,}05$) the curves are nearly symmetric about the vertical through $\omega/\omega_0 = 1$. The peak value of $|H(\omega)|$ occurs in the immediate vicinity of $\omega/\omega_0 = 1$ and is given by

$$|H(\omega)| \doteq \frac{1}{2\zeta} = Q \tag{14}$$

where Q is known as the **quality factor.**

For the curve of $\zeta = 0{,}1$ for example, the points P_1 and P_2 where the amplitude of $|H(\omega)|$ reduces to $Q/\sqrt{2}$ of its peak value are called the **half power points.** (If the ordinate is plotted on a logarithmic scale, P_1 and P_2 are points where the amplitude of $|H(\omega)|$ reduces by 3 dB and are thus called the –3 dB points). The difference in the frequencies of points P_1 and P_2 is called the 3 dB **bandwidth** of the system, and for **light damping** it can be shown that

$$\Delta\omega = \omega_2 - \omega_1 = 2\zeta\omega_o \tag{15}$$

where $\Delta\omega$ is the 3 dB bandwidth

ω_1 is the frequency at point P_1

ω_2 is the frequency at point P_2

From eqs. (14) and (15) we obtain

$$\frac{\omega_2 - \omega_1}{\omega_0} = 2\frac{c}{c_c} = \frac{1}{Q} = \eta \tag{16}$$

where η is called the **Loss Factor.**

Fig.3b shows curves of phase angle θ against ω/ω_0 for various values of ζ plotted from eq. (10). It should be noted that all curves pass through the point $\theta = \pi/2$, $\omega/\omega_0 = 1$; in other words, no matter what the damping is, the phase angle between force and displacement at the undamped natural frequency $\omega/=\omega_0$ is 90°. Moreover, the phase angle tends to zero for $\omega/\omega_0 \rightarrow 0$ and to 180° for $\omega/\omega_0 \rightarrow \infty$.

To examine the variation of the in-phase Re(x) and quadrature Im(x) components of displacement, eqs. (7 & 8) are plotted as a function of ω/ω_0 in Figs.4a and 4b respectively. The curves of the real component of displacement in Fig.4a have a zero value at $\omega/\omega_0 = 1$ independent of damping (ζ), and exhibits a peak and a notch at frequencies

$$\left.\begin{aligned} \omega_1 &= \omega_0\sqrt{1-2\zeta} \\ \text{and} \quad \omega_2 &= \omega_0\sqrt{1+2\zeta} \end{aligned}\right\} \tag{17}$$

respectively.

As the damping decreases (ζ gets smaller), the peak and the notch increase in value and become closer together. In the limit when $\zeta = 0$, the curve has an asymptote at $\omega/\omega_0 = 1$. The frequencies ω_1 and ω_2 are often used to determine the damping of the system from the equation

$$\eta = 2\zeta = \frac{(\omega_2/\omega_1)^2 - 1}{(\omega_2/\omega_1)^2 + 1} \tag{18}$$

The curves of the imaginary component of displacement have a notch in close vicinity of $\omega/\omega_0 = 1$ and they are sharper than those of $|H(\omega)|$ in Fig.3a for corresponding values of ζ.

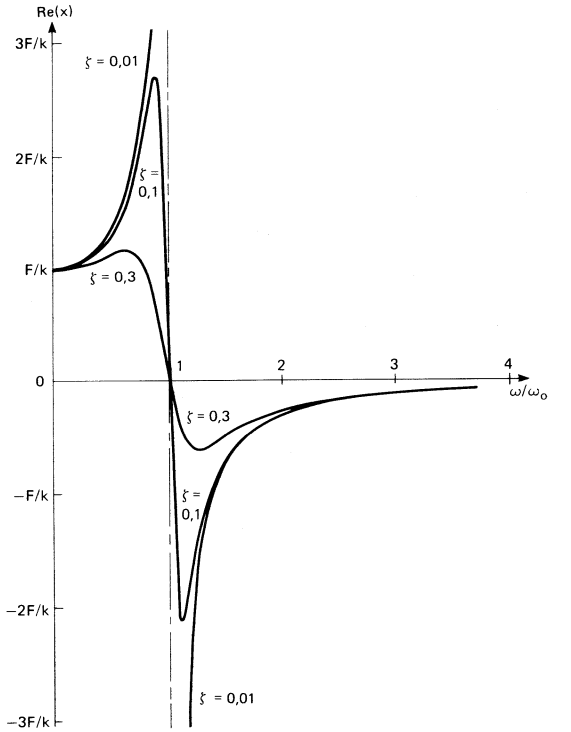

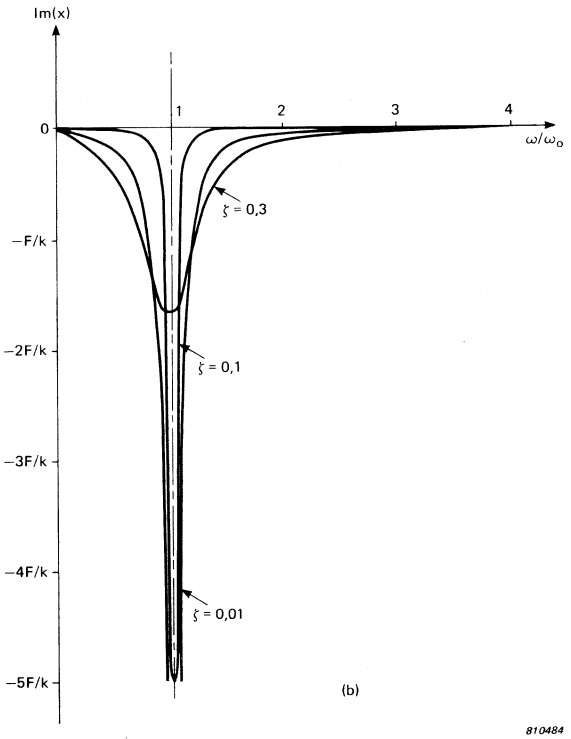

Fig.4.a) Real component of displacement as a function of the dimensionless frequency ratio ω/ω_0 for various values of ζ
b) Imaginary component of displacement against ω/ω_0 for various values of ζ

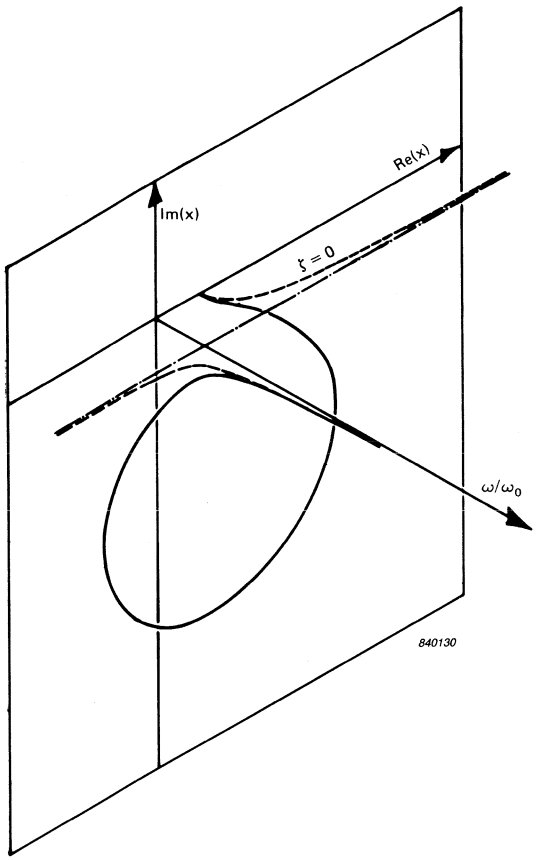

Fig.5. Three dimensional plot of real and imaginary components of displacement against frequency

If the real component, imaginary component and frequency ratio are plotted on three mutually perpendicular axes, the three dimensional curve obtained is that shown in Fig.5. The dashed line represents the curve for $\zeta = 0$ and lies wholly in the plane {Re(x),ω}. The curves of Fig.4a and 4b are in fact the projections of curves similar to that of Fig.5 in the {Re(x),ω} and {Im(x),ω} planes respectively. The third projection of the curve in the {Re(x), Im(x)} plane would look like the curves shown in Fig.6.

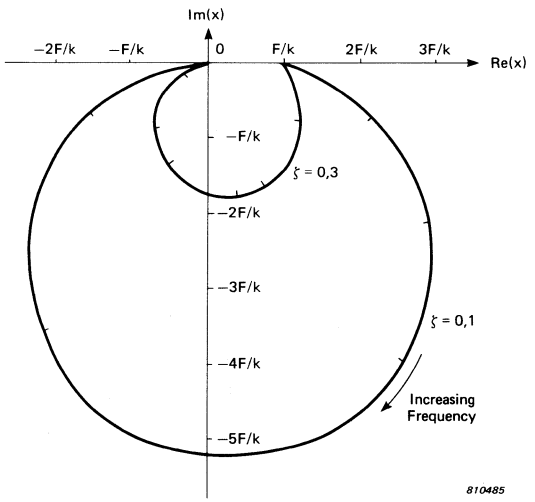

Fig.6. Complex plot of Real component against Imaginary component of displacement as the frequency is varied for various values of ζ

The right hand side of eqs. (7 & 8) are plotted on the X and Y axes of Fig.6 respectively, for varying values of ω/ω_0. The two curves are for ζ = 0,1 and ζ = 0,3. These curves could also have been obtained by plotting the total displacement given by expression (9) from the origin 0 at an angle θ from the Re(x) axis given by eq. (10). Thus the curve in Fig.6 is the locus in the Argand plane of the end of the line representing the total displacement for a particular ζ, as the frequency ratio ω/ω_0 is varied. It can be seen again in Fig.6 that no matter what the damping is, at the undamped natural frequency $\omega/\omega_0 = 1$ the real component is zero, or in other words, the phase angle between the force and the total displacement is 90°.

2.2. HYSTERETIC (STRUCTURAL) DAMPING

Another type of damping which permits setting up of linear damping equation, and which may often give a closer approximation to the damping process in practice, is the **hysteretic** damping, sometimes called **structural** damping. A large variety of materials, when subjected to cyclic stress (for strains below the elastic limit), exhibit a stress-strain relationship which is characterised by a hysteresis loop. The energy dissipated per cycle due to internal friction in the material is proportional to the area within the hysteresis loop, and hence the name hysteretic damping. It has been found [20] that the internal friction is independent of the rate of strain (independent of frequency) and over a significant frequency range is proportional to the displacement. Thus the damping force is proportional to the elastic force but, since energy is dissipated, it must be in phase with the velocity (in quadrature with displacement).

Thus for simple harmonic motion the damping force is given by

$$j\gamma kx = \gamma k \frac{\dot{x}}{\omega} \tag{19}$$

where γ is called the structural damping factor. The equation of motion for a single degree of freedom system with structural damping can thus be written

$$m\ddot{x} + \frac{\gamma k}{\omega}\dot{x} + kx = F e^{j\omega t} \tag{20}$$

or

$$m\ddot{x} + k(1 + j\gamma)x = F e^{j\omega t} \tag{21}$$

where $k(1 + j\gamma)$ is called the **complex stiffness.**
The steady state solution of eq. (21) is given by

$$x = X e^{j\omega t} = \left[\frac{1}{1 - (\omega/\omega_0)^2 + j\gamma}\right]\frac{F e^{j\omega t}}{k} \tag{22}$$

corresponding to eq. (4) for viscous damping.
By multiplying the numerator and the denominator of the square brackets by its complex conjugate, the real and the imaginary components of the displacement can be obtained:

$$x = \left[\frac{1 - (\omega/\omega_0)^2}{\{1 - (\omega/\omega_0)^2\}^2 + \gamma^2} - \frac{j\gamma}{\{1 - (\omega/\omega_0)^2\}^2 + \gamma^2}\right]\frac{F e^{j\omega t}}{k} \tag{23}$$

Thus

$$\mathrm{Re}(x) = \left[\frac{1 - (\omega/\omega_0)^2}{\{1 - (\omega/\omega_0)^2\}^2 + \gamma^2}\right]\frac{F e^{j\omega t}}{k} \tag{24}$$

and

$$\mathrm{Im}(x) = \left[\frac{-\gamma}{\{1 - (\omega/\omega_0)^2\}^2 + \gamma^2}\right]\frac{F e^{j\omega t}}{k} \tag{25}$$

The total displacement is given by

$$\left[\frac{1}{\sqrt{\{1-(\omega/\omega_0)^2\}^2+\gamma^2}}\right]\frac{F}{k}e^{j\omega t} \tag{26}$$

which lags behind the force vector by an angle θ given by

$$\theta = \tan^{-1}\left[\frac{\gamma}{1-(\omega/\omega_0)^2}\right] \tag{27}$$

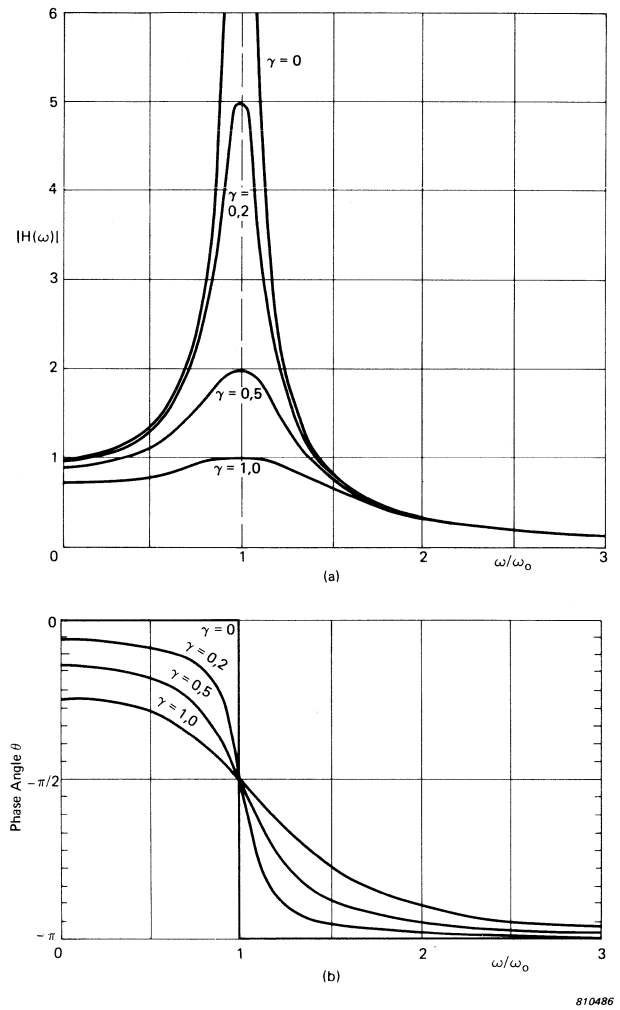

Fig.7.a) Magnification factor as a function of ω/ω_0 for various values of the structural damping factor γ

b) Phase lag of displacement behind force as a function of ω/ω_0 for various values of γ

The term in the square brackets of expression (26) (magnification factor) and θ are plotted against ω/ω_0 for various values of γ in Figs.7a and 7b respectively. The curves of Figs.7a and 7b can be seen to be similar to those of Figs.3a and 3b respectively for viscous damping; however, there are some minor differences. For hysteretic damping it can be seen from Fig.7a that the maximum response occurs exactly at $\omega/=\omega_0 = 1$ independent of damping γ. At very low values of ω/ω_0 the response for hysteretic damping depends on γ and the phase angle θ (Fig.7b) tends to $\tan^{-1}\gamma$ whereas it is zero for viscous damping.

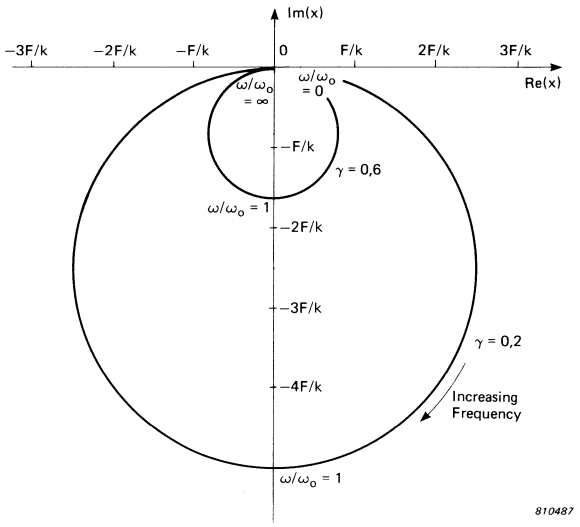

Fig.8. Complex plot of Real component against imaginary component of displacement as the frequency is varied for various values of γ

Fig.8 shows the complex plot (vector plot, polar plot, co-quad plot, Nyquist plot) obtained by plotting the right hand side of eqs. 24 and 25 in the Argand plane for values of $\gamma = 0{,}2$ and $\gamma = 0{,}6$. The two curves are seen to be completely symmetrical about the imaginary axis, except near the origin. At $\omega/\omega_0 = 1$ the real component is zero and the imaginary component is maximum.

3. MULTI-DEGREE OF FREEDOM SYSTEMS

In the previous sections a single degree of freedom system with a single mass, damper and spring was considered. Real structures have multiple degrees of freedom and their analysis is complicated by the large number of equations involved. To deal with them matrix methods are ideal, in that large arrays of equations can be manipulated in short-hand notation. Thus the reader unfamiliar with matrix methods is referred to **Appendices A** and **B** which should facilitate understanding of the following sections. To develop some of the concepts used in vibration theory in matrix form, a two degree of freedom system shown in Fig.9 will be used. Numerical examples will further elucidate these concepts which form the basis for the treatment and understanding of the dynamical behaviour of large systems.

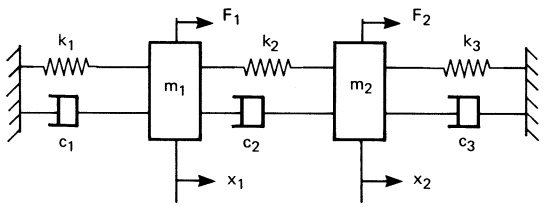

Fig.9. Two degree of freedom system

3.1. FREE VIBRATION

3.1.1. Eigenvalues and Eigenvectors

The equations of motion of the system shown in Fig.9 are

$$\begin{aligned} m_1\ddot{x}_1 + (c_1 + c_2)\dot{x}_1 - c_2\dot{x}_2 + (k_1 + k_2)x_1 - k_2x_2 &= F_1 \\ m_2\ddot{x}_2 - c_2\dot{x}_1 + (c_2 + c_3)\dot{x}_2 - k_2x_1 + (k_2 + k_3)x_2 &= F_2 \end{aligned} \tag{28}$$

which can be written in matrix form as

$$\begin{bmatrix} m_1 & 0 \\ 0 & m_2 \end{bmatrix} \begin{Bmatrix} \ddot{x}_1 \\ \ddot{x}_2 \end{Bmatrix} + \begin{bmatrix} c_1 + c_2 & -c_2 \\ -c_2 & c_2 + c_3 \end{bmatrix} \begin{Bmatrix} \dot{x}_1 \\ \dot{x}_2 \end{Bmatrix} + \begin{bmatrix} k_1 + k_2 & -k_2 \\ -k_2 & k_2 + k_3 \end{bmatrix} \begin{Bmatrix} x_1 \\ x_2 \end{Bmatrix} = \begin{Bmatrix} F_1 \\ F_2 \end{Bmatrix} \tag{29}$$

To determine the natural frequencies and natural mode shapes of the system, the undamped free vibration of the system is first considered. Thus the equations reduce to

$$[m]\{\ddot{x}\} + [k]\{x\} = 0 \qquad \text{where } [m] = \begin{bmatrix} m_1 & 0 \\ 0 & m_2 \end{bmatrix} \tag{30}$$

$$\text{and} \quad [k] = \begin{bmatrix} k_1 + k_2 & -k_2 \\ -k_2 & k_2 + k_3 \end{bmatrix}$$

Assuming harmonic motion $\ddot{x}_i = -\lambda_i x_i$ where $\lambda = \omega^2$ eq. (30) becomes

$$-\lambda [m] \{x\} + [k] \{x\} = 0$$

$$\text{or} \quad \left[-\lambda [m] + [k]\right] \{u\} = 0 \qquad \text{where } \{u\} = \{x\} \tag{31}$$

Premultiplying eq. (31) by $[m]^{-1}$ and rearranging we obtain

$$\left[[m]^{-1}[k] - \lambda [I]\right] \{u\} = 0 \tag{32}$$

where $[m]^{-1}[k]$ is called a **dynamic** matrix

and $[m]^{-1}[m] = [I]$ is a **unit** matrix, see Appendices A and B.

Eq. (32) is a set of simultaneous algebraic equations in u_i. From the theory of equations it is known, that for a non-trivial solution $\{u\} = 0$, the determinant of the coefficients of eq. (32) must be zero. Thus

$$\left|[m]^{-1}[k] - \lambda [I]\right| = 0 \tag{33}$$

which is known as the **characteristic equation** of the system. Eq. (33) when expanded can be rewritten as

$$\lambda^n + a_1\lambda^{n-1} + a_2\lambda^{n-2} + \ldots\ldots\ldots a_n = 0 \tag{34}$$

which is a polynomial in λ for an n degree of freedom system. The roots λ_i of the characteristic equation are called **eigenvalues** and the undamped natural frequencies of the system are determined from the relationship

$$\lambda_i = \omega_i^2 \tag{35}$$

By substituting λ_i into matrix equation (32) we obtain the corresponding **natural (or Principal) mode shape** $\{u_i\}$ which is also called an **eigenvector**. The us represent a deformation pattern of the structure for the corresponding natural frequency. As equations (32) are homogeneous, there is not a unique solution for the us, and we can only obtain a ratio among the us. Thus the natural mode shape is defined by the **ratio** of the amplitudes of motion at the various points on the structure when excited at its natural frequency. The actual amplitude on the other hand depends on the initial conditions and the position and magnitude of the exciting forces.

Consider a numerical example for the system shown in Fig.9 where

$$m_1 = 5 \text{ kg}; \quad m_2 = 10 \text{ kg}; \quad k_1 = k_2 = 2 \text{ N/m}; \quad k_3 = 4 \text{ N/m}$$

Substituting in eq. (29) we get

$$\begin{bmatrix} 5 & 0 \\ 0 & 10 \end{bmatrix} \begin{Bmatrix} \ddot{x}_1 \\ \ddot{x}_2 \end{Bmatrix} + \begin{bmatrix} 4 & -2 \\ -2 & 6 \end{bmatrix} \begin{Bmatrix} x_1 \\ x_2 \end{Bmatrix} = \begin{Bmatrix} 0 \\ 0 \end{Bmatrix} \tag{36}$$

Thus eq. (32) becomes

$$\left[\begin{bmatrix} 5 & 0 \\ 0 & 10 \end{bmatrix}^{-1} \begin{bmatrix} 4 & -2 \\ -2 & 6 \end{bmatrix} - \lambda \begin{bmatrix} 1 & 0 \\ 0 & 1 \end{bmatrix}\right] \begin{Bmatrix} u_1 \\ u_2 \end{Bmatrix} = \begin{Bmatrix} 0 \\ 0 \end{Bmatrix}$$

$$\left[\begin{bmatrix}1/5 & 0\\ 0 & 1/10\end{bmatrix}\begin{bmatrix}4 & -2\\ -2 & 6\end{bmatrix} - \lambda\begin{bmatrix}1 & 0\\ 0 & 1\end{bmatrix}\right]\begin{Bmatrix}u_1\\ u_2\end{Bmatrix} = \begin{Bmatrix}0\\ 0\end{Bmatrix}$$

$$\begin{bmatrix}4/5-\lambda & -2/5\\ -1/5 & 3/5-\lambda\end{bmatrix}\begin{Bmatrix}u_1\\ u_2\end{Bmatrix} = \begin{Bmatrix}0\\ 0\end{Bmatrix} \qquad (37)$$

For a non-trivial solution the determinant of the above equation must equal zero, thus

$$(4/5 - \lambda)\,(3/5 - \lambda) - (-1/5)\,(-2/5) = 0$$

i.e. $$\lambda^2 - \frac{7}{5}\lambda + \frac{2}{5} = 0 \quad \text{(characteristic equation)}$$

The roots of the above equation are

$$\lambda_{1,2} = \frac{7/5 \pm \sqrt{49/25 - 8/5}}{2} = \frac{7}{10} \pm \frac{1}{2}\sqrt{\frac{9}{25}}$$

Thus $\lambda_1 = 2/5$ and $\lambda_2 = 1$ and the two natural frequencies are given by

$$\omega_1 = \sqrt{\lambda_1} = \sqrt{2/5} \quad \text{and} \quad \omega_2 = \sqrt{\lambda_2} = 1$$

Substitution of λ_1 and λ_2 in turn in eq. (37) will give the two natural mode shapes. Thus the mode shape for λ_1 is given by

$$\begin{bmatrix}4/5-2/5 & -2/5\\ -1/5 & 3/5-2/5\end{bmatrix}\begin{Bmatrix}u_1\\ u_2\end{Bmatrix} = \begin{Bmatrix}0\\ 0\end{Bmatrix}$$

$$\frac{2}{5}u_1 - \frac{2}{5}u_2 = 0$$

i.e. $u_1 = u_2$

Thus the mode shape for the natural frequency ω_1 is $\{\phi_1\} = \begin{Bmatrix}u_1\\ u_1\end{Bmatrix}$ where u_1 is arbitrary

Similarly the mode shape for λ_2 is given by

$$\begin{bmatrix}4/5-1 & -2/5\\ -1/5 & 3/5-1\end{bmatrix}\begin{Bmatrix}u_1\\ u_2\end{Bmatrix} = \begin{Bmatrix}0\\ 0\end{Bmatrix}$$

$$-\frac{1}{5}u_1 - \frac{2}{5}u_2 = 0$$

i.e. $$u_2 = \frac{-u_1}{2}$$

Thus the mode shape for the natural frequency ω_2 is $\{\phi_2\} = \begin{Bmatrix}u_1\\ -u_1/2\end{Bmatrix}$

For an arbitrary deflection of $u_1 = 1$ the two mode shapes would be

$$\{\phi_1\} = \begin{Bmatrix}1\\ 1\end{Bmatrix} \qquad \text{for } \omega_1 = \sqrt{2/5}$$

and $$\{\phi_2\} = \begin{Bmatrix}1\\ -1/2\end{Bmatrix} \qquad \text{for } \omega_2 = 1$$

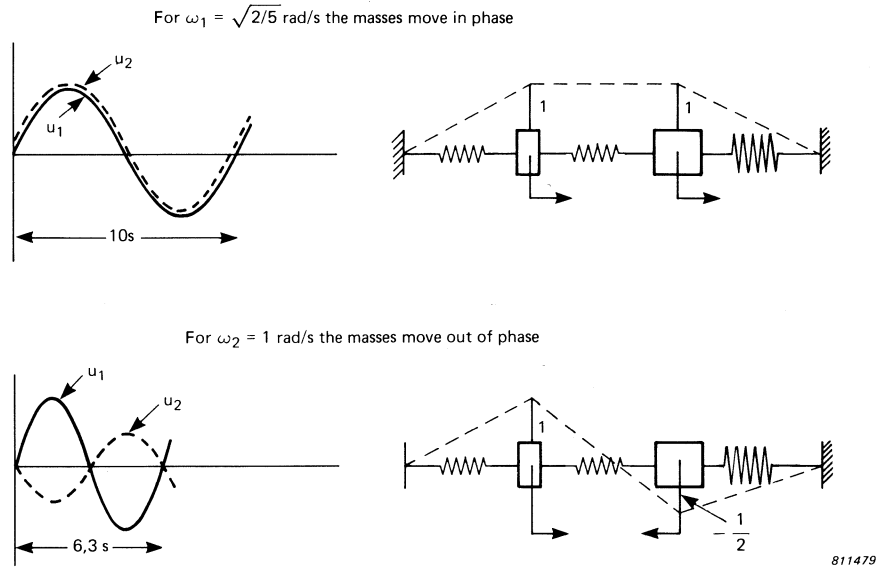

Fig.10. Frequency and mode shapes for the two degree of freedom system

The system can thus vibrate freely with simple harmonic motion when started in the correct way at one of two possible frequencies as shown in Fig.10. **Note that the masses move either in phase or 180° out of phase with each other. Since the masses reach their maximum displacements simultaneously, the nodal points are clearly defined.**

3.1.2. Eigenvectors from adjoint of system matrix

Another way of determining the eigenvectors is through the use of the adjoint matrix of the system. In eq. (32) let

$$\left[[m]^{-1}[k] - \lambda[I]\right] = \left[A\right] \tag{38}$$

It has been shown in Appendix B that

$$[A]^{-1} = \frac{[\hat{A}]}{|A|} \quad \text{where } [\hat{A}] \text{ is the adjoint of } [A] \tag{39}$$

Premultiplying the above equation by $|A|[A]$ we obtain

$$|A|[I] = [A][\hat{A}] \tag{40}$$

or in terms of the original expression for [A] we get

$$\left|[m]^{-1}[k] - \lambda[I]\right|[I] = \left[[m]^{-1}[k] - \lambda[I]\right]\left[\hat{A}\right] \tag{41}$$

If now $\lambda = \lambda_i$ a root of the characteristic equation (an eigenvalue) the determinant on the left hand side becomes zero and eq.(41) reduces to

i.e. $$0 = \left[[m]^{-1}[k] - \lambda_i[I]\right] \text{ adj } \left[[m]^{-1}[k] - \lambda_i[I]\right] \tag{42}$$

Eq. (42) is valid for all λ_i and represents the n equations for the n degrees of freedom system. By comparing equations (32) and (42) it can be seen that the adjoint matrix, adj. $[[m]^{-1}[k] - \lambda_i[I]]$ must consist of columns, each of which is proportional to the i th eigenvector $\{u_i\}$ (i th mode shape for λ_i).

For the numerical example considered, the system matrix [A] is given in eq. (37)

$$\text{i.e.} \quad [A] = \begin{bmatrix} 4/5 - \lambda & -2/5 \\ -1/5 & 3/5 - \lambda \end{bmatrix}$$

For the first mode $\lambda_1 = \frac{2}{5}$ we get

$$[A(\lambda_1)] = \begin{bmatrix} 2/5 & -2/5 \\ -1/5 & 1/5 \end{bmatrix}$$

The adjoint of $[A(\lambda_1)]$ is given by

$$\text{adj}\,[A(\lambda_1)] = \begin{bmatrix} 1/5 & 2/5 \\ 1/5 & 2/5 \end{bmatrix}$$

Thus both the columns of the systems adjoint matrix are proportional to the first mode shape.

Similarly for the second mode $\lambda_2 = 1$ the system matrix is

$$[A(\lambda_2)] = \begin{bmatrix} 4/5 - 1 & -2/5 \\ -1/5 & 3/5 - 1 \end{bmatrix} = \begin{bmatrix} -1/5 & -2/5 \\ -1/5 & -2/5 \end{bmatrix}$$

The adjoint of $[A(\lambda_2)]$ is given by

$$\text{adj}\,[A(\lambda_2)] = \begin{bmatrix} -2/5 & 2/5 \\ 1/5 & -1/5 \end{bmatrix}$$

Both the columns are seen to be proportional to the second mode shape.

3.1.3. Orthogonal Properties of Eigenvectors

It was shown in the previous section that solution of equation (31) yields n eigenvalues and n corresponding eigenvectors. Thus a particular eigenvalue ω_i and the eigenvector $\{\phi_i\}$ will satisfy eq. (31);

$$\text{i.e.} \quad [k]\{\phi_i\} = \lambda_i [m]\{\phi_i\} \tag{43}$$

Premultiply eq. (43) by the **transpose** of another mode shape $\{\phi_j\}$

$$\text{i.e.} \quad \{\phi_j\}^T [k]\{\phi_i\} = \lambda_i \{\phi_j\}^T [m]\{\phi_i\} \tag{44}$$

where the superscript T denotes a transpose matrix (see Appendix A).

We now write the equation for the j^{th} mode and premultiply by the transpose of the i^{th} mode

$$\text{i.e.} \quad \{\phi_i\}^T [k]\{\phi_j\} = \lambda_j \{\phi_i\}^T [m]\{\phi_j\} \tag{45}$$

As [m] and [k] are symmetric matrices

$$\{\phi_j\}^T [k] \{\phi_i\} = \{\phi_i\}^T [k] \{\phi_j\} \quad \text{(see Appendix A)} \tag{46}$$

and

$$\{\phi_j\}^T [m] \{\phi_i\} = \{\phi_i\}^T [m] \{\phi_j\}$$

Therefore subtracting eq. (45) from eq. (44) we obtain

$$0 = (\lambda_i - \lambda_j) \{\phi_i\}^T [m] \{\phi_j\} \tag{47}$$

If $\lambda_i \neq \lambda_j$ (implying two different natural frequencies)

$$\{\phi_i\}^T [m] \{\phi_j\} = 0 \tag{48}$$

and from eq. (45) it can be seen that

$$\{\phi_i\}^T [k] \{\phi_j\} = 0 \tag{49}$$

Equations (48) and (49) define the orthogonality properties of the mode shapes with respect to the system mass and stiffness matrices respectively. (The concept of orthogonality of vectors can be illustrated by, for example, the i j k unit vectors for the three dimensional cartesian coordinate system).

3.1.4. Generalized Mass and Generalized Stiffness

It can be seen that if i = j in eq. (47) then the two modes are not necessarily orthogonal and eq. (48) is equal to some scalar constant other than zero, e.g. M_i

$$\text{i.e.} \quad \{\phi_i\}^T [m] \{\phi_i\} = M_i \qquad i = 1, 2, 3, \ldots\ldots n \tag{50}$$

and from eq. (45) it follows that

$$\{\phi_i\}^T [k] \{\phi_i\} = \lambda_i M_i = \omega_i^2 M_i = K_i \qquad i = 1, 2, 3 \ldots\ldots n \tag{51}$$

M_i and K_i are called the **generalized mass** and **generalized stiffness** respectively.

The numerical values of the mode shapes calculated above will be used to determine the generalized mass and generalized stiffness. The mode shapes were found to be

$$\{\phi_1\} = \begin{Bmatrix} 1 \\ 1 \end{Bmatrix} \text{ for } \omega_1 = \sqrt{2/5} \quad \text{and} \quad \{\phi_2\} = \begin{Bmatrix} 1 \\ -1/2 \end{Bmatrix} \text{ for } \omega_2 = 1$$

Substituting $\{\phi_1\}$ in eq. (50) we obtain the generalized mass M_1 for the first mode:

$$\begin{Bmatrix} 1 \\ 1 \end{Bmatrix}^T \begin{bmatrix} 5 & 0 \\ 0 & 10 \end{bmatrix} \begin{Bmatrix} 1 \\ 1 \end{Bmatrix} = M_1$$

$$\text{i.e. } (1 \quad 1) \begin{bmatrix} 5 & 0 \\ 0 & 10 \end{bmatrix} \begin{Bmatrix} 1 \\ 1 \end{Bmatrix} = M_1$$

$$(5 \quad 10) \begin{Bmatrix} 1 \\ 1 \end{Bmatrix} = M_1$$

$$5 + 10 = M_1$$

$$M_1 = 15$$

Similarly substituting $\{\phi_2\}$ in eq. (50) we obtain

$$\begin{Bmatrix} 1 \\ -1/2 \end{Bmatrix}^T \begin{bmatrix} 5 & 0 \\ 0 & 10 \end{bmatrix} \begin{Bmatrix} 1 \\ -1/2 \end{Bmatrix} = M_2$$

$$\text{i.e.} \quad (5 \quad -5) \begin{Bmatrix} 1 \\ -1/2 \end{Bmatrix} = M_2$$

$$\therefore \quad 5 + 5/2 = M_2$$

$$\therefore M_2 = 15/2$$

Thus the generalized masses M_1 and M_2 for the first and second modes are 15 and 15/2 respectively.

The generalized stiffnesses K_1 and K_2 for the first and second modes are

$$K_1 = \omega_1^2 M_1 = 2/5 \times 15 = 6 \qquad \text{and} \qquad K_2 = \omega_2^2 M_2 = 1 \times 15/2 = 15/2$$

3.1.5. Normalization of Mode Shapes

If one of the elements of the eigenvector $\{\phi_i\}$ is assigned a certain value, the rest of the (n – 1) elements are also fixed because the ratio between any two elements is constant. Thus the eigenvector becomes unique in an absolute sense. This process of adjusting the elements of the natural modes to make their amplitude unique is called **normalization**, and the resulting scaled natural modes are called **orthonormal** modes. There are several ways to normalize the mode shapes, four of which are tabulated below;

1) The mode shapes can be normalized such that the generalized mass or modal mass M_i in eq. (50) is set to unity. This method has the advantage that eq. (51) yields directly the eigenvalues λ_i and thus the natural frequencies.

2) The largest element of the mode shape is set to unity, which may be convenient for plotting the mode shape.

3) A particular element of the mode shape is set to unity.

4) The length of the mode vector is set to unity.

The first method of normalization will be illustrated by the numerical example of the system shown in Fig.9. The mode shapes were shown to be

$$\{\phi_1\} = \begin{Bmatrix} u_1 \\ u_1 \end{Bmatrix} \text{ for } \omega_1 = \sqrt{2/5} \quad \text{and} \quad \{\phi_2\} = \begin{Bmatrix} u_1 \\ -u_1/2 \end{Bmatrix} \text{ for } \omega_2 = 1$$

Therefore substitution of $\{\phi_1\}$ in eq. (50) yields

$$\begin{Bmatrix} u_1 \\ u_1 \end{Bmatrix}^T \begin{bmatrix} 5 & 0 \\ 0 & 10 \end{bmatrix} \begin{Bmatrix} u_1 \\ u_1 \end{Bmatrix} = M_1 = 1$$

$$\text{i.e.} \qquad (u_1 \quad u_1) \begin{bmatrix} 5 & 0 \\ 0 & 10 \end{bmatrix} \begin{Bmatrix} u_1 \\ u_1 \end{Bmatrix} = 1$$

$$\text{i.e.} \quad (5u_1 \quad 10u_1) \begin{Bmatrix} u_1 \\ u_1 \end{Bmatrix} = 1$$

$$\therefore \quad 5u_1^2 + 10u_1^2 = 1 \qquad \text{i.e.} \quad u_1 = \sqrt{1/15}$$

Thus the normalized mode shape for $\omega_1 = \sqrt{2/5}$ is

$$\{\phi_1\} = \begin{Bmatrix} u_1 \\ u_1 \end{Bmatrix} = \begin{Bmatrix} \sqrt{1/15} \\ \sqrt{1/15} \end{Bmatrix} \tag{52}$$

Similarly for $\{\phi_2\}$ we get $\begin{Bmatrix} u_1 \\ -u_1/2 \end{Bmatrix}^T \begin{bmatrix} 5 & 0 \\ 0 & 10 \end{bmatrix} \begin{Bmatrix} u_1 \\ -u_1/2 \end{Bmatrix} = M_2 = 1$

$$\text{i.e.} \quad (5u_1 \quad -5u_1) \begin{Bmatrix} u_1 \\ -u_1/2 \end{Bmatrix} = 1$$

$$\therefore \quad 5u_1^2 + 5u_1^2/2 = 1 \qquad \text{i.e.} \quad u_1 = \sqrt{2/15}$$

Thus the normalized mode shape for $\omega_2 = 1$ is

$$\{\phi_2\} = \begin{Bmatrix} u_1 \\ -u_1/2 \end{Bmatrix} = \begin{Bmatrix} \sqrt{2/15} \\ -\sqrt{2/15}/2 \end{Bmatrix} \tag{53}$$

It can now be seen that these normalized mode shapes could also have been obtained by dividing the **natural** modes by the square root of their respective generalized masses calculated in the previous section.

i.e. For normalization of the first natural mode

$$\{\phi_1\} = \frac{1}{\sqrt{M_1}} \begin{Bmatrix} 1 \\ 1 \end{Bmatrix} = \frac{1}{\sqrt{15}} \begin{Bmatrix} 1 \\ 1 \end{Bmatrix} = \begin{Bmatrix} \sqrt{1/15} \\ \sqrt{1/15} \end{Bmatrix}$$

and for the second mode

$$\{\phi_2\} = \frac{1}{\sqrt{M_2}} \begin{Bmatrix} 1 \\ -1/2 \end{Bmatrix} = \frac{1}{\sqrt{15/2}} \begin{Bmatrix} 1 \\ -1/2 \end{Bmatrix} = \begin{Bmatrix} \sqrt{2/15} \\ -\sqrt{2/15}/2 \end{Bmatrix}$$

which are the same as calculated in eq. (52) and (53) respectively.

3.2. FORCED VIBRATION

3.2.1. Principal Coordinates (Normal Coordinates)

The equations of motion of the two degree of freedom system shown in Fig.9 without damping can be written as

$$\begin{aligned} m_1 \ddot{x}_1 \quad + (k_1 + k_2) x_1 \quad - k_2 x_2 &= F_1 \\ m_2 \ddot{x}_2 \quad - k_2 x_2 \quad + (k_2 + k_3) x_2 &= F_2 \end{aligned} \tag{54}$$

or in matrix form by eq. (29) as

$$\begin{bmatrix} m_1 & 0 \\ 0 & m_2 \end{bmatrix} \begin{Bmatrix} \ddot{x}_1 \\ \ddot{x}_2 \end{Bmatrix} + \begin{bmatrix} (k_1 + k_2) & -k_2 \\ -k_2 & (k_2 + k_3) \end{bmatrix} \begin{Bmatrix} x_1 \\ x_2 \end{Bmatrix} = \begin{Bmatrix} F_1 \\ F_2 \end{Bmatrix} \tag{55}$$

In solving the above equations for the response $\{x\}$ for a particular set of exciting forces, the major obstacle encountered is the coupling between the equations; i.e. both coordinates x_1 and x_2 occur in each of the equations (54). In equation (55) the coupling is seen by the fact that while the stiffness matrix is **symmetric** it is not diagonal (i.e. the off-diagonal terms are non-zero). This type of coupling is called **elastic coupling** or **static coupling** (non-diagonal stiffness matrix) and occurs for a lumped mass system, if the coordinates chosen are at each mass point. If the equations of motion had been written in terms of the extensions of each spring, the stiffness matrix would have been diagonal but not the mass matrix. This kind of coupling is termed **inertial coupling** or **dynamic coupling** (non-diagonal mass matrix). It is thus seen that the way in which the equations are coupled depends on the choice of coordinates. If the system of equations could be uncoupled, so that we obtained diagonal mass and stiffness matrices, then each equation would be similar to that of a single degree of freedom system, and could be solved independent of each other. Indeed, the process of deriving the system response by transforming the equations of motion into an independent set of equations is known as **modal analysis**.

Thus the coordinate transformation we are seeking, is one that decouples the system inertially and elastically simultaneously, and therefore yields us diagonal mass and stiffness matrices. It is here that the orthogonal properties of the mode shapes discussed above come into use. It was shown by eq. (50), that if the mass or the stiffness matrix is post and pre-multiplied by a mode shape and its transpose respectively, the result is some scalar constant. Thus with the use of a matrix $[\phi]$ whose columns are the mode shape vectors, we already have at our disposal the necessary coordinate transformation. The x coordinates are transformed to η by the equation

$$\{x\} = [\phi]\{\eta\} \tag{56}$$

where

$$[\phi] = \begin{bmatrix} \begin{Bmatrix} u_1 \\ u_2 \\ \vdots \\ u_n \end{Bmatrix}_1 & \begin{Bmatrix} u_1 \\ u_2 \\ \vdots \\ u_n \end{Bmatrix}_2 & \cdots\cdots & \begin{Bmatrix} u_1 \\ u_2 \\ \vdots \\ u_n \end{Bmatrix}_n \end{bmatrix} \tag{57}$$

$[\phi]$ is referred to as the **modal matrix** and $\{\eta\}$ is called **principal coordinates, normal coordinates** or **modal coordinates.**

Eq. (55) can be written as

$$[m]\{\ddot{x}\} + [k]\{x\} = \{F\} \tag{58}$$

and substituting eq. (56) into (58) yields

$$[m][\phi]\{\ddot{\eta}\} + [k][\phi]\{\eta\} = \{F\} \tag{59}$$

Pre-multiplying eq. (59) by the transpose of the modal matrix i.e. $[\phi]^T$ we obtain

$$[\phi]^T[m][\phi]\{\ddot{\eta}\} + [\phi]^T[k][\phi]\{\eta\} = [\phi]^T\{F\} \tag{60}$$

In eq. (50) the mass matrix was post and pre-multiplied by **one** mode shape and its transpose, giving a scalar quantity, while in eq. (60) the mass matrix is post and pre-multiplied by all the mode shapes and their transpose. Thus the product is a matrix $[M]$ whose diagonal elements are some constants while all the off-diagonal terms are zero, i.e.

$$[\phi]^T [m] [\phi] = [M] \tag{61}$$

Similarly

$$[\phi]^T [k] [\phi] = [K] \tag{62}$$

where [M] and [K] are diagonal matrices.

Hence eq. (60) can be written as

$$[M]\{\ddot{\eta}\} + [K]\{\eta\} = [\phi]^T \{F\} \tag{63}$$

Eq. (63) represents n equations of the form

$$M_i \ddot{\eta}_i + K_i \eta_i = \{\phi_i\}^T \{F\} = F_i \tag{64}$$

where $\{\phi_i\}$ is the i th column of the modal matrix i.e. the i th mode shape. M_i and K_i can be recognised as the i th modal mass (generalized mass) and i th modal stiffness (generalized stiffness) respectively, see eqs. (50) and (51). Eq. (64) is the equation of motion for single degree of freedom systems shown in Fig.11.

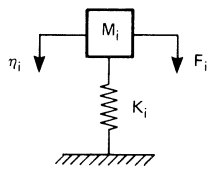

Fig.11. Single degree of freedom system defined by eq. (64)

Since $K_i = \omega_i^2 M_i$ see eq. (51), eq. (64) can be written as

$$\ddot{\eta}_i + \omega_i^2 \eta_i = \frac{F_i}{M_i} = \frac{\{\phi_i\}^T \{F\}}{\{\phi_i\}^T [m] \{\phi_i\}} \tag{65}$$

Once the solution (time responses) of eq. (63) for all ηs is obtained, the solution in terms of the original coordinates x can be obtained by transforming back, i.e. substituting for ηs in eq. (56) $\{x\} = [\phi]\{\eta\}$

It should, however, be noted, that the modal matrix $[\phi]$ of eq. (57) can also be made up of columns of the **normalized mode shapes** (such that $M_i = 1$). Such a matrix is called a **weighted modal matrix** $[\tilde{\phi}]$. If this matrix is used instead of the matrix with natural mode shapes, (see section on Normalization of Mode Shapes), eq. (65) would be simplified to

$$\ddot{\eta}_i + \omega_i^2 \eta_i = F_i = \{\phi_i\}^T \{F\} \tag{66}$$

Thus the modal mass would be unity and the modal stiffness would be the square of the natural frequency of the i th mode.

Let us consider our numerical example of the system of Fig.9 with forcing functions F_1 and F_2. Thus eq. (36) becomes

$$\begin{bmatrix} 5 & 0 \\ 0 & 10 \end{bmatrix} \begin{Bmatrix} \ddot{x}_1 \\ \ddot{x}_2 \end{Bmatrix} + \begin{bmatrix} 4 & -2 \\ -2 & 6 \end{bmatrix} \begin{Bmatrix} x_1 \\ x_2 \end{Bmatrix} = \begin{Bmatrix} F_1 \\ F_2 \end{Bmatrix} \tag{67}$$

The natural frequencies and natural mode shapes were

$$\omega_1 = \sqrt{2/5} \qquad \left\{\phi_1\right\} = \begin{Bmatrix} 1 \\ 1 \end{Bmatrix}$$

$$\omega_2 = 1 \qquad \left\{\phi_2\right\} = \begin{Bmatrix} 1 \\ -1/2 \end{Bmatrix}$$

Thus the modal matrix $[\phi]$ using **natural** mode shapes* is

$$[\phi] = \begin{bmatrix} 1 & 1 \\ 1 & -1/2 \end{bmatrix}$$

The x coordinates are transformed by the equation

$$\{x\} = [\phi]\{\eta\} \tag{68}$$

i.e.

$$\begin{Bmatrix} x_1 \\ x_2 \end{Bmatrix} = \begin{bmatrix} 1 & 1 \\ 1 & -1/2 \end{bmatrix} \begin{Bmatrix} \eta_1 \\ \eta_2 \end{Bmatrix} \tag{69}$$

Substituting eq. (68) into eq. (67) and pre-multiplying by $[\phi]^T$ gives

$$[\phi]^T \begin{bmatrix} 5 & 0 \\ 0 & 10 \end{bmatrix} [\phi] \begin{Bmatrix} \ddot{\eta}_1 \\ \ddot{\eta}_2 \end{Bmatrix} + [\phi]^T \begin{bmatrix} 4 & -2 \\ -2 & 6 \end{bmatrix} [\phi] \begin{Bmatrix} \eta_1 \\ \eta_2 \end{Bmatrix} = [\phi]^T \begin{Bmatrix} F_1 \\ F_2 \end{Bmatrix}$$

---

* As mentioned above, the modal matrix can also be made up of columns of the normalized mode shapes (such that $M_i = 1$). Using the normalized mode shapes from eqs. (52) and (53), the weighted modal matrix $[\tilde{\phi}]$ is given by

$$[\tilde{\phi}] = \begin{bmatrix} \sqrt{1/15} & \sqrt{2/15} \\ \sqrt{1/15} & -\sqrt{2/15}/2 \end{bmatrix}$$

Thus the products $[\tilde{\phi}]^T[m][\tilde{\phi}]$ and $[\tilde{\phi}]^T[k][\tilde{\phi}]$ are given by

$$[\tilde{\phi}]^T [m] [\tilde{\phi}] = \begin{bmatrix} \sqrt{1/15} & \sqrt{1/15} \\ \sqrt{2/15} & -\sqrt{2/15}/2 \end{bmatrix} \begin{bmatrix} 5 & 0 \\ 0 & 10 \end{bmatrix} \begin{bmatrix} \sqrt{1/15} & \sqrt{2/15} \\ \sqrt{1/15} & -\sqrt{2/15}/2 \end{bmatrix} = \begin{bmatrix} 1 & 0 \\ 0 & 1 \end{bmatrix}$$

$$[\tilde{\phi}]^T [k] [\tilde{\phi}] = \begin{bmatrix} \sqrt{1/15} & \sqrt{1/15} \\ \sqrt{2/15} & -\sqrt{2/15}/2 \end{bmatrix} \begin{bmatrix} 4 & -2 \\ -2 & 6 \end{bmatrix} \begin{bmatrix} \sqrt{1/15} & \sqrt{2/15} \\ \sqrt{1/15} & -\sqrt{2/15}/2 \end{bmatrix} = \begin{bmatrix} 2/5 & 0 \\ 0 & 1 \end{bmatrix}$$

It can thus be seen that by using the weighted modal matrix for coordinate transformation the mass matrix becomes a unit matrix and the stiffness matrix is diagonalized with the diagonal terms equal to the eigenvalues – the square of the natural frequencies.

In general

$$[\tilde{\phi}]^T [m] [\tilde{\phi}] = [1]$$

and

$$[\tilde{\phi}]^T [k] [\tilde{\phi}] = [\Lambda]$$

where

$$[\Lambda] = \begin{bmatrix} \lambda_1 & 0 & 0 \cdots 0 \\ 0 & \lambda_2 & 0 \cdots 0 \\ \vdots & & \\ 0 & 0 & \cdots \lambda_n \end{bmatrix}$$

The products $[\phi]^T[m][\phi]$ and $[\phi]^T[k][\phi]$ are calculated to be

$$[\phi]^T\,[m]\,[\phi] = \begin{bmatrix} 1 & 1 \\ 1 & -1/2 \end{bmatrix} \begin{bmatrix} 5 & 0 \\ 0 & 10 \end{bmatrix} \begin{bmatrix} 1 & 1 \\ 1 & -1/2 \end{bmatrix} = \begin{bmatrix} 15 & 0 \\ 0 & 15/2 \end{bmatrix}$$

$$[\phi]^T\,[k]\,[\phi] = \begin{bmatrix} 1 & 1 \\ 1 & -1/2 \end{bmatrix} \begin{bmatrix} 4 & -2 \\ -2 & 6 \end{bmatrix} \begin{bmatrix} 1 & 1 \\ 1 & -1/2 \end{bmatrix} = \begin{bmatrix} 6 & 0 \\ 0 & 15/2 \end{bmatrix}$$

Substituting these products into the equation above we obtain

$$\begin{bmatrix} 15 & 0 \\ 0 & 15/2 \end{bmatrix} \begin{Bmatrix} \ddot{\eta}_1 \\ \ddot{\eta}_2 \end{Bmatrix} + \begin{bmatrix} 6 & 0 \\ 0 & 15/2 \end{bmatrix} \begin{Bmatrix} \eta_1 \\ \eta_2 \end{Bmatrix} = \begin{bmatrix} 1 & 1 \\ 1 & -1/2 \end{bmatrix} \begin{Bmatrix} F_1 \\ F_2 \end{Bmatrix}$$

Thus the equations of motion in η are

$$\begin{aligned} 15\ddot{\eta}_1 + 6\eta_1 &= F_1 + F_2 \\ 15/2\ddot{\eta}_2 + 15/2\eta_2 &= F_1 - F_2/2 \end{aligned} \tag{70}$$

The generalized masses and stiffnesses for the two modes can be seen to be the same as those calculated under **section 3.1.4. Generalized Mass and Generalized Stiffness.** Thus the original set of equations (67) are shown to be uncoupled; in other words the two degree of freedom system is broken down to two single degree of freedom systems shown in Fig.12.

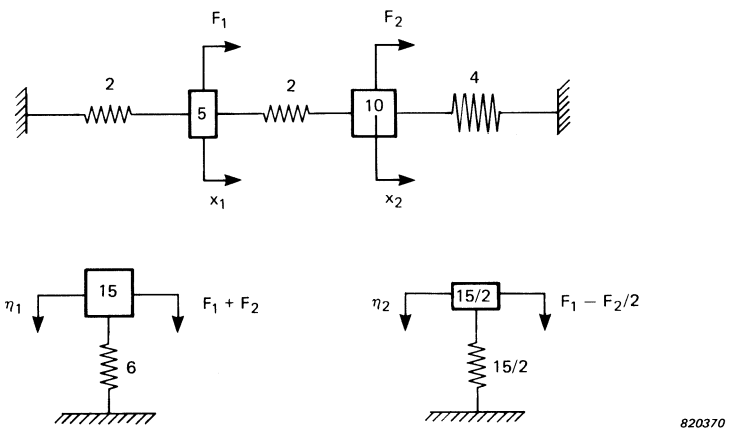

Fig.12. The undamped two degree of freedom system shown in Fig.9, broken down to two single degree of freedom systems

Once the time responses for η_1 and η_2 have been determined from eq. (70), they can be substituted in eq. (69) to give the time response in terms of the original coordinates x, thus

$$\begin{aligned} x_1(t) &= \eta_1(t) + \eta_2(t) \\ x_2(t) &= \eta_1(t) - \frac{1}{2}\eta_2(t) \end{aligned} \tag{71}$$

Eq. (71) in fact illustrates a very important principle in vibration, namely that any possible **free** motion can be written as the sum of the motion in each principal mode in some proportion and relative phase. In general for an n degree of freedom system

$$\begin{Bmatrix} x_1 \\ x_2 \\ \vdots \\ x_n \end{Bmatrix} = \eta_1 \begin{Bmatrix} u_1 \\ u_2 \\ \vdots \\ u_n \end{Bmatrix}_1 \cos(\omega_1 t - \theta_1) + \eta_2 \begin{Bmatrix} u_1 \\ u_2 \\ \vdots \\ u_n \end{Bmatrix}_2 \cos(\omega_2 t - \theta_2)$$

$$+ \cdots\cdots \eta_n \begin{Bmatrix} u_1 \\ u_2 \\ \vdots \\ u_n \end{Bmatrix}_n \cos(\omega_n t - \theta_n) \qquad (72)$$

If the two degree of freedom system discussed above is given arbitrary starting conditions, the resulting motion would be the sum of the two principal modes in some proportion and would look as shown in Fig.13.

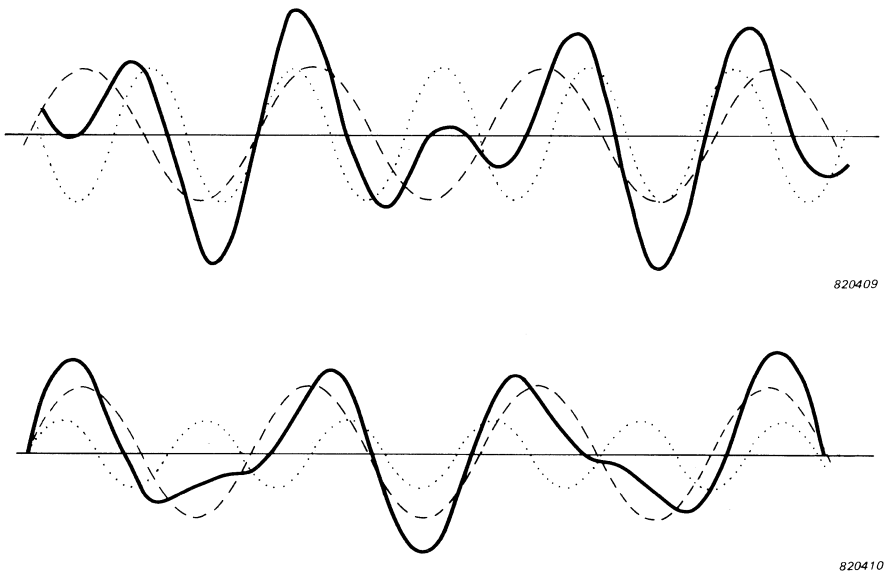

Fig.13. Response of the two degree of freedom system when given arbitrary starting conditions

3.3. FORCED DAMPED VIBRATION – PROPORTIONAL DAMPING

The assumption that systems have no damping is only hypothetical, since all structures have internal damping. As there are several types of damping, viscous, hysteretic, coulomb, aerodynamic etc., it is generally difficult to ascertain which **type** of damping is represented in a particular structure. In fact a structure may have damping characteristics resulting from a combination of all the types. In many cases, however, the damping is small and certain simplifying assumptions can be made.

3.3.1. Viscous Damping

The equations of motion of the two degree of freedom system with damping, shown in Fig.9, are given by eq. (29)

$$\text{i.e. } \begin{bmatrix} m_1 & 0 \\ 0 & m_2 \end{bmatrix} \begin{Bmatrix} \ddot{x}_1 \\ \ddot{x}_2 \end{Bmatrix} + \begin{bmatrix} c_1 + c_2 & -c_2 \\ -c_2 & c_2 + c_3 \end{bmatrix} \begin{Bmatrix} \dot{x}_1 \\ \dot{x}_2 \end{Bmatrix} + \begin{bmatrix} k_1 + k_2 & -k_2 \\ -k_2 & k_2 + k_3 \end{bmatrix} \begin{Bmatrix} x_1 \\ x_2 \end{Bmatrix} = \begin{Bmatrix} F_1 \\ F_2 \end{Bmatrix} \quad (73)$$

In short form they can be written as

$$[m]\{\ddot{x}\} + [c]\{\dot{x}\} + [k]\{x\} = \{F\} \quad (74)$$

Two assumptions are taken for granted before attempting solution of these equations. Firstly, that the **type** of damping is viscous, and secondly that the **distribution** of damping is **proportional**. By proportional damping it is implied that the damping matrix [c] is proportional to the stiffness matrix or the mass matrix – or to some linear combination of these two matrices. Mathematically it means that

$$\begin{aligned} &\text{either} && [c] = \alpha [m] \\ &\text{or} && [c] = \beta [k] \\ &\text{or} && [c] = \alpha [m] + \beta [k] \end{aligned} \quad (75)$$

where α and β are constants.

Because of the assumption of proportional damping, the coordinate transformation (using the modal matrix for the free undamped case) which diagonalizes the mass and stiffness matrices, will also diagonalize the damping matrix. Thus the coupled equations of motion for a proportionally damped system can also be uncoupled to single degree of freedom systems as shown in the following.

Substituting the coordinate transformation of eq. (56) into eq. (74) we obtain

$$[m][\phi]\{\ddot{\eta}\} + [c][\phi]\{\dot{\eta}\} + [k][\phi]\{\eta\} = \{F\} \quad (76)$$

Pre-multiplying eq. (76) by the transpose of the modal matrix i.e. $[\phi]^T$ we obtain

$$[\phi]^T[m][\phi]\{\ddot{\eta}\} + [\phi]^T[c][\phi]\{\dot{\eta}\} + [\phi]^T[k][\phi]\{\eta\} = [\phi]^T\{F\} \quad (77)$$

It was shown before, (see eq. 61 and 62), that because of the orthogonal properties of the mode shapes the mass and stiffness matrices are diagonalized, i.e.

$$[\phi]^T[m][\phi] = [M]$$

and

$$[\phi]^T[k][\phi] = [K]$$

Because of proportional damping i.e.

$$[c] = \alpha [m] + \beta [k]$$

we have

$$\begin{aligned} [\phi]^T[c][\phi] &= [\phi]^T \left[\alpha [m] + \beta [k]\right] [\phi] \\ &= \alpha [\phi]^T[m][\phi] + \beta [\phi]^T[k][\phi] \end{aligned}$$

i.e.

$$[\phi]^T[c][\phi] = \alpha [M] + \beta [K] = [C]$$

where $[C]$ is a diagonal matrix.

Thus substitution into eq. (77) gives

$$[M]\{\ddot{\eta}\} + [C]\{\dot{\eta}\} + [K]\{\eta\} = [\phi]^T\{F\} \tag{78}$$

Eq. (78) represents an uncoupled set of equations for **damped** single degree of freedom systems. The i-th equation is

$$M_i\ddot{\eta}_i + C_i\dot{\eta}_i + K_i\eta_i = \{\phi_i\}^T\{F\} = F_i \tag{79}$$

which represents the equation of motion of a system shown in Fig.14.

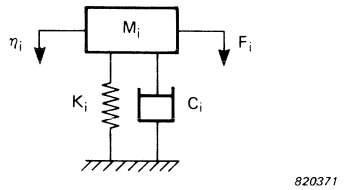

Fig.14. Single degree of freedom system defined by eq. (79)

Since $K_i = \omega_i^2 M_i$, see eq. (51), eq. (79) can be written as

$$\ddot{\eta}_i + 2\zeta_i\omega_i\dot{\eta}_i + \omega_i^2\eta_i = \frac{\{\phi_i\}^T\{F\}}{M_i} = \frac{F_i}{M_i} \tag{80}$$

where

$$\zeta_i = \frac{C_i}{2\sqrt{K_i M_i}} \tag{81}$$

The solution of a damped single degree of freedom system, as described by eq. (80) has been discussed previously. Once the solution of eq. (80) is obtained for all ηs, the solution in terms of the original coordinates x can be deduced by transforming back, i.e. substituting for ηs in eq. (56).

It should be noted that if the damping matrix is proportional to the stiffness matrix i.e. [c] α [k] then from eq. (80) we see that

$$\zeta_i \propto \frac{K_i}{\sqrt{K_i M_i}} \propto \omega_i$$

which means that the higher frequency modes will have higher damping ratios.

3.3.2. Hysteretic Damping

Hysteretic or structural damping was discussed under single degree of freedom systems. It was shown, that in this case the damping force is proportional to the elastic force, but as energy is dissipated, the force is in phase with the velocity. Thus for simple harmonic motion the damping force is given by $j\gamma kx$, see eq. (19). For a multi-degree of freedom system, the equations of motion with hysteretic damping can be written as

$$[m]\{\ddot{x}\} + j\gamma[k]\{x\} + [k]\{x\} = \{F\} \tag{82}$$

Changing to Principal Coordinates as shown in the section above leads to

$$[M]\{\ddot{\eta}\} + (1 + j\gamma)[K]\{\eta\} = [\phi]^T\{F\} \tag{83}$$

Thus each equation is of the form

$$M_i\ddot{\eta}_i + (1 + j\gamma)K_i\eta_i = \{\phi_i\}^T\{F\}$$

i.e.

$$\ddot{\eta}_i + (1 + j\gamma)\omega_i^2\eta_i = \frac{\{\phi_i\}^T\{F\}}{M_i} \tag{84}$$

If

$$\{F\} = \{\overline{F}\}e^{j\omega t}$$

then

$$\{\eta\} = \{\overline{\eta}\}e^{j\omega t}$$

Substituting in eq. (84) we obtain

$$-\omega_i^2\overline{\eta}_i + (1 + j\gamma)\omega_i^2\overline{\eta}_i = \frac{\{\phi_i\}^T\{\overline{F}\}}{M_i} = \frac{\overline{F}_i}{M_i} \tag{85}$$

the solution of which has been discussed previously.

3.4. FORCED DAMPED VIBRATION – NON PROPORTIONAL DAMPING

3.4.1. State-Space Method

When the damping matrix is not proportional to the mass or the stiffness matrix, neither the modal matrix nor the weighted modal matrix will diagonalize the damping matrix. In this general case of damping, the coupled equations of motion have to be solved simultaneously, or they need to be uncoupled using the **state-space method** which is briefly introduced here.

Basically, by this method the set of n second order differential equations are converted to an equivalent set of 2n first order differential equations, by assigning new variables (referred to as **state variables**) to each of the original variables and their derivatives. To illustrate the procedure, the equations of motion for the two degree of freedom system shown in Fig.9 are written as

$$\begin{bmatrix} m_1 & 0 \\ 0 & m_2 \end{bmatrix}\begin{Bmatrix} \dot{x}_1 \\ \dot{x}_2 \end{Bmatrix} - \begin{bmatrix} m_1 & 0 \\ 0 & m_2 \end{bmatrix}\begin{Bmatrix} \dot{x}_1 \\ \dot{x}_2 \end{Bmatrix} = \begin{Bmatrix} 0 \\ 0 \end{Bmatrix}$$

$$\begin{bmatrix} m_1 & 0 \\ 0 & m_2 \end{bmatrix}\begin{Bmatrix} \ddot{x}_1 \\ \ddot{x}_2 \end{Bmatrix} + \begin{bmatrix} c_1 + c_2 & -c_2 \\ -c_2 & c_1 + c_2 \end{bmatrix}\begin{Bmatrix} \dot{x}_1 \\ \dot{x}_2 \end{Bmatrix} + \begin{bmatrix} k_1 + k_2 & -k_2 \\ -k_2 & k_1 + k_2 \end{bmatrix}\begin{Bmatrix} x_1 \\ x_2 \end{Bmatrix} = \begin{Bmatrix} F_1 \\ F_2 \end{Bmatrix} \tag{86}$$

or in partitioned matrix form as

$$\begin{bmatrix} \begin{bmatrix} 0 & 0 \\ 0 & 0 \end{bmatrix} & \begin{bmatrix} m_1 & 0 \\ 0 & m_2 \end{bmatrix} \\ \begin{bmatrix} m_1 & 0 \\ 0 & m_2 \end{bmatrix} & \begin{bmatrix} c_1 + c_2 & -c_2 \\ -c_2 & c_1 + c_2 \end{bmatrix} \end{bmatrix}\begin{Bmatrix} \ddot{x}_1 \\ \ddot{x}_2 \\ \dot{x}_1 \\ \dot{x}_2 \end{Bmatrix} + \begin{bmatrix} -\begin{bmatrix} m_1 & 0 \\ 0 & m_2 \end{bmatrix} & \begin{bmatrix} 0 & 0 \\ 0 & 0 \end{bmatrix} \\ \begin{bmatrix} 0 & 0 \\ 0 & 0 \end{bmatrix} & \begin{bmatrix} k_1 + k_2 & -k_2 \\ -k_2 & k_1 + k_2 \end{bmatrix} \end{bmatrix}\begin{Bmatrix} \dot{x}_1 \\ \dot{x}_2 \\ x_1 \\ x_2 \end{Bmatrix} = \begin{Bmatrix} \begin{Bmatrix} 0 \\ 0 \end{Bmatrix} \\ \begin{Bmatrix} F_1 \\ F_2 \end{Bmatrix} \end{Bmatrix}$$

Substituting

$$x_1 = z_1 \qquad \dot{x}_1 = \dot{z}_1 = z_3 \qquad \ddot{x}_1 = \dot{z}_3$$

$$x_2 = z_2 \qquad \dot{x}_2 = \dot{z}_2 = z_4 \qquad \ddot{x}_2 = \dot{z}_4$$

we get

$$\begin{bmatrix} \begin{bmatrix} 0 & 0 \\ 0 & 0 \end{bmatrix} & \begin{bmatrix} m_1 & 0 \\ 0 & m_2 \end{bmatrix} \\ \begin{bmatrix} m_1 & 0 \\ 0 & m_2 \end{bmatrix} & \begin{bmatrix} c_1+c_2 & -c_2 \\ -c_2 & c_1+c_2 \end{bmatrix} \end{bmatrix} \begin{Bmatrix} \begin{Bmatrix} \dot{z}_3 \\ \dot{z}_4 \end{Bmatrix} \\ \begin{Bmatrix} \dot{z}_1 \\ \dot{z}_2 \end{Bmatrix} \end{Bmatrix} + \begin{bmatrix} -\begin{bmatrix} m_1 & 0 \\ 0 & m_2 \end{bmatrix} & \begin{bmatrix} 0 & 0 \\ 0 & 0 \end{bmatrix} \\ \begin{bmatrix} 0 & 0 \\ 0 & 0 \end{bmatrix} & \begin{bmatrix} k_1+k_2 & -k_2 \\ -k_2 & k_1+k_2 \end{bmatrix} \end{bmatrix} \begin{Bmatrix} \begin{Bmatrix} z_3 \\ z_4 \end{Bmatrix} \\ \begin{Bmatrix} z_1 \\ z_2 \end{Bmatrix} \end{Bmatrix} = \begin{Bmatrix} \begin{Bmatrix} 0 \\ 0 \end{Bmatrix} \\ \begin{Bmatrix} F_1 \\ F_2 \end{Bmatrix} \end{Bmatrix} \tag{87}$$

which can be abbreviated to

$$[A]\{\dot{z}\} + [B]\{z\} = \{Q\} \tag{88}$$

where $[A] = \begin{bmatrix} [0] & [m] \\ [m] & [c] \end{bmatrix}$ $[B] = \begin{bmatrix} [m] & [0] \\ [0] & [k] \end{bmatrix}$ and $\{Q\} = \begin{Bmatrix} \{0\} \\ \{F\} \end{Bmatrix}$

It can be seen that whilst the second order equations have been reduced to first order equations, the number of equations have been doubled adding to the burden of computation. The solution of the above equations will not be given here, but can be found in Refs. [19, 21, 22].

The solution of above equations for free vibration reveals, that damped natural modes do exist, however, they are not identical to the undamped natural modes. For the undamped modes, various parts of the structure move either in phase or 180° out of phase with each other. For the non-proportionally damped structures, there are phase differences between the various parts of the structure, which result in complex mode shapes. This difference is manifested by the fact, that for undamped natural modes all points on the structure pass through their equilibrium positions simultaneously, which is not the case for the complex modes. Thus the undamped natural modes have well-defined nodal points or lines and appear as a "standing wave", while for complex modes the nodal lines are not stationary.

3.4.2. Forced Normal Modes of Damped Systems (Characteristic Phase-Lag Modes)

For an n degree of freedom system with viscous damping, the equations of motion for steady state sinusoidal excitation can be written in its general form as

$$[m]\{\ddot{x}\} + [c]\{\dot{x}\} + [k]\{x\} = \{F\} \sin \omega t \tag{89}$$

where the system inertia, damping and stiffness matrices [m], [c] and [k] respectively, are assumed to be real symmetric and positive – definite. If the damping is hysteretic the second term would be given by $1/\omega\,[d]\,\{\dot{x}\}$, where [d] is the hysteretic damping matrix. In the general case damping would be non-proportional and thus the damping matrix cannot be diagonalized using the normal mode transformation. For an arbitrary

set of forces $\{F\}$ and excitation frequency ω the solution of eq. (89) is rather complicated. Although the responses at each coordinate x are harmonic with the excitation frequency, they are not all in phase with each other or with the excitation force. If, however, a system with n degrees of freedom is excited by n number of forces which are either 0° or 180° out of phase (often called monophase or coherently phased forces), then for a particular ratio of forces, the response at each of the coordinates will be in phase with each other and lag behind the force by a common angle θ (called the characteristic phase lag).

Thus we have to determine the conditions which will produce a solution of the form

$$\begin{Bmatrix} x_1 \\ x_2 \\ x_3 \\ \vdots \\ x_n \end{Bmatrix} = \begin{Bmatrix} X_1 \\ X_2 \\ X_3 \\ \vdots \\ X_n \end{Bmatrix} \sin(\omega t - \theta) = \{\psi\} \sin(\omega t - \theta) \tag{90}$$

For any given excitation frequency ω, there exist n solutions of the type given by eq. (90), where each of the modes $\{\psi_i\}$ is associated with a definite phase θ_i and a corresponding distribution of forces $\{\Gamma_i\}$ which is required for its excitation. The response under these conditions is called the **"forced normal modes"** of the damped system, since every point of the system moves in phase and passes through its equilibrium position simultaneously with respect to the other points. The existence of these modes appears to have been first pointed out by Fraeijs de Veubeke in what is termed as the "Characteristic Phase-Lag Theory" [23]. The theory has been expounded by other authors, namely Bishop and Gladwell [8] but can also be found in Refs. [9, 10, 21, 24].

Substituting eq. (90) in eq. (89) gives

$$\sin(\omega t - \theta)\left[[k] - \omega^2 [m]\right]\{\psi\} + \omega \cos(\omega t - \theta)[c]\{\psi\} = \{F\} \sin \omega t \tag{91}$$

Expanding the sin $(\omega t - \theta)$ and the cos $(\omega t - \theta)$ terms and separating the sin ωt and cos ωt terms we obtain

$$\cos\theta \left[[k] - \omega^2 [m]\right]\{\psi\} + \omega \sin\theta [c]\{\psi\} = \{F\} \tag{92}$$

$$\sin\theta \left[[k] - \omega^2 [m]\right]\{\psi\} - \omega \cos\theta [c]\{\psi\} = \{0\} \tag{93}$$

These equations contain three unknowns $\{F\}$, $\{\psi\}$ and θ since ω is given. If $\cos\theta \neq 0$, eq. (93) may be divided by $\cos\theta$ to give

$$\left[\tan\theta \left[[k] - \omega^2 [m]\right] - \omega [c]\right]\{\psi\} = \{0\} \tag{94}$$

Eq. (94) has a non-trivial solution if the determinant

$$\left|\tan\theta \left[[k] - \omega^2 [m]\right] - \omega [c]\right| = 0 \tag{95}$$

It is evident, that for a given ω there are n values of $\tan\theta_i$ (i = 1,2---n) corresponding to the n eigenvalues, and for each $\tan\theta_i$ there is a corresponding eigenvector $\{\psi_i\}$ satisfying the equation

$$\left[\tan\theta_i \left[[k] - \omega^2 [m]\right] - \omega [c]\right]\{\psi_i\} = \{0\} \tag{96}$$

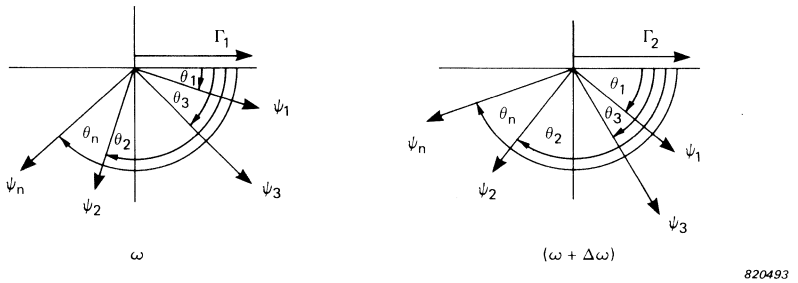

Fig.15. Eigenvectors relative to the force vector for each ω. At each θ the displacements at all points are in phase

Fig.15 illustrates the eigenvectors relative to the force vector for each frequency.

If eq. (96) is premultiplied by the transpose $\{\psi_i\}^T$ and rearranged, we obtain

$$\tan\theta_i = \frac{\omega \{\psi_i\}^T [c] \{\psi_i\}}{\{\psi_i\}^T [[k] - \omega^2 [m]] \{\psi_i\}} \tag{97}$$

From eq. (97) it can be seen that each of the roots $\tan\theta_i$ is a continuous function of ω. For low values of ω, $\tan\theta_i$ is small i.e. θ_i is a small angle. As ω increases and approaches ω_1 the undamped natural frequency, one of the roots θ_i (which can be named θ_1) approaches the value $\pi/2$. As ω is increased above ω_1 the denominator of eq. (97) gets negative and $\theta_1(\omega)$ gets larger than $\pi/2$. When ω tends to ∞, $\theta_1(\omega)$ tends to π. In a similar manner the remaining roots θ_i (i = 2, 3, --- n) can be plotted as a function of frequency ω, where θ_i (i = 2, 3 --- n) is equal to $\pi/2$ at the ith undamped natural frequency ω_i. Thus θ_k is that root which has the value $\pi/2$ at the undamped natural frequency $\omega = \omega_k$. (The numerical example given at the end of the section will make this point clearer. See also Fig.17).

Having examined the variation of eigenvalues ($\tan\theta_i$) as a function of frequency, the mode shapes can now be investigated. It can be seen from eqs. (95) and (96) that at any one frequency the mode shapes depend only on the shape of the damping matrix and not on its intensity. If every element in the matrix [c] is multiplied by a constant factor, then eq. (95) shows that the roots $\tan\theta_i$ will all be increased by the same ratio. Thus eq. (96) which determines the mode shapes, will be multiplied throughout by the same factor and the mode shape $\{\psi_i\}$ will be unchanged.

Eq. (96) can be re-written as

$$\left[[k] - \omega^2 [m] - \frac{\omega [c]}{\tan\theta_i}\right] \{\psi_i\} = \{0\} \tag{98}$$

When ω is equal to one of the undamped natural frequencies, say $\omega = \omega_1$, then one of the roots θ_1 is 90° as shown above. Thus eq. (98) which determines the mode shape for this root becomes

$$[[k] - \omega_1^2 [m]] \{\psi_1\} = \{0\} \tag{99}$$

It can thus be seen, that when the frequency is equal to one of the undamped natural frequencies, the mode shape for one of the roots (which is equal to $\pi/2$) is identical to the Principal or Normal mode shape (see eq.31).

Attention can now be paid to the force ratio that is required to excite any one mode $\{\psi_i\}$ for the corresponding root $\tan \theta_i$ at any one frequency. The force ratio required can be calculated from eq. (92) namely

$$\cos \theta_i \left[[k] - \omega^2 [m]\right] \{\psi_i\} + \omega \sin \theta_i [c] \{\psi_i\} = \{\Gamma_i\} \tag{100}$$

In the special case when $\omega = \omega_1$ one of the undamped natural frequencies, one of the roots $\theta_i = \theta_1 = 90°$ and eq. (100) reduces to

$$\omega_1 [c] \{\psi_1\} = \{\Gamma_1\} \tag{101}$$

To illustrate the concepts discussed above consider the same numerical example of the two degree of freedom system of Fig.9, but with the values of damping added as shown in Fig.16.

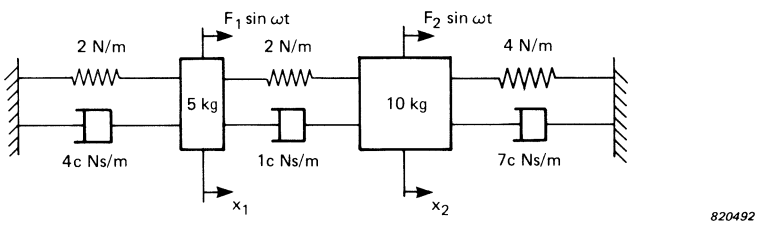

Fig.16. Two degree of freedom system with non-proportional damping

Thus the equations of motion according to eq. (29) become

$$\begin{bmatrix} 5 & 0 \\ 0 & 10 \end{bmatrix} \begin{Bmatrix} \ddot{x}_1 \\ \ddot{x}_2 \end{Bmatrix} + \begin{bmatrix} 5c & -1c \\ -1c & 8c \end{bmatrix} \begin{Bmatrix} \dot{x}_1 \\ \dot{x}_2 \end{Bmatrix} + \begin{bmatrix} 4 & -2 \\ -2 & 6 \end{bmatrix} \begin{Bmatrix} x_1 \\ x_2 \end{Bmatrix} = \begin{Bmatrix} F_1 \\ F_2 \end{Bmatrix} \sin \omega t$$

For a non-trivial solution the determinant of eq. (95) must be equal to zero, i.e.

$$\left| \tan \theta \begin{bmatrix} 4 & -2 \\ -2 & 6 \end{bmatrix} - \omega^2 \begin{bmatrix} 5 & 0 \\ 0 & 10 \end{bmatrix} - \omega c \begin{bmatrix} 5 & -1 \\ -1 & 8 \end{bmatrix} \right| = 0$$

i.e.
$$\begin{vmatrix} \tan \theta \ (4 - 5\omega^2) - 5\omega c & \tan \theta \ (-2) + \omega c \\ \tan \theta \ (-2) + \omega c & \tan \theta \ (6 - 10\omega^2) - 8\omega c \end{vmatrix} = 0$$

i.e. $\{\tan \theta \ (4 - 5\omega^2) - 5\omega c\} \{\tan \theta \ (6 - 10\omega^2) - 8\omega c\} - \{\tan \theta \ (-2) + \omega c\}^2 = 0$

which reduces to

$$(20 - 70\omega^2 + 50\omega^4) \tan^2 \theta - 2 (29 - 45\omega^2) \omega c \tan \theta + 39 \omega^2 c^2 = 0 \tag{102}$$

The undamped natural frequencies of the system are given by letting c = 0, i.e. by the equation

$$(20 - 70\omega^2 + 50\omega^4) = 0$$

They are found to be $\omega_1 = \sqrt{2/5} = 0{,}63$ rad/s and $\omega_2 = 1$ rad/s, which obviously should be the same as those calculated under **section 3.1. Free Vibration.**

Dividing eq. (102) by $\tan^2\theta$ and substituting $\sigma = \dfrac{\omega c}{\tan\theta}$ we get

$$39\sigma^2 - 2(29 - 45\omega^2)\sigma + (20 - 70\omega^2 + 50\omega^4) = 0$$

The roots of this equation are given by

$$\sigma = \frac{\omega c}{\tan\theta} = \frac{(29 - 45\omega^2) \pm \sqrt{(29 - 45\omega^2)^2 - 39\,(20 - 70\omega^2 + 50\omega^4)}}{39} \qquad (103)$$

When ω is equal to one of the undamped natural frequencies ω_1 or ω_2 the equation reduces to

$$\sigma = \frac{\omega c}{\tan\theta} = \frac{(29 - 45\omega^2) \pm (29 - 45\omega^2)}{39}$$

Thus when $\omega = \omega_1$ we get

$$\sigma = \frac{\omega_1 c}{\tan\theta} = \frac{(29 - 45{\omega_1}^2) \pm (29 - 45{\omega_1}^2)}{39}$$

so that $\theta_1 = 90°$ for the negative sign and

$$\theta_2 = \tan^{-1}\left(\frac{39\omega_1 c}{2(29 - 45{\omega_1}^2)}\right) \quad \text{for the positive sign.}$$

Similarly when $\omega = \omega_2$ we get

$$\sigma = \frac{\omega_2 c}{\tan\theta} = \frac{(29 - 45\,{\omega_2}^2) \pm (29 - 45\,{\omega_2}^2)}{39}$$

so that $\theta_2 = 90°$ for the negative sign and

$$\theta_1 = \tan^{-1}\left(\frac{39\,\omega_2 c}{2(29 - 45\,{\omega_2}^2)}\right) \quad \text{for the positive sign.}$$

The variation of θ_1 and θ_2 can be plotted as a function of frequency using eq. (103). The curves are shown in Fig.17 for three values of damping c, corresponding roughly to **light, medium** and **heavy** damping. The shape of the curves are seen to be similar to those of Fig.3b.

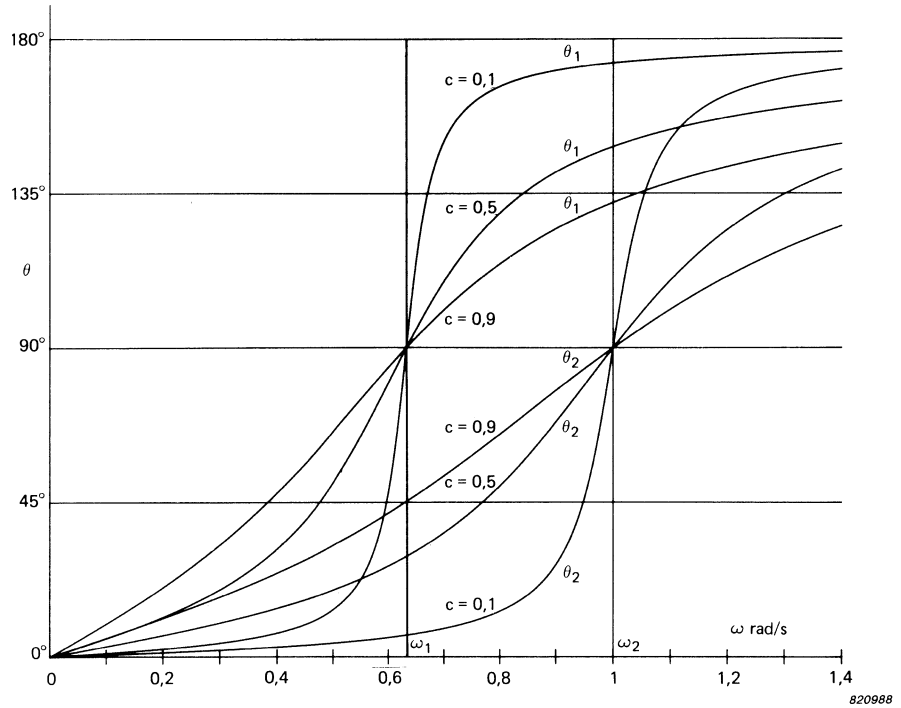

Fig.17. Variation of the roots θ_1 and θ_2 as a function of frequency for three values of damping

The mode shapes are obtained by substituting numerical values for the matrices [m], [c] and [k] in eq. (96), i.e.

$$\left[\tan\theta_i \left[\begin{bmatrix}4 & -2\\ -2 & 6\end{bmatrix} - \omega^2\begin{bmatrix}5 & 0\\ 0 & 10\end{bmatrix}\right] - \omega c\begin{bmatrix}5 & -1\\ -1 & 8\end{bmatrix}\right]\left\{\begin{matrix}u_1\\ u_2\end{matrix}\right\}_i = \left\{\begin{matrix}0\\ 0\end{matrix}\right\}$$

i.e.
$$\begin{bmatrix}\tan\theta_i\,(4-5\,\omega^2) - 5\,\omega c & \tan\theta_i\,(-2) + \omega c\\ \tan\theta_i\,(-2) + \omega c & \tan\theta_i\,(6-10\,\omega^2) - 8\,\omega c\end{bmatrix}\left\{\begin{matrix}u_1\\ u_2\end{matrix}\right\}_i = \left\{\begin{matrix}0\\ 0\end{matrix}\right\} \quad (i = 1,2)$$

Expanding the first equation we get

$$\{\tan\theta_i\,(4-5\,\omega^2) - 5\,\omega c\}\,u_1 + \{\tan\theta_i\,(-2) + \omega c\}\,u_2 = 0$$

Thus $$\left\{\frac{u_1}{u_2}\right\}_i = \frac{2\tan\theta_i - \omega c}{\tan\theta_i\,(4-5\,\omega^2) - 5\,\omega c} = \frac{2 - \omega c/\tan\theta_i}{(4-5\,\omega^2) - 5\,\omega c/\tan\theta_i}$$

Substituting for $\omega c/\tan\theta$ from eq. (103) we obtain

$$\left\{\frac{u_1}{u_2}\right\}_i = \frac{49 + 45\,\omega^2 \pm \sqrt{61 + 120\,\omega^2 + 75\,\omega^4}}{11 + 30\,\omega^2 \pm 5\sqrt{61 + 120\,\omega^2 + 75\,\omega^4}} \qquad (104)$$

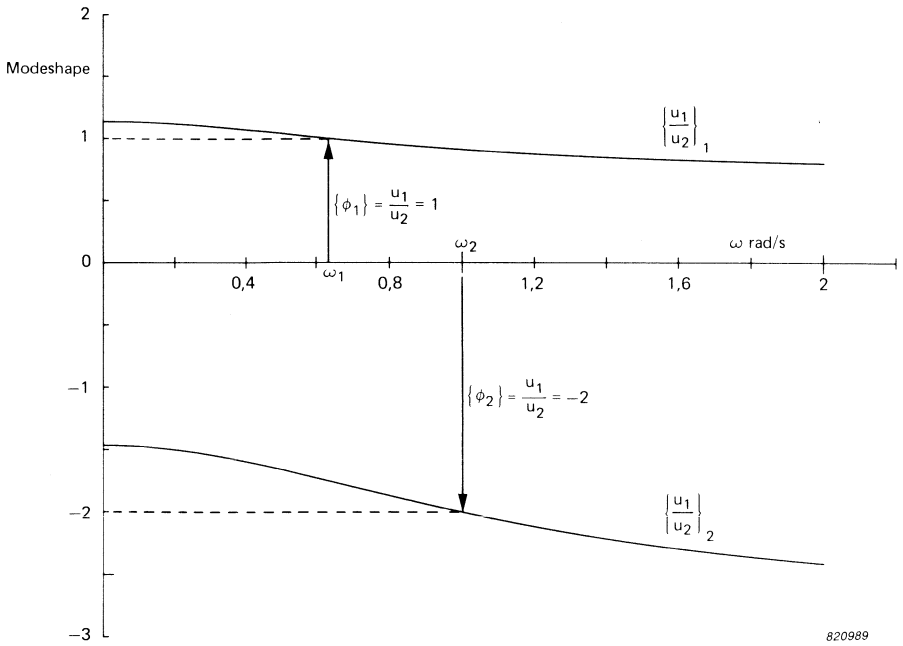

Fig.18. The characteristic phase lag modes as a function of frequency

The characteristic phase lag modes are plotted as a function of frequency using eq. (104) in Fig.18. The positive sign now corresponds to i = 1 for the first mode and the negative sign corresponds to i = 2 for the second mode. Note, in the special case when ω is equal to the first undamped natural frequency $\omega_1 = \sqrt{2/5}$ for i = 1 we obtain

$$\left\{\psi_1\right\}_{\omega_1} = \left\{\frac{u_1}{u_2}\right\}_1 = \frac{49 + 18 + 11}{11 + 12 + 55} = 1$$

which is the same as the first Principal Mode Shape $\{\phi_1\}$ (see **section 3.1.1.**).

At $\omega = \omega_1 = \sqrt{2/5}$ for i = 2 we obtain

$$\left\{\psi_2\right\}_{\omega_1} = \left\{\frac{u_1}{u_2}\right\}_2 = \frac{49 + 18 - 11}{11 + 12 - 55} = \frac{-56}{32}$$

Similarly, when ω is equal to the second undamped natural frequency $\omega_2 = 1$ for i = 1 we obtain

$$\left\{\psi_1\right\}_{\omega_2} = \left\{\frac{u_1}{u_2}\right\}_1 = \frac{49 + 45 + 16}{11 + 30 + 80} = \frac{110}{121}$$

At $\omega = \omega_2 = 1$ for i = 2 we obtain

$$\left\{\psi_2\right\}_{\omega_2} = \left\{\frac{u_1}{u_2}\right\}_2 = \frac{49 + 45 - 16}{11 + 30 - 80} = \frac{-2}{1}$$

which is the same as the second Principal Mode Shape $\{\phi_2\}$.

The force ratio required to excite any one mode $\{\psi_i\}$ for the corresponding root $\tan\theta_i$ at any one frequency can be calculated from eq. (100), i.e.

$$\cos\theta_i \left[\begin{bmatrix}4 & -2\\ -2 & 6\end{bmatrix} - \omega^2\begin{bmatrix}5 & 0\\ 0 & 10\end{bmatrix}\right]\begin{Bmatrix}u_1\\ u_2\end{Bmatrix}_i + \omega c \sin\theta_i \begin{bmatrix}5 & -1\\ -1 & 8\end{bmatrix}\begin{Bmatrix}u_1\\ u_2\end{Bmatrix}_i = \begin{Bmatrix}F_1\\ F_2\end{Bmatrix} \quad (105)$$

The force ratio for each root can be plotted as a function of frequency by substituting the value of θ for each ω and the corresponding mode shape. Fig.19 shows the force ratios required as a function of frequency for the two θs.

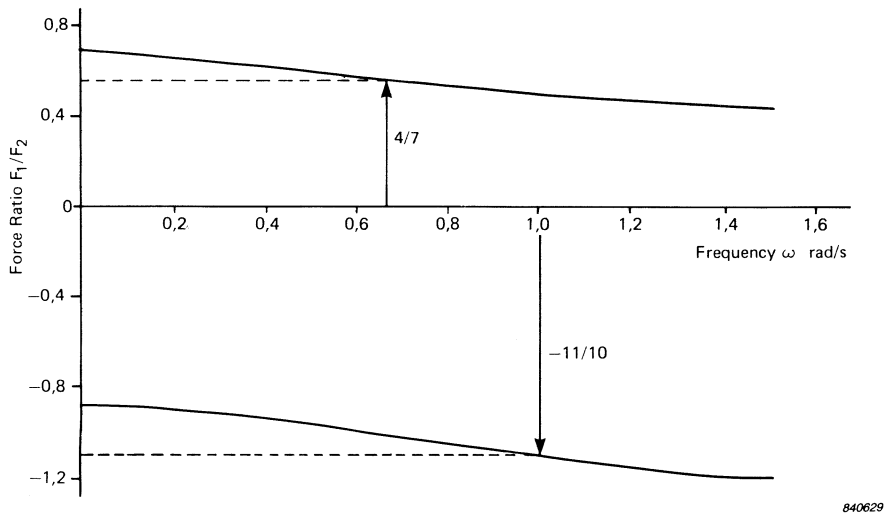

Fig.19. Force ratios required to excite the two modes as a function of frequency

It is, however, interesting to calculate the force ratios at the undamped natural frequencies. As shown previously, at any one undamped natural frequency, one of the roots $\tan\theta_i = \infty$, i.e. one of the $\theta_i = 90°$, and for that root the mode shape obtained is the Principal Mode Shape.

Thus eq. (105) reduces to (see eq. 101)

$$\omega c \begin{bmatrix}5 & -1\\ -1 & 8\end{bmatrix}\begin{Bmatrix}u_1\\ u_2\end{Bmatrix} = \begin{Bmatrix}F_1\\ F_2\end{Bmatrix}$$

which gives the force ratio required to excite the Principal Mode shape at the corresponding undamped natural frequency.

Substituting the first undamped natural frequency $\omega_1 = \sqrt{2/5}$ and $u_1/u_2 = 1$ we obtain

$$\sqrt{2/5}\, c \begin{bmatrix}5 & -1\\ -1 & 8\end{bmatrix}\begin{Bmatrix}1\\ 1\end{Bmatrix} = \begin{Bmatrix}F_1\\ F_2\end{Bmatrix}$$

i.e.

$$\sqrt{2/5}\ c\ 4 = F_1$$

$$\sqrt{2/5}\ c\ 7 = F_2$$

i.e.

$$F_1/F_2 = 4/7 = \{\Gamma_1\}$$

Substituting the second undamped natural frequency $\omega_2 = 1$ and $u_1/u_2 = -2/1$ we obtain

$$1\,c \begin{bmatrix} 5 & -1 \\ -1 & 8 \end{bmatrix} \begin{Bmatrix} -2 \\ 1 \end{Bmatrix} = \begin{Bmatrix} F_1 \\ F_2 \end{Bmatrix}$$

i.e

$$c\,(-11) = F_1$$

$$c\,10 = F_2$$

i.e.

$$F_1/F_2 = -11/10 = \{\Gamma_2\}$$

Before concluding this section it is important to recapitulate the following points:

1) For each frequency of excitation there are as many characteristic phase angles as there are number of degrees of freedom, corresponding to certain sets of forces.

2) For each characteristic phase lag there is a corresponding mode shape which varies with frequency. At the undamped natural frequencies one of the mode shapes is identical to the corresponding undamped Principal mode.

3) The mode shapes depend on the shape of the damping matrix and not on the intensity of damping.

4) In each mode the responses at the coordinates are all in phase, but lag behind the excitation force by an angle θ. At the undamped natural frequency, $\theta = 90°$ for one of the modes which is the Principal mode.

5) Orthogonal properties of phase lag modes also exist as shown in the footnote*.

*** Footnote**

The orthogonal properties of the principal modes of vibration were demonstrated previously in **section 3.1.3.**. To derive analogous properties of forced modes. eq. (94) can be written for the i th eigenvalue and eigenvector and premultiplied by the transpose of the j th eigenvector. The procedure is repeated with i and j interchanged giving the following two equations,

$$\tan\theta_i \{\psi_j\}^T [[k] - \omega^2 [m]] \{\psi_i\} - \omega \{\psi_j\}^T [c] \{\psi_i\} = 0 \quad (106)$$

$$\tan\theta_j \{\psi_i\}^T [[k] - \omega^2 [m]] \{\psi_j\} - \omega \{\psi_i\}^T [c] \{\psi_j\} = 0 \quad (107)$$

Since [m], [c] and [k] are symmetric matrices eq. (107) can be transposed to obtain

$$\tan\theta_j \{\psi_j\}^T [[k] - \omega^2 [m]] \{\psi_i\} - \omega \{\psi_j\}^T [c] \{\psi_i\} = 0 \quad (108)$$

Subtracting eq. (108) from eq. (106) we obtain the orthogonal properties as

$$\{\psi_j\}^T [[k] - \omega^2 [m]] \{\psi_i\} = 0 \quad (109)$$

and

$$\{\psi_j\}^T [c] \{\psi_i\} = 0 \quad (110)$$

provided $\tan\theta_i \neq \tan\theta_j$.

Combining eqs. (109) and (110) with eq. (92) we obtain the third relation

$$\{\psi_j\}^T \{F_i\} = 0 = \{\psi_i\}^T \{F_j\} \quad (111)$$

EXPERIMENTAL METHODS

4. INTRODUCTION

The first part of this book deals with the theoretical analysis of free and forced vibration of undamped and damped multi-degree of freedom systems. Such systems are described by [m], [c] and [k] matrices and it was shown how their responses are obtained in terms of the modal parameters. To provide experimental data to validate the theoretical model, the problem facing the experimentalist is the inverse of this; to deduce the matrices from the vibration. However, the [m], [c] and [k] matrices are not directly measurable, and have to be deduced from measurable quantities, such as the natural frequencies, dampings of the system and the mode shapes. Therefore, the first step for the experimentalist, is to treat the continuous structure that he has to test, as one that possesses a finite number of degrees of freedom. The properties of a continuous structure can be simulated to any desired accuracy by a system possessing a finite number of degrees of freedom n, provided n is large enough. Each of these degrees of freedom can then be examined individually. Since each degree of freedom corresponds to a natural frequency and a mode shape, it is interesting to see how they manifest themselves in the frequency and the modal domains.

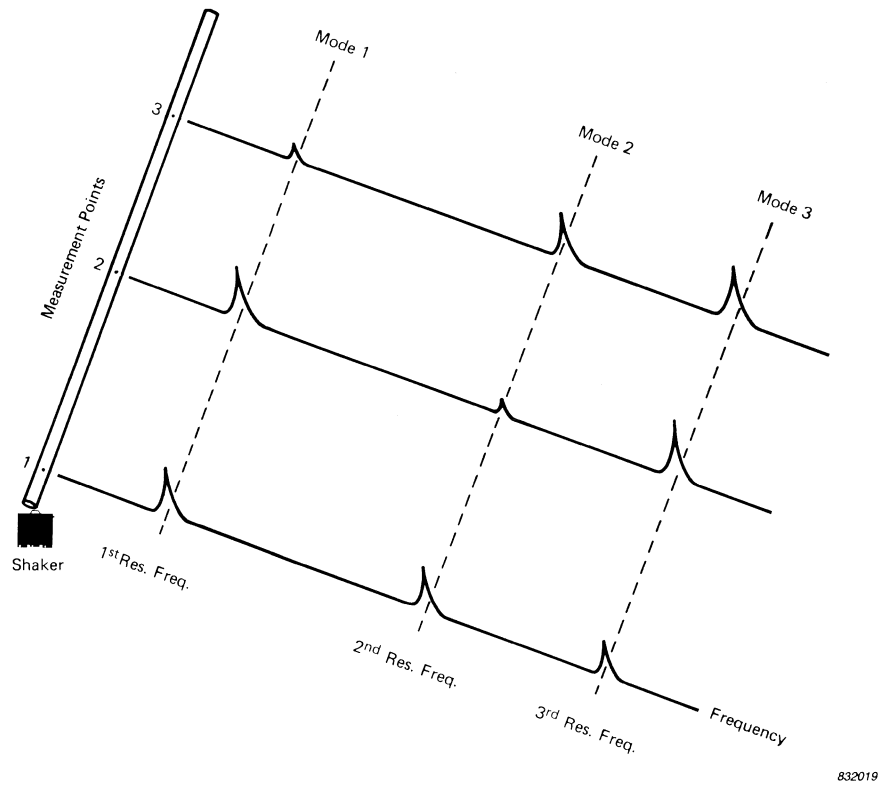

Fig.20 Frequency response of a free-free beam at three measurement points

Consider a simple free-free beam shown in Fig.20, and assume it has only the first three degrees of freedom. To determine the total vibration of the beam, it must be excited at some point and the vibration measured at several points on the beam. If this time domain information is transformed to the frequency domain, the frequency response curves obtained at the three points would be as shown in Fig.20. It can be seen, that the sharp peaks (resonances) occur at the same frequencies, independent of where they are measured on the beam. The only difference we observe, as we move from point to point, is the relative height of the resonances. Although phase information is just as important, it is not taken into account in Fig.20 for clarity of the figures. Whilst the magnitude of the frequency response curves gives the magnitude of the mode shape, the phase gives the direction of the deflection.

In Fig.21 the frequency response curves are obtained at several accelerometer positions on the beam. By connecting the peaks of the resonances of a given mode, and taking the phase into account, the mode shape at each resonance frequency can be traced out. Thus by viewing the figure along the distance axis we obtain a combined frequency response. The figure when viewed along the frequency axis shows the three mode shapes, and is referred to as the **modal domain** view. Just as any real waveform can be expressed as a sum of simple sine waves, any vibration can be represented as a sum of principal modes. The right side of Fig.21 shows the total vibration envelope, as a sum of the three modes.

It can be seen that the same amount of information is available from the three dimensional plot of Fig.21, whether it is viewed in the frequency domain or in the modal domain. In other words there is no loss of information by this change of perspective, similar to the case of transforming data mutually between the frequency and the time domain. To determine the mode shapes, therefore, one can either excite the structure at the resonance frequencies and measure the structural deformation in each vibration mode, or they can be deduced from the frequency responses measured at various points on the structure. Whilst sinusoidal excitation is used for the former method, wide band excitation can be used for the latter. These methods can be further sub-divided into two categories—single shaker techniques, and multiple shaker techniques generally required for the excitation of larger structures. In the following chapters, the various techniques used for obtaining the modal parameters, will be viewed from three aspects:

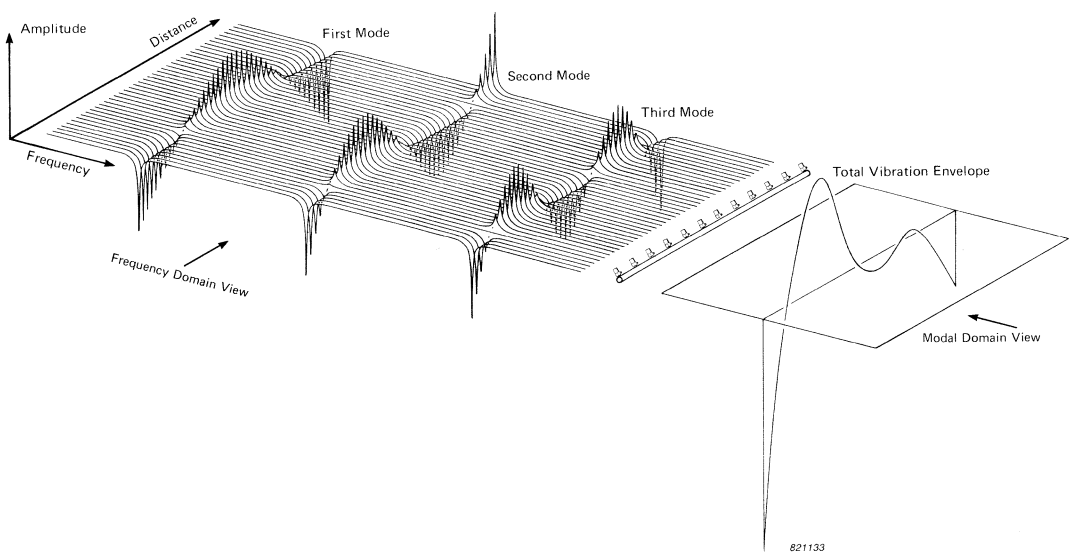

Fig.21. Three dimensional view illustrating the frequency and the modal domain

1) The way in which the structure is excited and the instrumentation required,

2) The data obtained and its presentation, and

3) The analysis of the data

Furthermore, the advantages and disadvantages of the various techniques developed over the course of years will be discussed. Particular emphasis is placed on the limitations of the different methods, to elucidate the reasons for the on-going development of more sophisticated techniques in the continuing search for an ideal modal test. This is briefly touched upon in the following.

The simplest and most commonly used technique is the **"peak amplitude"** method, in which the structure is excited by a sinusoidal force from a single shaker and the **"response curves"** of total amplitude, obtained at several points on the structure, are recorded as a function of frequency. The required information is then extracted from these curves. However, this method has inherent deficiencies, in that not enough is measured, and what is measured is displayed unsatisfactorily. De Vries [28] (1942) and Kennedy and Pancu [1] (1947), having recognized the inadequacies of this method, suggested the use of vector response plots which is widely used today for estimation of damping and the natural frequencies. The mode shapes obtained with this technique, using a single shaker, may not always be acceptable; however, they will, in general, be better than those obtained with the peak amplitude method.

Since the vibratory response of a structure is due to the response in all the principal modes simultaneously, the measured mode shapes are often distorted. This problem is further exacerbated in the case of structures with close natural frequencies where separation of modes becomes mandatory. Stahle [2] has described a "Phase Separation Technique" for isolating the individual modes with simple methods of excitation for lightly damped structures.

With the advent of the two channel real time FFT-analyzers, measurement of response to wide band excitation signals (in contrast to the traditional sinusoidal excitation) has been made possible. In this technique, the frequency response function of a structure can be measured at a single point, due to impulse excitation at various points on the structure, or the structure can be excited at a single point using various forms of wide band random signals, and the frequency response function measured at several points. The modal parameters are then extracted by analytic curve-fitting the measured data in both the time and the frequency domains. Exhaustive amounts of technical literature exist today on methods and algorithms for the extraction of modal parameters. The drastic reduction in experimental time achieved by real time analysis has therefore rightly made this the dominant technique for modal testing of structures since the early 1970's. Furthermore, on account of the price of real time analyzers being affordable, these techniques have emerged in the last decade from research laboratories to become part of the practitioner's repertoire.

Since the accuracy of the modal parameters depends on how precisely the admittance or the frequency response function matrix can be measured, significiant consideration should be given to exciting the structure adequately, in order to maintain the vibration amplitudes as close as possible to the operating levels in all areas of interest. This is relatively easy for simple structures and individual components which can be excited evenly. In the case of large structures, such as aircraft wings, automobiles, train car bodies and other large assemblies with numerous joints, vibration energy is quickly dissipated within the structure, producing widely different vibration amplitudes at various locations. Additionally, non-proportional damping, non-linear effects and closely spaced modes are often encountered in large structures, which not only impede in

locating the frequencies at which to identify the modes, but also the mode shapes based on one exciter position may not agree with those based on another exciter position. To mitigate some of these difficulties, multi-point excitation can be used, by which a larger amount of energy can be fed more uniformly into the structure than with single point excitation. Here again two forms of excitation can be used — sinusoidal and wide band random.

The theoretical requirements for exciting a structure with multiple shakers using sinusoidal excitation was laid down by Fraeijs de Veubeke [23] known as the **Characteristic Phase Lag Theory** which is briefly described in **Section 3.4.2.**

The testing of large structures is carried out in two steps: In the first step the number of modes and their resonant frequencies are roughly established using single shaker sweeps. The presence of modes are indicated by resonant phenomena and phase shifts in the response, and can be difficult to detect when modes have similar shapes and natural frequencies. Once the existence of a mode has been established, the second step involves isolation (tuning) of the mode. This is achieved by distributing the available number of shakers around the structure, guided by experience and heuristic reasoning, and adjusting (appropriating) the amplitudes of the mono-phase* forces on the shakers, such that only the mode of interest is dominantly excited in that particular frequency range. The structure thus responds predominantly in the principal mode as a single degree of freedom system, and the modal parameters can then be easily calculated. The number of shakers used and their judicious distribution around the structure govern the accuracy of the results.

Since the early fifties most full scale modal tests have been based on the approach outlined originally by Lewis and Wrisley [3] (1950). In general his method involves iterative adjustment of the mono-phase forces at the shakers and the excitation frequency, until the velocity response at all points on the structure is coherent (all in phase or 180° out of phase with the force vector). This objective can only be fulfilled if there is strict equilibrium between the applied and damping forces everywhere in the structure. Since the dissipative forces in a real structure are distributed continuously throughout the structure, this objective cannot be fully achieved in practice with a limited number of shakers, and therefore the iterative procedure is stopped when the differences in the phase responses are found to be a minimum [4, 5, 6, 25]. This is a laborious and time consuming process and isolation of modes in regions of high modal density can be difficult. In an effort to alleviate the problem and automate the force appropriation task, Asher [7] (1958) proposed a quantitative method, which detects both natural frequencies and provides the force distributions, using only experimental transfer admittance data as input.

In Asher's method the admittance matrix is measured using single shaker sweeps at various points on the structure. The determinant of the real part of the admittance matrix is now plotted as a function of frequency, and the frequencies at which the determinant vanishes, give excellent approximations to the undamped natural frequencies. The force ratios required to tune a particular principal mode can then be calculated from any one column of the adjoint of the real part of the admittance matrix evaluated at the corresponding undamped natural frequency. A narrow band frequency sweep around the natural frequency with the calculated force ratios is now performed to refine modal parameter estimates.

Unfortunately, Asher was not able to implement his method because of equipment limitations. The lack of sophisticated data acquisition and processing equipment there-

* Mono-phase is used adjectivally with either forces or responses to describe a set whose angles relative to one another are all 0° or 180°.

fore discouraged attempts also throughout the 1960's to apply Asher's method in the laboratory. Nonetheless, his method was considered to be significant enough to be discussed, implemented and elaborated upon with renewed interest as illustrated by Refs.[8-15, 31, 36, 42, 44].

The excitation of structures using dual input random signals to obtain frequency response functions has also been attempted by Allemang et al [38-40]. Application of Asher's modal tuning procedures to frequency response function matrix is equally possible, and in fact has been carried out by Ensminger and Turner [44] (1979), Hallauer et al [10, 31] (1979), and Craig et al [36, 42] (1982). Ensminger and Turner in [44] have developed also another technique, which has been referred to as the "**Minimum coincident response method**" by Craig et al.

These methods are outlined in the following chapters with some illustrations of results obtained by Asher's method on synthesized analytical models. Although the software for the various methods is obviously different, the instrumentation required for implementation of these techniques is more or less the same, and is described briefly in Chapter 6. The essential features in the specifications, necessary for practical feasibility of these techniques are also pointed out. It might be worth mentioning, that apart from equipment limitations, the success or failure of a particular technique may depend on the malignancy of a structure, the cure of which may lie at the hands of an experienced engineer.

5. SINGLE EXCITER TECHNIQUES

5.1. PEAK AMPLITUDE METHOD

A dynamic test basically involves quantitative measure of the effect of a vibratory force on a structure. If the structure is linear and elastic and excited by a sinusoidal force, the resulting vibratory motion (response) is directly proportional to the exciting force and at the same frequency. Measurement of the exciting force and the resulting motion at a number of points over a range of frequencies would be sufficient to describe the vibratory behaviour of the structure. This information can be presented by, for example, plotting the ratio of motion to force as a function of frequency.

The motion can be measured either in terms of displacement, velocity or acceleration and as a result different terms have been used for the ratios of motion to force. Following is the terminology in common use:

$$\frac{\text{acceleration}}{\text{force}} = \text{Inertance (Accelerance according to ANSI 2.31-1979)}$$

$$\frac{\text{velocity}}{\text{force}} = \text{Mobility}$$

$$\frac{\text{displacement}}{\text{force}} = \text{Receptance, Compliance, Admittance}$$

These ratios are further qualified by the term **point**, if the excitation and measurement points coincide, and by the term **transfer,** if they are different, for example, **point inertance** and **transfer inertance.**

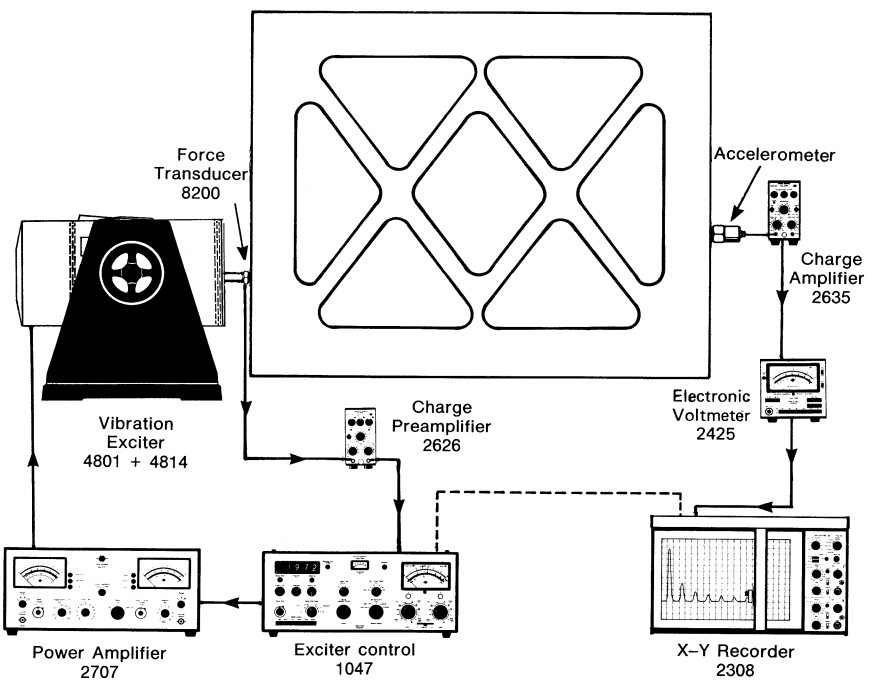

Fig.22. Instrumentation set-up for the peak amplitude method

Fig.22 shows an instrumentation set-up used for obtaining a response curve in which the vibration exciter is fed with a certain amount of power at a slowly changing frequency. Due to resonances in the test specimen and the vibration exciter, the power necessary to subject the test specimen to a constant force level will not, however, remain constant during the test, but will be a function of frequency. To keep the force level constant a servo-loop is used in which the output from the force transducer, mounted between the shaker and the specimen, is fed back to the exciter control via a preamplifier. The output from the accelerometer mounted on the specimen is fed to an X-Y recorder which traces out a response curve as the frequency is scanned. **The response should be measured at enough points on the structure to ensure that all modes will display their resonant characteristics in the response curve of at least one of the points**. This is the most commonly used method of carrying out a resonance test.

Fig.23 shows a typical point inertance curve plotted on linear scales of a free-free beam excited at constant force as shown. The first piece of information that can be extracted from an amplitude response curve is the natural frequencies of the specimen, which are usually identified as the frequencies where peaks are attained – and thus the name **peak-amplitude** method. It has been shown, however, in Ref. [8] that theoretically the peaks do not occur exactly at the natural frequencies but at a frequency displaced slightly on one or the other side of them. This is partly due to the damping which couples the modes (non-proportional damping) and partly due to the contribution from the other off-resonant modes at that frequency (see **Section 5.1.1.**). The latter contribution will still be there, even if the damping does not couple the motion in the principal modes. However, if the system is lightly damped and the natural frequencies are widely spaced, these errors would be relatively small compared to the experimental errors involved in locating the peaks.

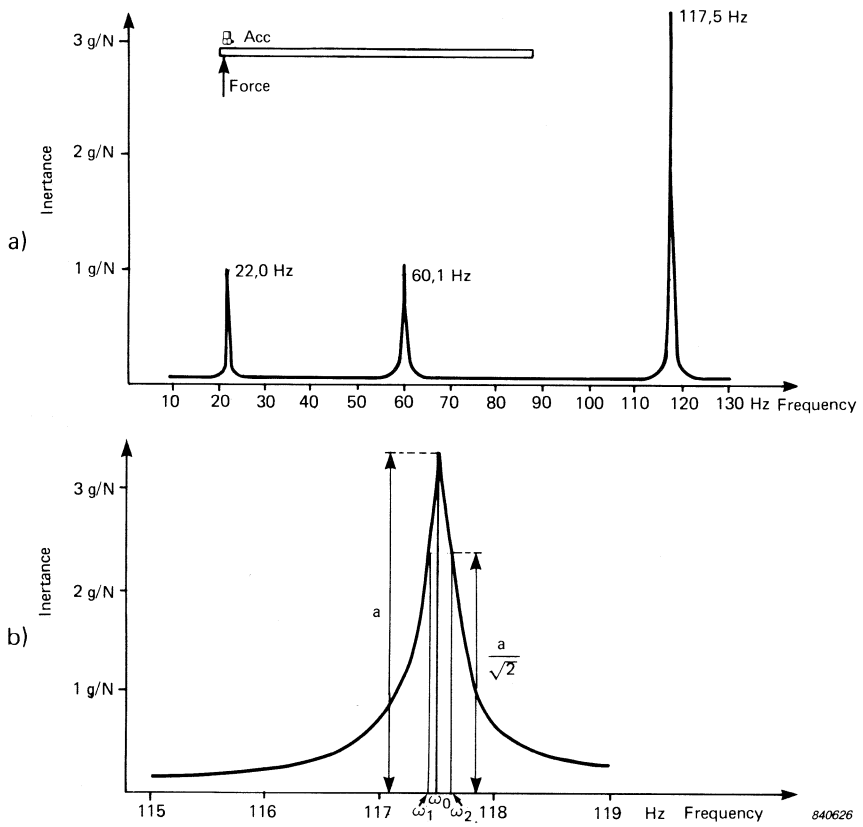

Fig.23.a) Point inertance curve for a free-free beam plotted on linear scales
b) Third resonance plotted on enlarged linear scales

The second piece of information that can be extracted from a response curve is the amount of damping in a particular mode. Damping is determined from the sharpness of the peak (Fig.23 b) and is normally measured in terms of the Loss Factor η given by

$$\eta = \frac{\omega_2 - \omega_1}{\omega_0}$$

where ω_0 is the natural frequency and ω_1 and ω_2 are frequencies on either side of the natural frequency where the peak amplitude is reduced by a factor of $\sqrt{2}$, (see eq. 16). (If the amplitude is plotted on a log scale in dBs, ω_1 and ω_2 are frequencies where the amplitudes are 3 dBs below the peak amplitude).

Other parameters in terms of which damping is quoted are all related to each other and are given by

$$\eta = \frac{2c}{c_c} = \frac{1}{Q} = \frac{\delta}{\pi} = \tan\alpha = \frac{E}{2\pi w} \qquad (112)$$

where $\frac{c}{c_c}$ is the dimensionless damping ratio (see eq. 2)

c_c is the critical damping

Q is the quality factor (see eq. 14)

δ is the logarithmic decrement

$\tan\alpha$ is the loss tangent

E is the energy dissipated per cycle at resonance

and w is the energy stored in the system.

It should be noted, as pointed out in Ref. [8], that in the calculation of the damping by this method it is assumed that each peak represents motion in only one mode, i.e. the contribution from the off-resonant modes is negligible – as assumption very often conveniently forgotten in practice. For resonances that are well separated, however, sufficiently accurate estimates of damping can be achieved, provided $\eta < 0{,}1$.

If the off-resonant vibration is not negligible, but however, constant (as assumed by Kennedy & Pancu [1]), it may appear at first sight that the off-resonant vibration could be extracted from the measured amplitude. Unfortunately, this cannot be done directly, as accelerations are vector quantities and phase angles of the responses have to be taken into consideration. Thus the effect of the off-resonant vibration will be different above and below resonance of the mode under consideration, resulting in a non-symmetrical peak. This is explained further in **Section 5.1.2.**

To determine the mode shape, the structure is excited at a natural frequency, and the ratios of the amplitudes at various points on the structure are determined. Fig.24 shows the mode shape for the third natural frequency. As the acceleration goes through a phase change of 180° as one passes through a node, the relative phase of the accelerations at various points should also be taken into account.

Since the beam has uniform cross-section, the mode shape should ideally be symmetrical; however, the asymmetry of the mode shape is evident. This is because more than one mode is represented in general, at any one frequency, and therefore the mode shape is not a true principal mode. In other words, the phase angle between the force and the acceleration would not be exactly 90° at all points on the beam.

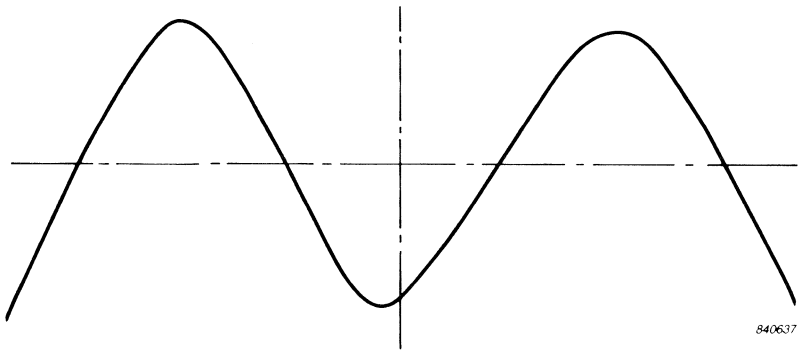

Fig.24. Mode shape for the third natural frequency

While the loss factor is evaluated from a single peak, the mode shape is evaluated from the ratio of a number of peaks. Thus if an error is made in the estimation of a peak due to the contribution from other modes, the inaccuracies in the principal mode shape will be greater than those involved in the determination of the damping.

5.1.1. Contribution from Off-Resonant Modes

It has been shown in the theoretical section that the response of a continuous structure (multiple degree of freedom system) can be represented by the superposition of the responses in its individual modes, considering each mode to respond as a single degree of freedom system. Differences between the resonance characteristics of the response of a single degree of freedom system and those of a multiple degree of freedom system are, however, manifested by the contribution of the off-resonant modes to the mode that is excited. This has been illustrated by Stahle in Ref.[2] whose example will be briefly described in the following.

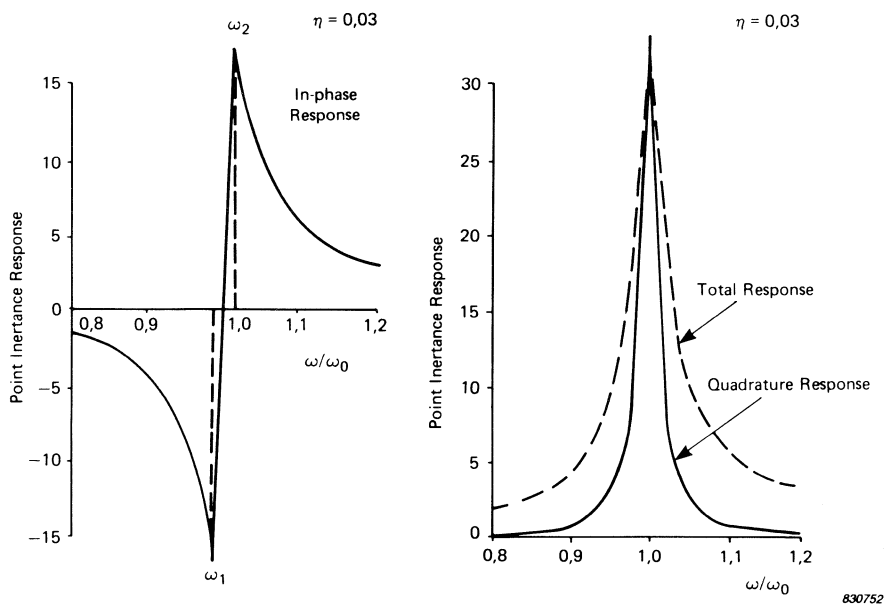

Fig.25.a) Theoretical in-phase point inertance response of a single degree of freedom system

b) Theoretical quadrature and total point inertance response of a single degree of freedom system

The full lines in Fig.25a) and Fig.25b) show the real part (in-phase component) and the imaginary part (quadrature component) of the point inertance response of a single degree of freedom system respectively. The dashed line in Fig.25b) shows the total point inertance response. These responses can be derived from eq.(23). It can be seen that the quadrature response peaks more sharply than the total response, and is equal to the total response at resonance, since the in-phase response is zero. The total response on either side of resonance is relatively large, because the in-phase response varies more slowly than the quadrature response. Whilst the in-phase response is asymptotic to 1/m above resonance, the quadrature response rapidly approaches zero on either side of resonance.

To compare these responses with those of a multiple degree of freedom system, Stahle in Ref.[2] has theoretically calculated the in-phase, quadrature, and the total point inertance response of a free-free beam excited at one end, using the principle of superposition of modes. Fig.26a) and Fig.26b) show these calculated responses as a function of frequency. It can be seen that the amplitudes of the quadrature response away from the resonance frequencies are relatively small, and that the peak values accurately determine the resonant response of the individual modes. For the fourth mode the quadrature response at the resonance frequency is approximately 1/2% greater than the response of the individual mode.

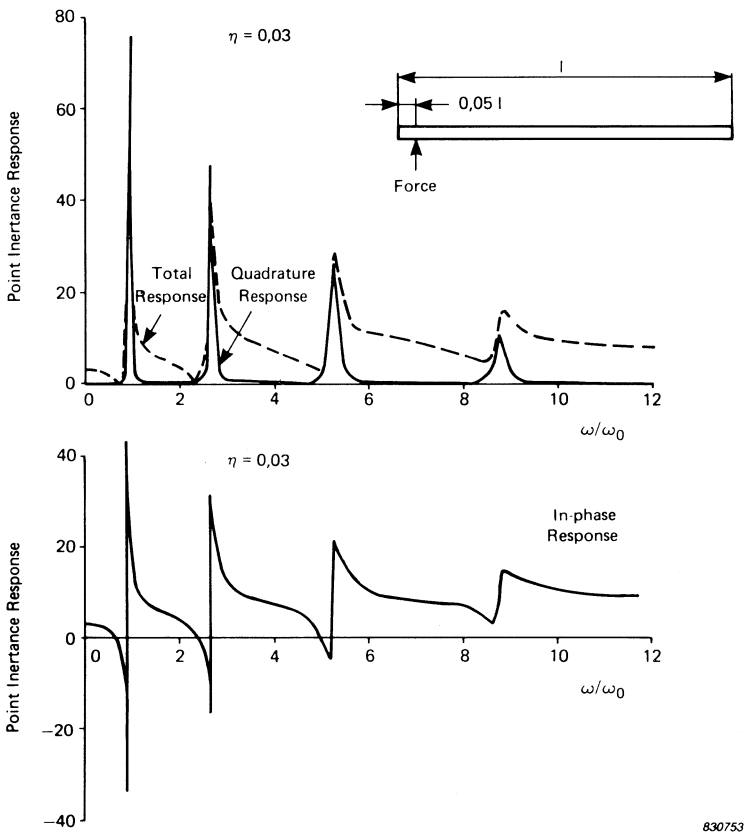

Fig.26.a) Theoretical quadrature and total point inertance response of a free-free beam excited at one end

b) Theoretical in-phase point inertance response of a free-free beam excited at one end

The total response, however, is more susceptible to the effects of the non-resonant modes, which is evidenced by the increasing differences between the peak values of the total response and the corresponding peak values of the quadrature response. This is because the in-phase response starts at a relatively low amplitude, but continually builds up due to the in-phase response in the various elastic modes. The in-phase response is not zero at the resonance frequencies as was the case for the single degree of freedom system. Since the total response is the vector sum of the in-phase and quadrature responses, the total response at resonance is greater than the response of the individual resonant mode. Thus significant distortion of the mode shape will result, if it is determined from the total response, since the in-phase response becomes appreciable for the higher modes.

For the free-free beam, the effects of the non-resonant modes are evident at the resonance of the fourth mode, which is enlarged in Fig.27 for clarity. It can be seen that the amplitude of the total response is larger than that of the quadrature response, and that the peak of the total response occurs above the true resonant frequency. Although the difference in the frequency of the two peaks is small, the relative amount of the non-resonant mode response at the frequency of the peak total response is increased. Since the response of the resonant mode varies rapidly with frequency, the contribution of non-resonant modes to the total response is increased from approximately 25% at the actual resonant frequency to approximately 65% at the apparent resonant frequency indicated by the peak of the total response.

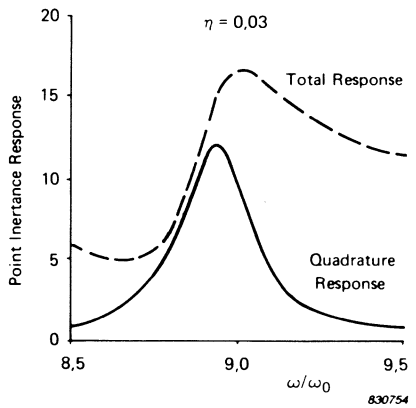

Fig.27. Theoretical quadrature and total point inertance response of the fourth mode of a free-free beam excited at one end

If the mode shape was determined from the quadrature response, adequate mode shape measurement would be obtained, since the error in the amplitude of the fourth mode as determined by the quadrature response is negligible for this simple system. In practical structures, however, resonant modes are often close to each other, causing modal interaction in the quadrature response. It is then necessary to separate the individual modes from the quadrature response for which a method has been outlined by Stahle in Ref.[2]. The problem of "close resonances" is further elucidated in the next section.

5.1.2. Close Resonances

Fig.28 shows two modes that are closely spaced in the frequency domain. Each mode responds to a sinusoidal excitation at any frequency. This response is small unless the excitation frequency is in the immediate vicinity of the mode's resonant frequency. Although the off-resonant contribution is relatively small at the frequency of the mode to be excited, it adds to the distortion of the data and must, therefore be removed.

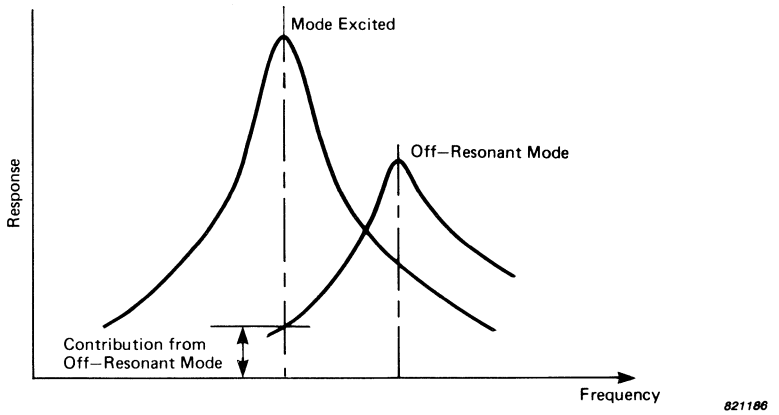

Fig.28. Two closely spaced modes illustrating contribution from the off-resonant mode

Kennedy & Pancu [1] (whose method will be described in the next section) assume that the off-resonant vibration is constant (in amplitude and phase) as the excitation frequency is scanned through the resonance. Therefore, at first sight one might be inclined to extract the off-resonant vibration from the measured amplitude. Unfortunately, this cannot be done legitimately, as accelerations (or displacements) are vector quantities. Therefore phase angles of the measured amplitude and of the off-resonant vibration have to be taken into account, and subtraction carried out vectorially. Although the off-resonant vibration does not go through a marked change in the phase response, the phase angle of the response in the resonant mode changes from a small angle to almost π as it passes through the resonant frequency.

The dashed lines in Figs.29a) and 29b) show the amplitude and phase response of two single closely spaced resonant modes. The full line shows the response when the two individual modes are added together. The way in which the vectorial addition of the two modes is carried out is illustrated in Fig.29c). OB and OC are equal amplitudes on either side of the resonant frequency ω_1 of the first resonant mode (Fig.29a)). The phase angles of these amplitudes relative to the force are –60° and –120° respectively, as seen from Fig.29b). Thus OB and OC are drawn in Fig.29c) at –60° and –120° relative to the force vector which is parallel to the Real Axis. The off-resonant vibration contribution OA from the second mode is assumed constant in amplitude and phase over the frequency range ω_B to ω_C. Thus the amplitude of OA is plotted at an angle of –22° from the Real Axis in Fig.29c) and added vectorially to OB and OC the amplitudes of the resonant mode. The resultant vectors are OD and OE respectively, which are the amplitudes at ω_B and ω_C of the total vibration as shown in Fig.29a).*

* It should be noted that the off-resonant vibration is assumed to be constant in amplitude and phase for simplifying the explanation of the vector diagram of Fig.29c). The full line curve of Fig.29a) in fact takes into account the amplitude and phase variation of the off-resonant vibration.

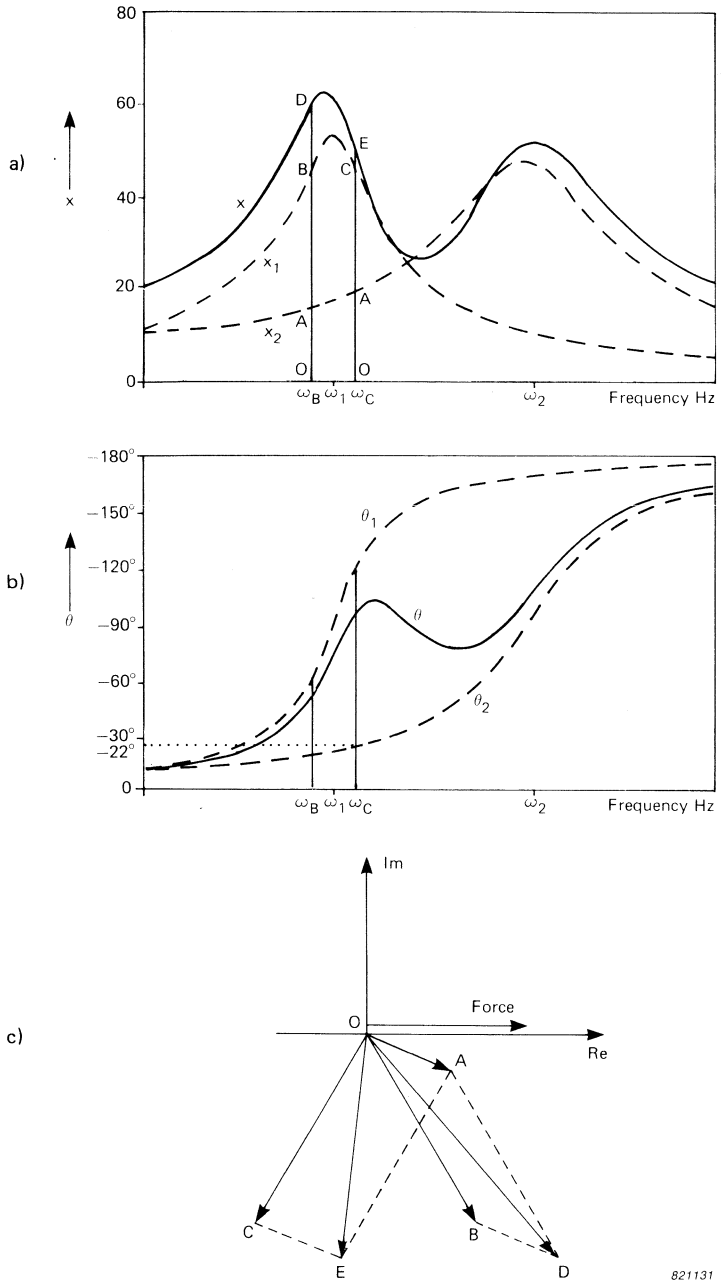

Fig.29. The dashed lines in a) and b) show the amplitude and phase response of two single closely spaced modes respectively. The full lines show the sum of the two modes. c) shows vectorial addition of the off-resonant vibration from the second mode to the first mode at frequencies ω_B and ω_C

It can thus be seen from the figure, that even if the off-resonant vibration is constant (in amplitude and phase), it's contribution to the measured amplitude below and above resonance will not be the same — giving rise to a non-symmetrical peak. Just as the off-resonant vibration of the second mode distorts the first mode, the off-resonant vibration of the first mode distorts the second resonant mode.

Another difficulty that arises in analyzing the amplitude frequency curves is when there is heavy damping. Firstly, a heavily damped mode may be completely obscured from some of the curves. Secondly, at the resonant frequency of a heavily damped mode, the amplitude of the off-resonant vibration may be comparable to the vibration in the

resonant mode. This can induce serious errors in the estimation of damping and the principal modes.

The limitations of the **Peak Amplitude** method, when there are close resonances (which may be further aggrevated by heavy damping) are summarized in the following:

1) A mode may be completely missed out

2) Errors may occur in estimation of damping and the principal modes

3) If the damping is very light experimental difficulties lie in making measurements around the resonant frequencies.

To overcome these limitations, either the off-resonant vibration has to be extracted from the response, or the structure must be excited in such a manner, so that only the mode of interest is excited (i.e. the resonant mode must be **isolated**).

In the following, the method of Kennedy & Pancu [1] will be described in which the off-resonant vibration is extracted, as well as multiple-shaker techniques which are required for isolating a principal mode.

5.2. KENNEDY AND PANCU METHOD

Instead of plotting the amplitude and phase response as a function of frequency, as shown in Figs.7a) and 7b) for a single degree of freedom, the complex admittance can be plotted in the Argand plane as shown in Fig.30a). The amplitude X_i is plotted as the vector OX_i at angle θ_i from the real axis, where θ_i is the phase angle between the exciting force and the displacement response at frequency ω_i. If the measured response was of a single degree of freedom system, the curve obtained by plotting the amplitude at the respective phase angles, would be as that shown in Fig.30a). The point Y which is furthest from the real axis corresponds to the point of maximum amplitude (depending on the type of damping), and also where the response is in quadrature with the exciting force (i.e. the real component is zero). At this point where the frequency corresponds to the natural frequency ω_0, the distance along the curve is maximum for equal increments in frequency as can be seen from the crosses in Fig.30a).

In dealing with a multiple degree of freedom system, Kennedy and Pancu made the assumption that for structures with small damping "the mode shapes, phase relations between motions at various points, and couplings between the various degrees of freedom will be unaffected" by the damping. (In terms of mathematics this means that the damping matrix is diagonal, when referred to the principal coordinates). Under this assumption the measured response of each mode as it passes through resonance will lie on an arc of a circle such as that shown in Fig.30a), if the contribution form the off-resonant modes is negligible. In practice, however, the contribution is not negligible, but if it is somewhat constant over a range of frequencies, then the measured points would be shifted relative to the origin as shown in Fig.30b). **The greater the range of frequency over which the contribution is constant, the greater will be the part of the loop coinciding with the circle.**

Whilst all the frequencies coincided at point Y in Fig.30a) for the single degree of freedom, they spread out for the multi-degree of freedom system as shown by points 1–4 in Fig.30b).

Point 1 is the frequency at which the maximum amplitude is obtained, (point furthest from the origin),

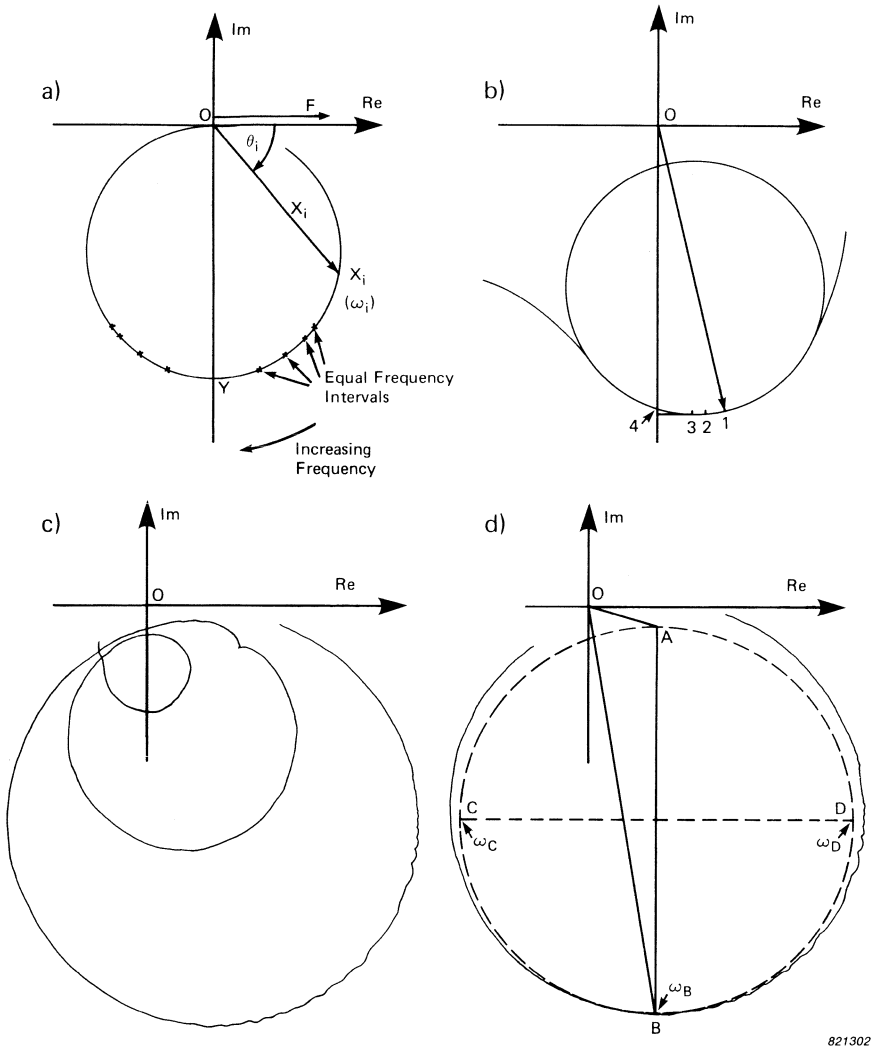

Fig.30.a) Complex admittance of a single degree of freedom plotted in the Argand plane
b) Illustration of various criteria for natural frequencies
c) Response of the first three modes of a simple free-free beam plotted in the Argand plane
d) Extraction of the off-resonant vibration from the total amplitude for determining the loss factor

Point 2 is the frequency at which maximum spacing on the arc occurs for equal frequency increments,

Point 3 is the frequency at which the maximum quadrature component is obtained, and

Point 4 is the frequency at which the force and response vectors are in quadrature (real component zero).

In the past various authors have used different criteria 1–4 for defining the "resonance" frequency.

Kennedy and Pancu have shown that by using criterion 2 the accuracy in obtaining the natural frequency is less affected by the presence of other modes than using the peak amplitude criterion. Also criterion 2 is more reliable in showing up the existence of modes.

To illustrate the method of Kennedy and Pancu for estimation of damping and the principal modes, a simple free-free steel beam was excited at one end, and the response measured at the same end.

Fig.30c) shows the response traced out of the first three modes of the steel beam in the Argand plane. In Fig.30d) the loop corresponding to the first mode of vibration is reproduced. In applying the Kennedy and Pancu method to the measured response, the natural frequency is first of all determined according to criterion 2. The best circle is then fitted to the arc near the natural frequency as shown by the dotted line in Fig.30d).

The point A (which would coincide with O but for the off-resonant vibration), corresponds to the displaced origin and the vector OA represents the contribution from the off-resonant modes. Thus the measured amplitude OB is composed of the contribution from the off-resonant modes OA plus the true peak amplitude of the mode AB. By determining the ratio of the true peak amplitudes (diameters of the circles) at various points on the structure using the above method, the principal mode shape can be found at this natural frequency. The procedure is then repeated for the other natural frequencies for obtaining their mode shapes.

The experimental curves obtained are seen to be almost circular, indicating that the contribution from the off-resonant modes is constant over a wide range of frequencies. This is partly due to the fact that the off-resonant contributions are reasonably small and partly because the natural frequencies are relatively widely spaced apart.

In the determination of the loss factor by the peak amplitude method, it was assumed that the peak was generated solely by the vibration in the resonant mode. As it is possible to separate the contribution of the off-resonant modes (vector OA) and the peak amplitude vibration (vector AB) from the total vibration (vector OB) by the Kennedy and Pancu method, a better estimate of the loss factor can be made.

In Fig.30d) the diameter CD is drawn parallel to the real axis. It can be seen that relative to the new displaced origin A, the amplitudes AD and AC are $1/\sqrt{2}$ the amplitude AB (similar to the peak amplitude method), and the argument of these vectors are $\tan^{-1}(\pm 1)$. If ω_C and ω_D are the frequencies at C and D respectively, the loss factor in this mode is determined from

$$\eta = \frac{\omega_C - \omega_D}{\omega_B} \tag{113}$$

In determining ω_C and ω_D the scale of ω is required on the response locus.

The method can be seen to be analogous to the peak amplitude method, except for the fact that the information is derived relative to the displaced origin and thus without the contribution from the off-resonant modes.

Another construction which can be used for evaluation of the loss factor is shown in Fig.31. The crosses show the experimental data obtained at equal frequency intervals $\Delta\omega$. The best circle is fitted through the measured points and the centre of the circle is established. By drawing the radii through the measured points the largest arc length for given frequency increment can be determined, which would in fact correspond to the largest angle α included between two adjacent radii. Thus the natural frequency ω_0 would be midway between ω_1 and ω_2 the frequencies at the two ends of the maximum arc length. The loss factor can then be determined from

$$\eta = \frac{2\Delta\omega}{\omega_0 \tan(\alpha/2)} = \frac{2(\omega_2 - \omega_1)}{\omega_0 \tan(\alpha/2)} \qquad (114)$$

for $\alpha/2 < 45°$.

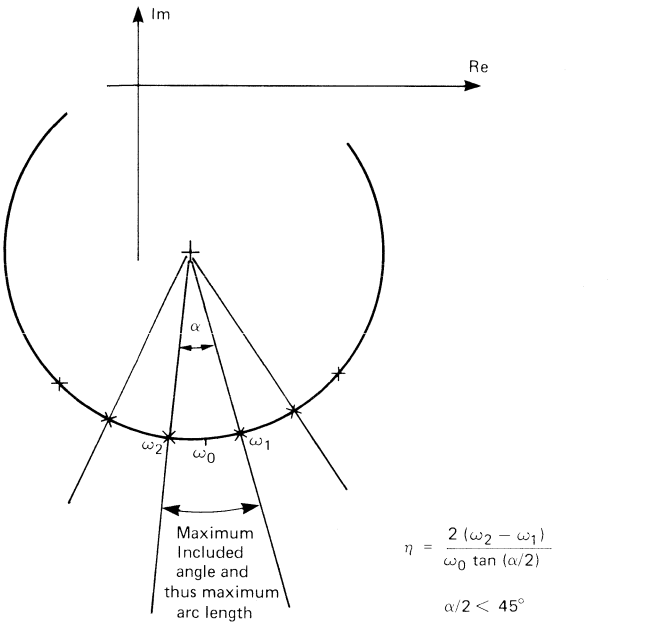

Fig.31. Construction for evaluating the loss factor

6. MULTIPLE EXCITER TECHNIQUES

Since a structure when excited vibrates in several modes simultaneously, and thus causes difficulties in the analysis of the results, the unwanted modes have to be somehow eliminated. This can be achieved for simple structures by placing the exciters or pick-ups at nodal points of the unwanted modes, or by making use of the symmetrical and anti-symmetrical properties of the mode shapes, (see **Section 6.3. Experimental Procedure**). In a complex structure, however, this is not always possible, and systematic methods have to be used for exciting the structure with multiple shakers and forcing them to vibrate in their Principal modes. However, this requires rather sophisticated equipment both on the excitation side, as well as on the data acquisition side, on account of the large number of pick-ups, necessary for determining the mode shapes. To facilitate understanding of the multi-shaker technique, it is necessary to first describe the instrumentation required, and the features that have been incorporated, that are obligatory for functioning of the test. (In **Appendix D** a simple system with two shakers is described, which is ideal for education and demonstration purposes in laboratories to illustrate the principles).

6.1. INSTRUMENTATION FOR EXCITATION

Fig.32 shows an instrumentation set-up for testing of large structures using multiple shakers. The system is such, that it can be readily expanded to incorporate any number of shakers and accelerometer channels. All the equipment below the structure constitutes the excitation part of the system, while the instrumentation above the structure is used for data acquisition and further processing and analysis of the results.

For sinusoidal excitation of the structure, the principle of operation of this set-up is basically the same as that of Fig.22. However, on account of the multiplicity of shakers and accelerometers, automatic control of the system is imperative, although manual operation is possible. This can be achieved by the Digital System Controller, which could be, for example, a desk-top calculator having sufficient memory and speed commensurate with the sophistication of the analysis software.

The fundamental requirement on the excitation side is the accurate control of the amplitude and phase of the force, applied by each shaker to the test structure at a single frequency. Either a Precision Generator Type 5819 or the sinusoidal generator built-in the Dual Channel Signal Analyzer Type 2032 or 2034, can be used to feed the signal to the shakers, via a power amplifier and a Phase & Amplitude Controller. Whilst the latter controls the voltage input, and thus the force output from each shaker, via the IEC/IEEE Interface, monitoring of the forces into the structure is carried out by force transducers mounted between each shaker and the test structure.

On the data acquisition side, the acceleration signals have to be measured at several points on the structure, and conditioned, before they are displayed on the Multiplexer Type 5797 as Lissajous figures. The Multiplier Type 5795 extracts the Real and the Imaginary components of the acceleration signals, while the Control Unit Type 5794 digitizes these signals, and controls the Group Selectors Type 5820 for out-scanning of the system.

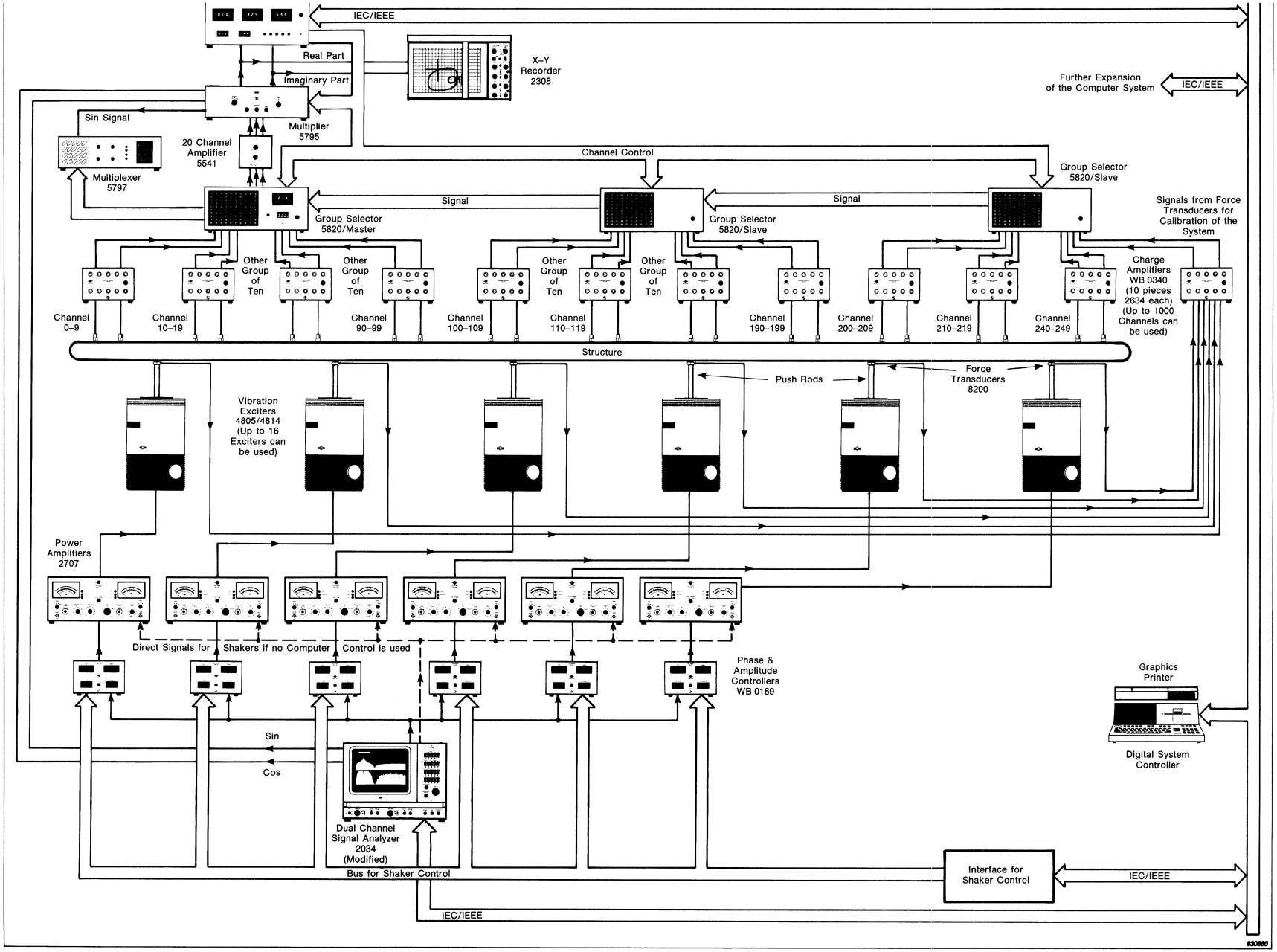

Fig.32. Instrumentation set-up for testing of large structures using multiple shakers

For wideband excitation of the structure using a single shaker, the signal from the force transducer of the corresponding shaker is fed to channel A of the Dual Channel Signal Analyzer Type 2032 or 2034, and the total amplitude output from the Multiplier 5795 is fed to channel B. The accelerometer channel for this output is selected by the Digital System Controller via the Control Unit 5794.

For techniques involving wideband excitation of the structure using multiple shakers, additional hardware is required (not shown in Fig.32). In the following the individual instruments will be described and the essential features which are incorporated in them.

6.1.1. Precision Generator Type 5819

Large metal structures have relatively low damping and often very close natural frequencies. Thus stable excitation of these modes places stringent requirements on the generator, which should have the following features:

a) Low distortion as harmonic components may excite undesired resonances.

b) High frequency resolution and stability because of the narrow resonant bandwidths of the structure.

c) Low phase jitter to avoid side bands around the excitation frequency.

The Precision Generator Type 5819 operating on the synthesizer principle has a frequency resolution of 2 mHz and fulfils the above requirements. The frequency range covered is 1,000 – 9999,9998 Hz. The sweep rate of the Generator can be chosen between 0,00100 – 100 Hz/s or oct/min.

Facility for compressor (servo) loop is available as an option for keeping a constant level excitation if desired. Both frequency and level control can be input digitally or adjusted manually.

The Precision Generator outputs a sine and cosine voltage at the same frequency, both of which are fed to the Amplitude and Phase Adjustment Units types WB 0169. The cosine voltage is used as the force reference. Both the voltages are also fed to the Multiplier Type 5795 to be multiplied with the selected acceleration signal for producing the in-phase and quadrature components of the acceleration output.

Frequency marking signal for the X-Y Recorder type 2308 is available from the Generator. This is especially useful in locating the maximum spacing for equal frequency intervals on the Nyquist plot for the determination of natural frequencies by the Kennedy and Pancu method. It was shown above that in order to excite a principal mode, the force distribution has to be found for which the acceleration at all points on the structure is in quadrature with the force input. The real part of the acceleration signal at a selected point can be fed from the Multiplier Type 5795 to the automatic frequency control of the Generator. By maintaining the real part zero, the Generator achieves the quadrature relationship while the correct force distribution is found manually or automatically.

6.1.2. Dual Channel Signal Analyzer Type 2032/2034

Instead of the Precision Generator Type 5819, the sine wave generator built-in the Dual Channel Analyzer Type 2032 or 2034 can also be used. The frequency range

covered by the generator is 15 mHz to 25,6 kHz, with a resolution of 15 mHz. However, the frequency sweep of the generator needs to be controlled by the desk-top calculator (Digital System Controller) via the IEC/IEEE interface.

The advantages of using the Dual Channel Analyzer, on the other hand, are that the structure can also be excited using random noise, pseudo-random noise or an impulse from the built-in generator. Furthermore, it is a zooming generator, so that with a random or pseudo-random noise output, the noise spectrum is bandlimited to match the selected frequency span, (see Ref [45]). Its 801 line resolution is of special importance with respect to measurements on mechanical system for identifying the modes. The analyzer can thus be used in conjunction with software packages developed by SMS (Structural Measurement Systems), for modal analysis of structures using wide band excitation described in **Section 7.4.3.**

6.1.3. Power Amplifier Type 2707

If the sinusoidal voltage generated by the Precision Generator is to be used as a force reference, it is necessary to eliminate any phase shift between the generator signal and the excitation force. The power amplifier has been designed such, that when it operates in the "high impedance" mode the output current is proportional to the input voltage with negligible phase shift. Thus any variation in the exciter impedance will have negligible effect on the coil current of the exciter. The phase shift between the coil current and the force on the coil has also been minimised.

6.1.4. Phase and Amplitude Controller Type WB 0169

As it is now possible to adjust the force applied to the structure by means of the current, a Phase and Amplitude Controller Type WB 0169 can be inserted between the Generator and the Power Amplifier for each channel. By this instrument the amplitude and phase of the force signal can be varied between 0° and 180° relative to the reference signal of the generator, either manually or remotely. (Normally 0° or 180° would be used for principal mode excitation).

6.1.5. Force Transducer Type 8200

A Force Transducer Type 8200 is placed between each vibration exciter and the structure. The outputs of the force transducers are fed to the Digital System Controller via a Group Selector and IEC/IEEE interface. It is thus possible to calibrate the system by force transducers, so that the current constant of the shakers may be checked.The force delivered by the vibration exciters can now be monitored.

6.2. INSTRUMENTATION FOR DATA ACQUISITION AND ANALYSIS

6.2.1. Accelerometer Types 4371 and Multiple Preamplifier Unit Type WB 0340

The use of unigain Accelerometers Types 4371 significantly simplifies simultaneous monitoring of acceleration at several points on the structure. This is because switching of the accelerometers does not lead to loss of calibration. Each Multiple Preamplifier Unit Type WB 0340 contains ten Charge Preamplifiers Types 2634 with their power supplies.

6.2.2. Group Selector Type 5820

The outputs from the Multiple Preamplifier Units is fed to a Group Selector Type 5820 which can accept up to 100 channels. Nine other Group Selectors may be connected in parallel as slaves, extending the number of channels to 1000. The 5820 divides the 100 channels into groups of ten, and outputs two groups at a time to the Multiplier Type 5795 via a Twenty Channel Amplifier Type 5541. Channel selection on the 5820 is carried out either manually by three digit thumb-wheels or remotely. The least significant digit selects the channel number that is to be output from the Multiplier 5795, while the middle digit selects one of the ten groups to be output from the 5820. The most significant digit selects one of the ten Group Selectors connected in parallel.

6.2.3. Twenty Channel Amplifier Type 5541

This unit amplifies the twenty signals from the Group Selector in steps of 0, + 20 dB or + 40 dB before feeding them to the Multiplier Type 5795.

6.2.4. Multiplier Type 5795

Each of the twenty input signals are here multiplied simultaneously by the sine and cosine voltage signals from the Precision Generator and low pass filtered. Thus two DC voltages proportional to the in-phase (real part) and quadrature component (imaginary part) of each acceleration signal relative to the reference cosine voltage signal of the Generator are produced, see **Appendix D**. The low pass filtering removes the harmonics of the signals, if any, thus eliminating the need of a tracking filter. The real and imaginary components of the ten acceleration signals at a time are fed through a remote controlled multiplexer to the Control Unit Type 5794. While one group of ten channels is being output, the second group of ten settles down and is ready for output, the sequence being controlled by the Control Unit Type 5794. For recording of the response curves in the Argand plane for the Kennedy and Pancu method, the real and imaginary parts of the signals can also be fed to the X-Y Recorder Type 2308. The total amplitude is also available as an output for the Peak Amplitude method.

6.2.5. Control Unit Type 5794

Type 5794 controls the digital measuring system. Two A/D converters digitize the real and the imaginary parts of the signal for feeding outputs to the Digital System Controller via the IEC/IEEE interface. The digitized values of the real and imaginary parts are also displayed on the front panel. The multiplex control logic through a microprocessor controls the Group Selector for out-scanning of the system. When a "channel scan" is desired, for example, at a natural frequency for obtaining the mode shapes, the real and imaginary parts of all the accelerometer signals are printed out in succession on the Digital System Controller.

In the case of a "frequency scan", the real and imaginary parts of the accelerometer signal selected on the Control Unit will be printed out against frequency at read-out intervals set by the Controller.

6.2.6. Multiplexer Unit Type 5797

The Multiplexer Unit accepts twenty accelerometer signals chosen from the Group Selector by means of a pin-board arrangement. The signals are converted to oscilloscope levels, lowpass filtered, and fed to the Y input of a twenty channel oscilloscope for displaying Lissajous figures. It is well known [26], that if two signals of equal amplitude are fed to the X and Y input of the oscilloscope, the Lissajous figures displayed will be as shown in Fig.33, for phase angles of 0°, 45°, 90°, 135° and 180° between the two signals.

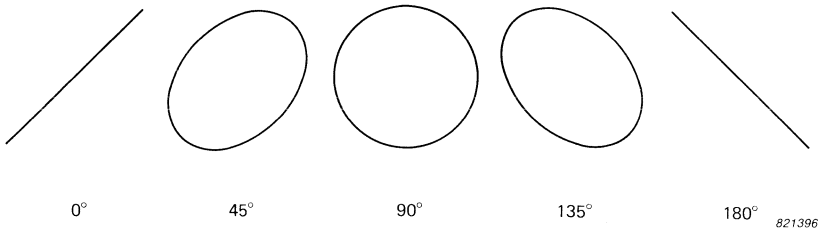

Fig.33. Lissajous figures for phase angles of 0°, 45°, 90°, 135° and 180° between two signals of equal amplitude

Thus, if the cosine voltage, which is in phase with the force signal, is fed from the Precision Generator Type 5819 (or the Dual Channel Analyzer) to the X input of the oscilloscope, a circle would be displayed when the principal mode was excited on account of the quadrature relationship between force and acceleration. However, such a display is rather inconvenient in establishing exactly if the quadrature relationship is fulfilled. If, instead, the sine voltage from the Generator via the Multiplier is fed to the X input of the oscilloscope, straight line Lissajous figures would be displayed when the quadrature relationship was satisfied.

6.3. EXPERIMENTAL PROCEDURE

Before describing the experimental procedure, it is necessary to illustrate in practical terms the theoretical considerations for multiple shaker excitation, laid down by Fræijs de Veubeke and Bishop & Gladwell [23, 8] and which is briefly described in the theoretical **Section 3.4.2.**

In words it can be stated, that if a structure is proportionally damped, it can be excited at any frequency by a particular set of forces which are in phase or anti-phase with each other (mono-phase), such that the measured responses at all points are all in phase (or anti-phase), and that the common phase lag (termed characteristic phase lag) between the force and the response is unique at this frequency. Furthermore, at this frequency there are as many characteristic phase lags with their associated linearly independent force distribution, as there are degrees of freedom in the structure. The structure when excited in this manner for a particular ratio of forces will vibrate in the principal mode, and thus as a single degree of freedom system.

If the structure is non-proportionally damped, the structure can be excited in its principal mode, only at the corresponding natural frequency by a set of mono-phase forces. In this case the response will be in quadrature with the forces at all points on the structure.

If the structure has n degrees of freedom, n number of shakers are required ideally to isolate a mode. To exemplify this statement, consider the mode shapes of the first

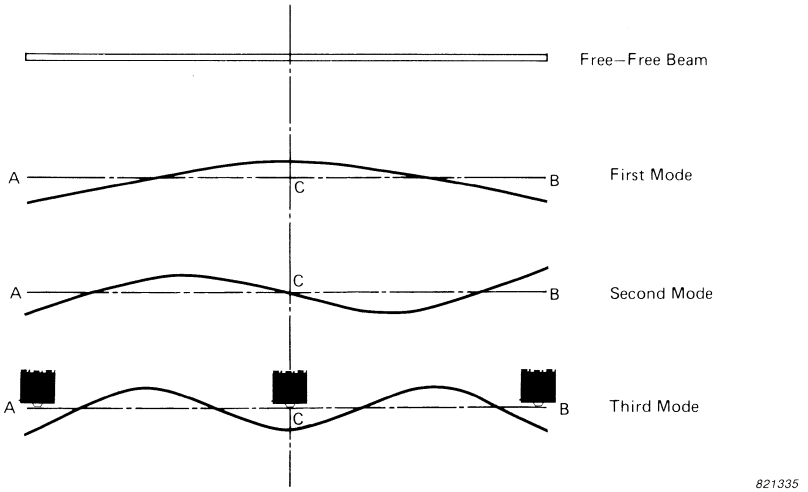

Fig.34. Positioning of shakers to excite the third mode of a free-free beam

three degrees of freedom of a free-free beam shown in Fig.34. It can be seen, that in order to excite the third mode only, three shakers in phase would be required, one at each of the points A, B and C. If only two shakers with equal force amplitudes were used in phase at A and B, the second mode could be eliminated, as points A and B move in anti-phase, however, the first mode would be excited together with the third one. Again, if only two shakers were used in phase at A and C, the first mode could be eliminated, as points A and C move in anti-phase, however, the second mode could not be eliminated.

From this example, it can be appreciated how the symmetrical and anti-symmetrical properties of the mode shapes can be used to advantage, for judicious positioning of the shakers. In complex structures, however, this is not always possible. Furthermore, as continuous structures have infinite number of degrees of freedom, infinite number of shakers would be required. In practice, obviously a limited number of shakers are used, such that only the mode of interest is dominantly excited in a particular frequency range.

As mentioned in the **Introduction**, the testing of large structures is carried out in two stages. In the first step the number of modes and their natural frequencies are roughly established using single shaker sweeps, by either plotting the peak amplitude or the quadrature component as a function of frequency, or preferably using the complex plot (polar plot) and using the Kennedy and Pancu method. The response should be monitored at several points to ensure that none of the modes is missed out in the frequency range of interest. Once the existence of a mode has been established, the second step involves isolation (tuning) of the mode using multiple shakers. The theoretical requirements for multi-shaker excitation has been excellently interpreted in practical terms for carrying out the test by Taylor et al in Ref.[6] and is as follows. The test is started using a single shaker (placed preferably at an anti-node of the mode to be excited) with an arbitrary force, and the response from an accelerometer placed at the same shaker (or an anti-node) is fed back to the generator. The natural frequency of the mode to be examined is now found by adjusting the frequency of the generator, and observing the relevant Lissajous figure on the oscilloscope until it becomes a straight line, indicating that a quadrature relationship between the exciting force and the response is established. The automatic **frequency** control loop is now closed so that subsequent frequency adjustment is automatic. With the first shaker operating on automatic frequency control, the force level on the second shaker is adjusted on its power amplifier, until the quadrature relationship for it is established on its Lissajous figure. The force level now is similarly adjusted on the third shaker,

which may, however, cause a phase difference on the Lissajous figure of the second shaker. Thus the force levels on the second and third shakers must be systematically adjusted. When force levels on more shakers are brought into play they would have effects on each others phase response. Thus iterative adjustment of force levels on the shakers is generally necessary to minimize the phase error on the Lissajous figures of all the shakers.

It will be found that as more and more forces are applied and adjusted, the more uniform in phase are the various points on the structure, and the responses in quadrature with the forces. Furthermore, the frequency at which the generator was initially set when the force to the first shaker was applied, would have drifted and approached the true natural frequency of the mode being excited. These trends give definite indications that a principal mode is being approached.

When the correct force distribution has been determined, it may be found that the overall force input is too low for accurate response measurements. This occurs if the force level chosen on the first exciter is incorrect. This can be overcome by increasing the voltage output from the generator, so that the forces at all the shakers are increased equally, maintaining the same force distribution. Furthermore, this feature is also useful in checking the amplitude linearity of the structure, by gradually increasing the overall force level and observing the response. Another situation which can arise if the force level chosen on the first exciter is incorrect, is that one or more of the forces at the other shakers may be at a maximum, before the correct force distribution is found. In this case the force at the first shaker has to be reduced and the force adjustment procedure repeated.

Once the correct force distribution has been obtained, such that the quadrature relationships have been established at the monitoring points, the rest of the structure should be examined for mono-phase response. If the phase scatter around the structure is unacceptably large, repositioning of the shakers and/or monitoring points of responses should be considered. If for some reason, for example, non-linearity in the structure, it is impossible to find the correct force distribution that gives a mono-phase response, it may be necessary to accept some phase error at a couple of excitation points. It should be remembered, that unless the automatic frequency control loop is offset, no phase error can occur at the first exciter. Thus if minimum error is sought, the possibility of having to accept some phase error at the first exciter should not be overlooked.

When there are fairly closely spaced resonances, care has to be exercised, as pointed out in Ref.[6] by the followig illustrative example. Fig.35 shows a polar plot obtained at the attachment point of shaker 1, used for the automatic frequency control loop. As can be seen, there are two modes with natural frequencies ω_1 and ω_2. If we wish to isolate mode 1, an arbitrary force would be selected at shaker 1 and the frequency of the generator would be adjusted to ω_1. If now the automatic frequency control loop was closed, the frequency of the generator would vary until the response was in quadrature with the force, i.e. the frequency at point P would be attained. When the forces on other shakers are brought into play the system will most likely end up exciting the mode of natural frequency ω_2. Thus it may be essential to determine approximately the correct force distribution for mode 1, before the automatic frequency control loop is closed. This situation can be avoided by having the shaker with the automatic frequency control loop mounted at a nodal point of mode 2.

With the correct force distribution established, a sinusoidal frequency sweep around the natural frequency is very useful in revealing the characteristics of the mode. If the damping is proportional (non-coupling) and hysteretic, the complex response in the Argand plane would be a perfect circle, centered on the imaginary axis with its highest

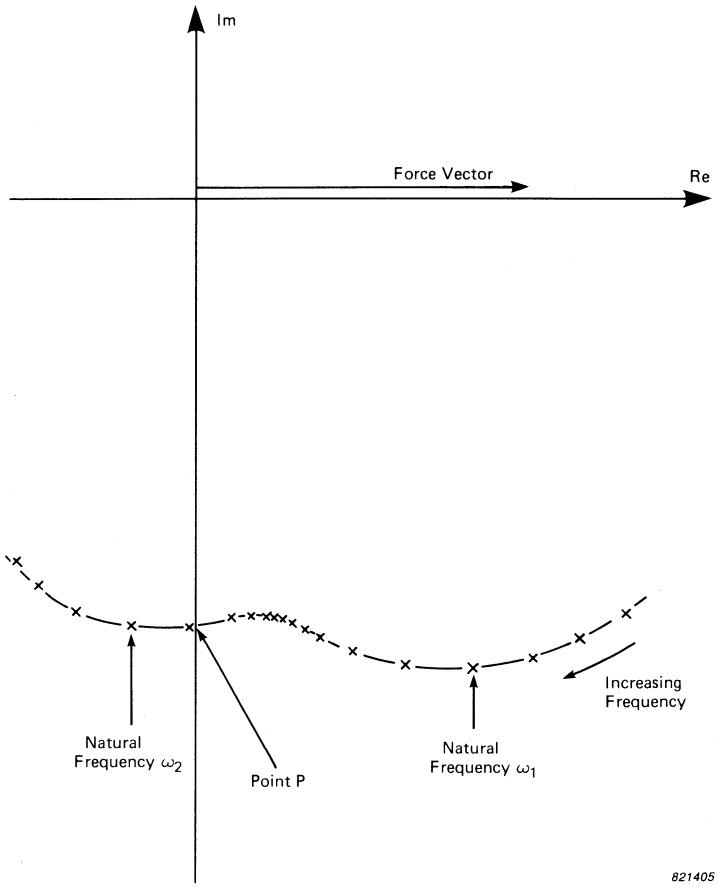

Fig.35. Polar plot of two closely spaced modes obtained at the attachment point of shaker 1

point passing through the origin. From this polar plot the modal damping as well as the mode shape component could be determined using the Kennedy and Pancu method. If the damping is proportional and viscous, the complex response would still be nearly circular. Even if the damping is non-proportional (i.e. damping couples the modes), the complex response plot is nevertheless useful in establishing the presence of a true mode. However, damping coupling of closely spaced modes causes deviation from circular shape of the polar plots, which may be difficult to interpret. It should be remembered that for non-proportional damping, according to the characteristic phase lag theory, the principal mode can be tuned only at the natural frequency, with the response in quadrature with the excitation force.

If the mode is isolated, and all the forces at the shakers are suddenly stopped (for example by setting the generator on standby), the resulting decay curves will not exhibit "beating" and will be of a single frequency (the natural frequency of the mode). The modal damping could then also be evaluated from the logarithmic decrement of the decay curves.

6.4. PRACTICAL DETAILS

6.4.1. Exciter Positions

Some prior knowledge of the mode shapes, obtained either from theoretical calculations or from experience of similar structures, will often expedite judicious positioning

of the shakers around the structure. Since nodal regions should be avoided, the extremities of free-free structures is generally a good choice. For exciting the symmetrical modes, positioning the shakers on the axis of symmetry is advisable, and conversely should be avoided for anti-symmetrical modes.

Since the aim of multiple shaker excitation is not only to excite the mode of interest, but also to cancel the contribution from the off-resonant modes, it should be remembered that the off-resonant component cannot be cancelled, if all the shakers are placed at the nodes of that unwanted mode. (The unwanted mode can nevertheless be excited due to damping coupling between it and the other modes).

6.4.2. Response Monitoring points for Force Control

As mentioned earlier, it is not always essential to have the response monitoring points for adjusting the forces, to be coincident with the corresponding shaker positions. The monitoring points should ideally be chosen in the region of anti-nodes, and in addition, where the component from off-resonant modes are initially large. These positions will therefore be sensitive to the mode being excited, as well as to the unwanted modes whose contribution could thus be reduced to a minimum.

6.4.3. Criterion for Modal Purity

From theory it is known, that if the structure is excited in a pure mode, the response at all points on the structure would be in quadrature with the forces. Therefore the minimum phase scatter that could be measured, would be the maximum phase error of the equipment. Unfortunately, structures are never ideal in practice, and therefore a realistic criterion for modal purity that is often used, is a phase scatter no greater than $\pm 10°$ around the quadrature components.

6.5. MEASUREMENT RESULTS

To illustrate isolation of the modes using multiple shakers, experiments were carried out on a free-free beam shown in Fig.36a). Fig.36b) shows the real and imaginary components of the response measured at point 1, as a function of frequency, when the beam is excited by a single shaker at the same point. From the response it can be seen that there are two resonances at frequencies 20,5 Hz and 47,8 Hz, corresponding to the first and second modes respectively. These resonances are indicated by the frequencies of the minima of the imaginary component. The real components can be seen to be practically zero at these frequencies. The peaks and notches below 10 Hz are caused by the low frequency suspension of the beam.

Fig.36c) shows the response at point 1 when the beam is excited by two shakers in phase positioned at points 1 and 2. It can be seen that the first mode is excited while the second mode is eliminated. Fig.36d) shows the response at point 3 for the same excitation conditions. The response curves are seen to be inverted i.e. a maximum occurs now for the imaginary component at the same frequency. The reason is that point 3 moves in anti-phase with point 1, as can be seen from the first mode shape. The fact that points 1 and 3 are moving in anti-phase, will also be indicated on their Lissajous figures. This is because the response at point 1 being 90° out of phase with the force signal at resonance, will display a line at 45° on the Lissajous figure, while the response at point 3 being 270° (–90°) out of phase with the force, will display a line at 135° from the horizontal on its Lissajous figure. This is a very useful feature in pointing out which points move in phase and which in anti-phase relative to each other at **resonance.**

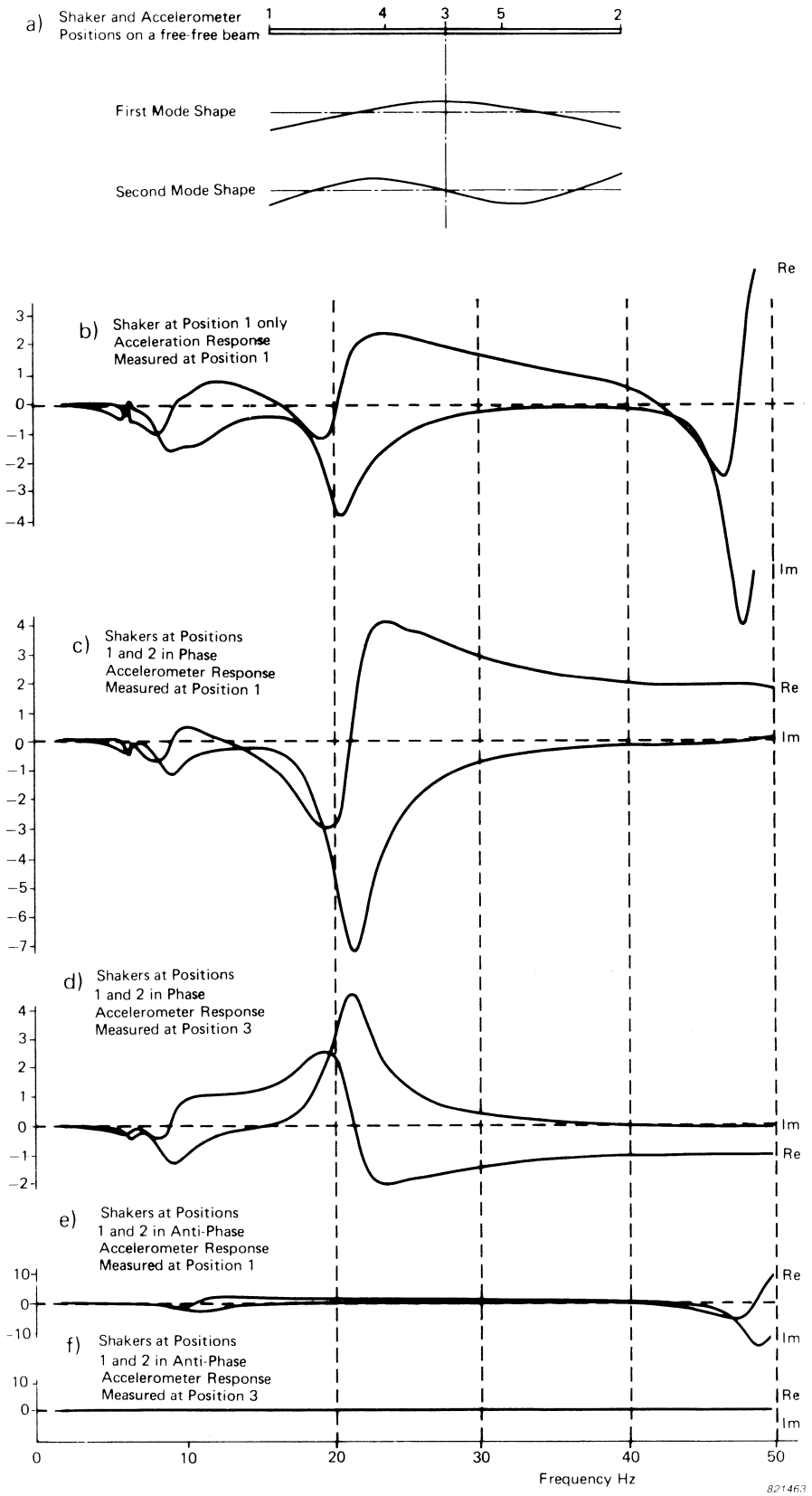

Fig.36. Real and Imaginary components of the response as a function of frequency measured at various points on a free-free beam excited under different conditions

Fig.36e) shows the response measured at Point 1 when the beam is excited by two shakers in anti-phase positioned at points 1 and 2. It can be seen that the second mode is excited, while the first mode is eliminated. Fig.36f) shows the response measured at point 3 for the same excitation conditions. Although mode 2 is excited, it can be seen that there is no response, simply because point 3 is a nodal point for the second mode. (The amplitude scales for Figs.36e) and f) are different to those of Figs.36b), c), and d).)

Fig.37a) shows the polar plot of response measured at point 1, when the beam is excited by a single shaker at the same point. With the beam excited by four shakers at points 1, 2, 4, and 5, and the forces adjusted to isolate the first mode, the polar plot response measured at point 1 is as shown in Fig.37b), when the frequency is scanned through the first resonance. Figs.37c) and d) show the polar plots similarly obtained for the second and the third modes respectively. The symmetry of the polar plots

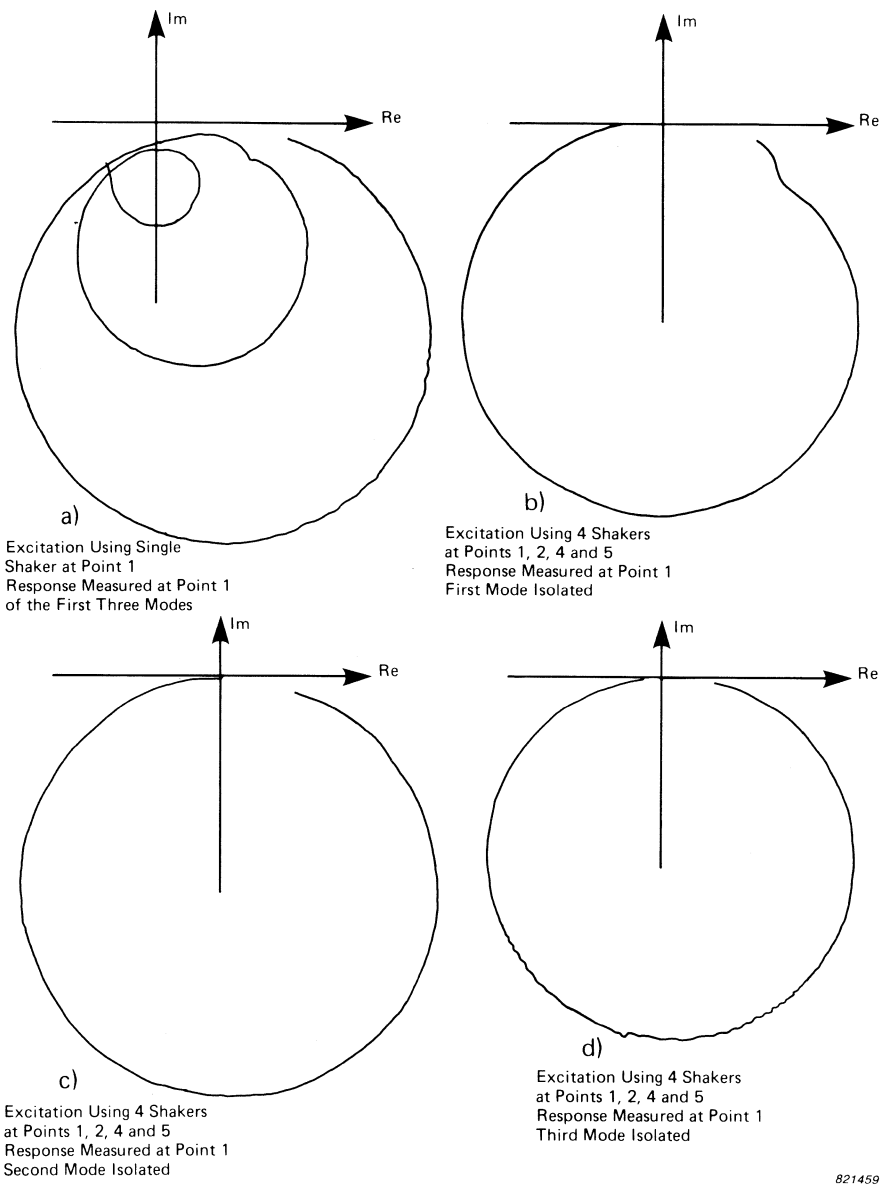

Fig.37. Polar plots of response measured at point 1 on a free-free beam excited using a single shaker, and using four shakers to isolate the first, second and the third modes

around the imaginary axis, with the highest point passing through the origin, gives a clear indication of the modes being isolated, when excited by the appropriated forces using multiple shakers. It should be noted that the results of Figs.36 and 37 can be obtained using the simple system described in **Appendix D**. However, as only two shakers can be used to isolate the modes with this simple system, the polar plots will not be as symmetrical and circular as those shown in Fig.37. Nevertheless, this simple system is ideal for education, in illustrating the principles behind the multiple shaker excitation and the Kennedy and Pancu techniques, as well as for less demanding practical applications.

Fig.38 shows the first three mode shapes of the beam when isolated using four shakers. Since the beam is uniform, the mode shapes theoretically should be symmetrical, which are confirmed by the practical results. However, compare the third mode shape with that shown in Fig.24 obtained using a single shaker.

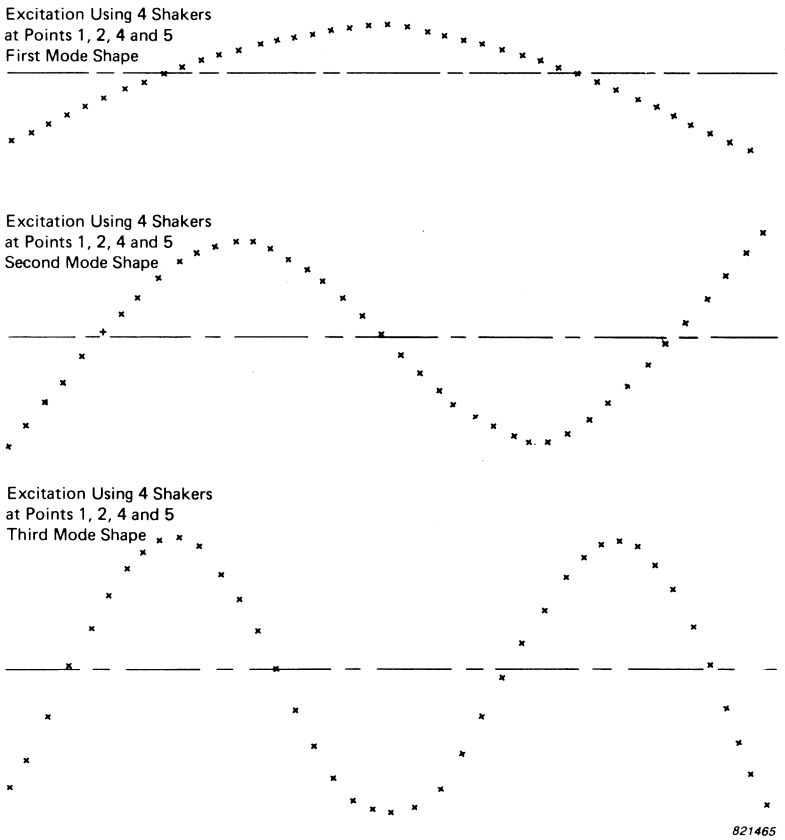

Fig.38. The first, second and the third mode shapes of a free-free beam obtained using four shakers with appropriated forces

7. AUTOMATIC FORCE APPROPRIATION TECHNIQUES

Under the **Experimental Procedure** section it was shown, that for isolating or tuning a mode using multi-shaker technique, it was necessary to adjust the mono-phase forces on the individual shakers at the natural frequency, until the acceleration response at all the mesurement points was in quadrature with the excitation forces. Thus some form of iterative procedure for force appropriation is required to optimize the phase coherence of the responses. Manual iterative procedures are carried out whilst observing some form of phase display. Generally, use of Lissajous figures is quite convenient, as closing of the ellipses at all points implies not only proper force appropriation, but also excitation at the resonant frequency.

Difficulties, however, arise when a large number of shakers have to be adjusted to isolate modes in frequency ranges of high modal density. Therefore to automate the force appropriation task, different methods have been put forward [16, 25, 29, 30]. In the following Deck's method [16] will be briefly touched upon, and Asher's method [7], which has been discussed by several authors, will be described in some detail.

7.1. DECK'S METHOD

For appropriating the forces, Deck proposes to iterate with multiple shakers to fulfil the criterion

$$R = \sum_{i=1}^{m} |A_i \sin \theta_i| \tag{115}$$

where A_i is the velocity amplitude response at point i.

θ_i is the phase angle between the velocity and force at point i, and n is the total number of measurement points.

Thus the function R is a minimum (and equal to zero) if all the velocity responses are in phase (acceleration responses are in quadrature) with the excitation forces — the conditions for an isolated mode. In his method, the amplitude of each shaker is adjusted in turn until R reaches a minimum. He also presents arguments for the convergence of this procedure and shows how adjustment of each force requires only two changes in the force.

Deck furthermore defines

$$Z = \frac{\sum_{i=1}^{m} |A_i \sin \theta_i|}{\sum_{i=1}^{m} |A_i \cos \theta_i|} \tag{116}$$

as a measure of modal isolation and resonance condition. The procedure for his method is as follows. The test is initiated by a few frequency sweeps to establish the natural frequencies. The structure is then excited at one of the estimated natural frequencies by a judiciously chosen initial force distribution. Each force is adjusted in turn (keeping the others fixed) by a two point evaluation of R. When each force is thus adjusted to minimize R, the excitation frequency is tuned to minimize Z to account for small changes in resonant frequency due to non-linear effects. Depending on the value of Z, the procedure may be repeated if desired, starting with the first force. The end result should give the correct force distribution for this mode. The whole procedure is of course repeated for the rest of the modes. Implementation of this algorithm based on a computer system is described by Deck in Ref. [16].

7.2. ASHER'S METHOD

Asher [7], apprehensive of other methods available at the time (1958) being capable of separating closely spaced modes, proposed a quantitative method, which detects the natural frequencies as well as provides the force ratios necessary for multiple-shaker tuning, using only experimental transfer admittance data as input.

Although Asher was unable to apply his method successfully on practical structures due to equipment limitations, his method was nevertheless considered to be promising and was discussed extensively by Bishop & Gladwell [8], (1961). Since then simulated modal testing has been carried out by Craig & Su [9], (1974) and also by Hallauer and Stafford [10], (1978) on theoretical five and eleven degrees of freedom models. Use of Asher's method on practical structures have been attempted and described in Refs. [11, 12, 13], (1976). Extensions of Asher's method have also been suggested in Refs. [15, 31, 36, 42].

To illustrate the method suggested by Asher consider eq. (89) which describes the harmonic motion of an n degree of freedom linear, damped system i.e.

$$[m]\{\ddot{x}\} + [c(\omega)]\{\dot{x}\} + [k]\{x\} = \{F\} \sin \omega t \tag{117}$$

The damping is considered to be rather general (see Ref. [10]), and is therefore represented by an arbitrarily frequency-dependent term

$$[c(\omega)] = [c] + 1/\omega\,[d] \tag{118}$$

where $[c(\omega)]$ encompasses any combination of the standard viscous and hysteretic types, given by [c] and [d] matrices respectively. Furthermore, in the general case, damping is non-proportional so that the damping matrix couples the otherwise uncoupled normal equations of motion.

The system is assumed to be excited by a set of mono-phase forces i.e. all the forces are either 0° or 180° out of phase with each other. Introducing complex notation (complex quantities are denoted by a bar) in eq. (117) yields

$$[m]\{\ddot{\bar{u}}\} + [c(\omega)]\{\dot{\bar{u}}\} + [k]\{\bar{u}\} = \{F\} e^{j\omega t} \tag{119}$$

where

$$\{x\} = \mathrm{Im}\{\bar{u}\} \tag{120}$$

Substituting the trial solution

$$\{\bar{u}\} = \{\bar{U}\}\, e^{j\omega t} \tag{121}$$

in eq. (119) yields

$$-\omega^2 [m]\{\bar{U}\} + j\omega [c(\omega)]\{\bar{U}\} + [k]\{\bar{U}\} = \{F\} \tag{122}$$

i.e.

$$[[k] - \omega^2 [m] + j\omega [c(\omega)]]\{\bar{U}\} = \{F\} \tag{123}$$

Eq. (123) may be written as

$$\{\bar{U}\} = [\bar{B}]\{F\} \tag{124}$$

where

$$[\bar{B}] = [[k] - \omega^2 [m] + j\omega [c(\omega)]]^{-1} \tag{125}$$

is called the complex admittance matrix. It can be written in its real and imaginary parts as

$$[\bar{B}] = [B'] + j[B''] \tag{126}$$

where [B'] is the real part of $[\bar{B}]$
and [B''] is the imaginary part of $[\bar{B}]$

The individual terms of the admittance matrix, the admittance functions, are the dynamic equivalent of the static flexibility influence coefficients. It has been shown in Appendix E, that the elements in each column of matrix $[\bar{B}]$ represents the complex displacement response (per force) at the different points on the structure at a single frequency, when the structure is excited at any one point. In other words the element $\bar{b}_{ij}$ represents the complex displacement at point i when the structure is excited at point j. (Thus the elements of the principal diagonal, ($\bar{b}_{ij}$ when i = j) represents the point admittances, while the off-diagonal elements represent the cross or transfer admittances).

In the section on **Forced Normal Modes of Damped Systems** it was shown, that by using the trial solution $\{x\} = \{\psi\} \sin(\omega t - \theta)$, eq. (117) can be written as

$$\cos\theta\, [[k] - \omega^2 [m]]\{\psi\} + \omega \sin\theta\, [c(\omega)]\{\psi\} = \{F\} \tag{127}$$

$$\sin\theta\, [[k] - \omega^2 [m]]\{\psi\} - \omega \cos\theta\, [c(\omega)]\{\psi\} = \{0\} \tag{128}$$

For the special case when $\theta = 90°$, i.e. all the displacements are in quadrature with the excitation forces, the equations reduce to

$$\omega [c(\omega)]\{\psi\} = \{\Gamma\} \tag{129}$$

$$[[k] - \omega^2 [m]]\{\psi\} = \{0\} \tag{130}$$

The only solution to eq. (130) is the normal mode solution (see eg.(31)), implying that the excitation frequency must be a natural freqency, and that the characteristic phase lag mode shape must be the principal mode shape ($\{\psi_i\} = \{\phi_i\}$) at that frequency. Furthermore, to establish this form of quadrature response, the force distribution required must be that given by $\{\Gamma_i\}$ from eq. (129).

It can thus be seen, that even if the damping is non-proportional, the Principal mode can be excited, as long as all the displacement responses are in quadrature with the excitation forces. However, this can only occur at the undamped natural frequency.

Substituting eq. (126) in eq. (124) yields

$$\{\bar{U}\} = [B']\{F\} + j[B'']\{F\} \tag{131}$$

Interpretation of the above statement when applied to eq. (131) implies, that when the displacement response is in quadrature with the excitation force, it is required that

$$[B']\{F\} = \{0\} \tag{132}$$

since the real parts of the displacement responses are zero. Eq. (132) represents a set of linear homogeneous equations which have a non-trivial solution if, and only if

$$|B'| = 0 \tag{133}$$

(giving a set of eigenvalues which are the undamped natural frequencies). As a corollary to this statement Craig & Su [9] concluded that "The response of a system will be in quadrature with the excitation if, and only if, the determinant of the real part of its complex admittance matrix [B'] is equal to zero". The corresponding force ratios required to isolate the modes will be given by eq. (132) using the eigenvalues obtained from eq. (133).

The theoretical results given by eqs. (132) and (133) were first stated by Asher [7]. His method can be described with reference to these equations in the context of an idealized modal test on a discrete n degree of freedom linear structure with linear damping. The test is started by measuring the (n x n) complex admittance matrix over the frequency range of interest. This can be carried out by exciting and measuring the response at each degree of freedom, either using sinusoidal sweep, or broadband excitation, see Ref. [13, 32]. The real part of the admittance matrix, [B'] is extracted, and the determinant of [B'] is plotted as a function of frequency. It can be seen from eq. (133) that this determinant is exactly zero at an undamped natural frequency. Thus n zero-crossings will be found on the frequency axis, and the frequencies at which they occur, are the undamped natural frequencies, even though damping is present. The admittance matrix is again measured, but this time only at the undamped natural frequencies just found $[\overline{B}(\omega_0)]$. The force ratios necessary to excite these modes **individually** are then calculated from eq. (132). (Any one column of the adjoint matrix $[\hat{B}'(\omega_0)]$ represents the solution to eq. (132), i.e. it is identical to the force ratios (to within constant multiples)). Using these force ratios, the individual modes are tuned exactly for a multiple-shaker sine dwell test. For the i^{th} mode the shakers are set to produce the force ratios

$$\{F_i\} \sin \omega_i t \tag{134}$$

and the displacement response is measured to be

$$\{x\} = \{\phi_i\} \sin(\omega_i t - \pi/2) \tag{135}$$

where $\{\phi_i\}$ is the principal mode shape for the i^{th} undamped natural frequency, even though there is damping in the system. Generally a narrow-band sweep about ω_0 with fixed $\{F_i\}$ is more useful than a dwell, as it permits the plotting of Nyquist graphs from which mode shapes and modal damping values can be calculated and modal purity evaluated.

From the above, it can be seen that Asher's method, in principle, can be used to determine the undamped natural frequencies, and to isolate the corresponding individual modes of an idealized discrete structure with n degrees of freedom and linear damping, using only experimental data as input.

Application of Asher's method to real hardware, however, is more involved, as structures are continuous in character and thus have an infinite number of degrees of freedom. As shakers and accelerometers can be positioned at only a few number of locations on the structure, the measurement of [B'] (the real part of the complex admittance matrix) using single shaker sweeps is not rigorously possible. Thus if an n degree of freedom system is excited by p number of shakers, it is feasible to measure only a (p × p) incomplete complex admittance matrix $[\overline{B}_*]$, where $p < n$. As it is not possible to satisfy the exact equations (132) and (133), the best that can be done is to solve analogous equations

$$[B'_*]\ \{F_*\} = \{0\} \tag{136}$$

$$|B'_*| = 0 \tag{137}$$

where $[B'_*]$ is the corresponding sub-matrix of [B'], and $\{F_*\}$ is the (p × 1) vector of the force amplitudes of the corresponding shaker locations. The solution of eq. (137) yields a set of frequencies ω_* which are called "test natural frequencies" in Ref.[9], as they may not be the true natural frequencies which satisfy eq. (133). Furthermore, if the force ratios are chosen to satisfy eq. (136), the displacement response at the p shaker locations will be in quadrature with the force. However, the response at the other (n – p) locations, may or may not be in quadrature.

In view of the simulation study results given in Ref.[10], Hallauer and Stafford conclude, that "the use of eqs. (136) and (137) can lead to the following possible consequences, listed in order of decreasing desirability:

1. a zero of det $[B'_*]$ may occur close to but not exactly at a natural frequency, and the vector $\{F_*\}$ will effectively tune the corresponding mode,

2. a zero of det $[B'_*]$ may occur close to a natural frequency, but the vector $\{F_*\}$ will not adequately isolate the mode from interfering modes,

3. a zero of det $[B'_*]$ may be totally unrelated to any of the natural frequencies;

4. det $[B'_*]$ may have no zero in the vicinity of a natural frequency."

The quoted references discuss various methods for the elimination of spurious frequencies, and note that shaker locations play an important part in determining the success of the method. It may be necessary to move the shakers around and repeat the test.

Although there is no rigorous mathematical justification to propose that eqs. (136) and (137) will yield accurate natural frequencies and the corresponding force distributions, these equations seem to give surprisingly good results. The physical explanation for this success offered by Hallauer, is that while the p degrees of freedom are constrained to respond exactly in quadrature phase with the p forces, the (n – p) unforced degrees of freedom having significant modal energy will "cooperate" by responding nearly in quadrature phase with the forces, if ω_* is close to a natural frequency, and if the p shakers are positioned appropriately to tune the mode. In this case the entire structure will vibrate very closely to the true principal mode.

7.3. USE OF ASHER'S METHOD ON ANALYTICAL MODELS

7.3.1. Numerical Simulation Studies

Simulation studies carried out by Hallauer and Stafford [10] on mathematical models will be described in the following to illustrate the effectiveness of Asher's method. As the parameters of a mathematical structural model are known precisely, and can also be designed to produce desired characteristics (such as high modal density), absolute values are available against which the simulated test results can be compared. Furthermore, they also aid in pin-pointing the specific causes for failures of the test method.

The structure used is a cantilevered plane grid shown in Fig.39, where five discrete masses are connected by identical massless bars at right angles in the α—β plane. The bars are flexible only in vertical bending and torsion, and the degrees of freedom are vertical (γ) translations of the masses. Two models 5H and 5V are considered which are structurally identical, but have different **coupled** damping matrices. Model 5H has hysteretic damping while model 5V has viscous damping.

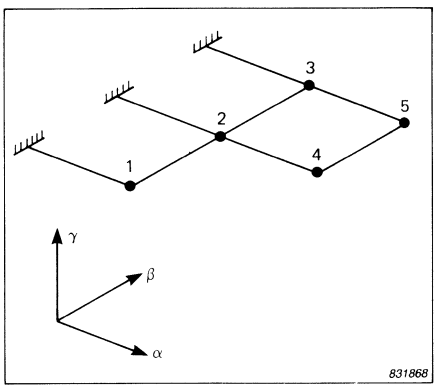

a)

Undamped normal modes of models 5H and 5V

r		1	2	3	4	5
ω_r (rad/sec)		10.908	32.055	53.500	55.409	94.924
ϕ_r	(mass)					
	(1)	0.126	0.943	−0.380	−0.595	0.121
	(2)	0.232	0.479	−0.075	0.478	−0.712
	(3)	0.337	−0.165	−0.703	0.320	0.217
	(4)	0.773	1.000	1.000	1.000	1.000
	(5)	1.000	−0.281	0.195	−0.342	−0.130

831755

b)

Fig.39. a) Structure of models 5H and 5V
b) Undamped normal modes of models 5H and 5V

By means of an optimization procedure [33], the structure was designed to have its third and fourth natural frequencies within 4% of each other. Damping values for the third and fourth modes were selected so that these modes were separated by less than one half-power bandwidth. The undamped natural frequencies and the corresponding normal modes are given in the table in Fig.39.

In Fig.40 the determinant of the real part of the admittance matrix, plotted as a function of frequency, is shown by solid lines when all the masses are excited, and by dashed lines when only masses 1 and 5 are excited for model 5H. The normalization scheme used is such that the lowest mode dominates the higher modes which consequently may disappear in the resolution of the graph. Thus Fig.40b and Fig.40c are redrawn on an expanded scale. It can be seen that the curves have a similar form to the real part of a frequency response function near the resonant frequencies. When all the masses are excited, the curves in Fig.40a and 40c have zero-crossings exactly at the undamped natural frequencies as predicted by the theory.

The force-amplitude distribution required to excite the fourth mode (the higher of the two closely spaced modes) of model 5H was calculated from $[B'(\omega_4)]\{\Gamma\} = \{0\}$. This distribution when applied to the model in a 3 rad/s narrow band sweep gave a polar plot of the admittance X_i of each mass as shown in Fig.41a. Tick marks on the response

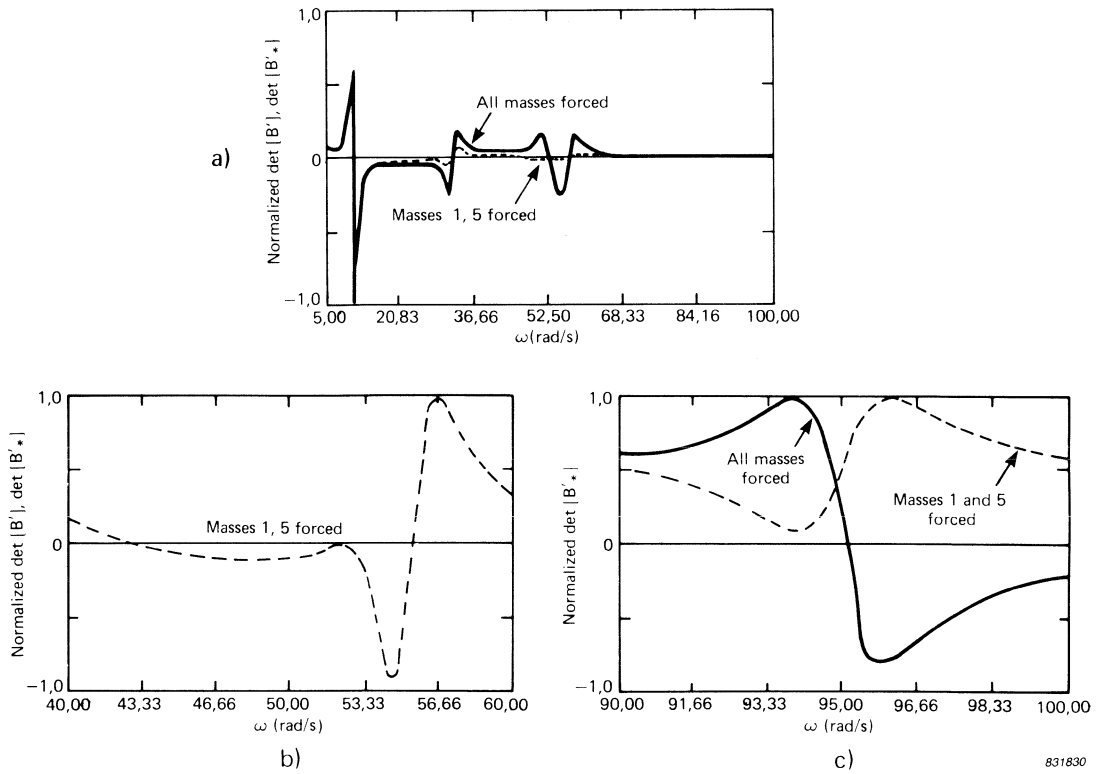

Fig.40. Determinant plots for complete and incomplete excitation of model 5H
a) 5-100 rad/s
b) 40-60 rad/s
c) 90-100 rad/s

curves indicate equal frequency increments, and arrows indicate starting frequency for each response. Conjugates of the curves are plotted when appropriate to have all the curves on the same side of the real axis. The mode shape vector $\{\phi_4\}$ indicated in the figure, was calculated from the quadrature components of the response at the zero-crossing frequency of the determinant. In this case, it is the exact mode shape according to theory.

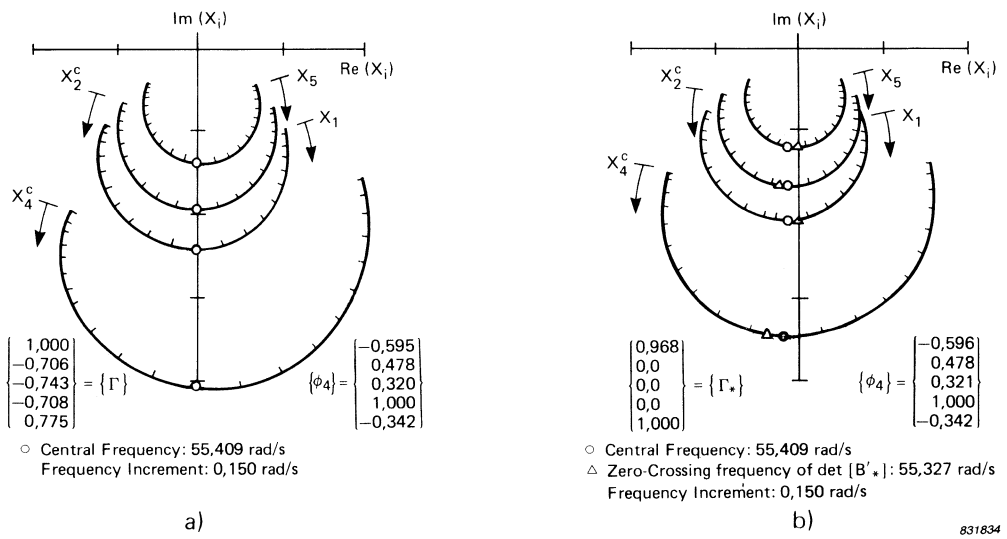

Fig.41. a) Perfect tuning with complete excitation: polar plot for the fourth mode of model 5H with all masses forced in a 3 rad/s narrow-band sine sweep
b) Excellent tuning with incomplete excitation: polar plot for the fourth mode of model 5H with masses 1 and 5 forced

If the damping had been non-coupling, then according to Kennedy & Pancu [1], each curve of the polar plot would be an arc of a perfect circle centred on the imaginary axis with its highest point passing through the origin. However, coupling damping causes deviation from circular shape, which is evident in Fig.41a where interference is introduced from the lower of the two closely spaced modes. As mentioned previously, according to theory perfect mode tuning is possible only at the undamped natural frequency for coupling damping, with responses in quadrature with the force, even though all degrees of freedom are excited.

From the table in Fig.39 it can be seen that for the first bending mode shape, all the responses are in phase. Thus intuitively one would expect all the tuning forces to be in phase as well. However, the normalized force vector for perfect tuning is given by

$$\{\Gamma\} = \begin{Bmatrix} -0{,}214 \\ -0{,}125 \\ 0{,}133 \\ 1{,}000 \\ 0{,}431 \end{Bmatrix}$$

On second thoughts the explanation is obvious, in that the appropriated forces required to tune the mode must cancel the damping forces, which are not generally distributed spatially as the mode shape.

The dashed curves of Fig.40a, b, and c show zero-crossings at 10,909, 32,070, and 55,327 rad/s which are very close to the natural frequencies of the first, second and fourth modes respectively. However, there is also a false mode crossing at 44,524 rad/s which is characterised by its gentle slope. In general, for lightly damped structures, true modes are indicated by steep slopes at the zero-crossings, and false modes by relatively gentler slopes. This can again be seen on the dashed curves of Fig.40b and c which do not have a zero-crossing for the third and the fifth modes, but nevertheless have a relatively steep slope in the vicinity of the natural frequency of the missed modes.

Fig.41b shows the polar plots of the admittance X_i of each mass obtained using incomplete excitation. The tuning corresponds to the fourth mode zero-crossing of the determinant at 55,327 rad/s on Fig.40a and b for masses 1 and 5 forced. The 5×1 force-

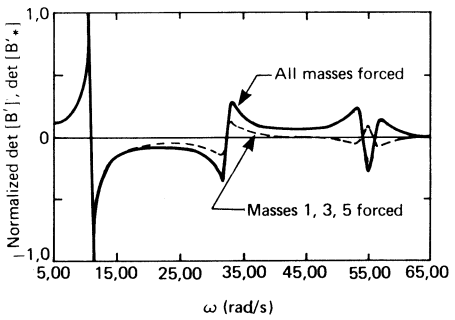

a)

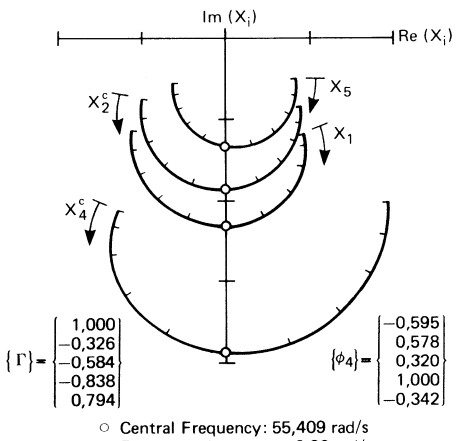

b)

831836

Fig.42. a) Determinant plots for complete and incomplete excitation of model 5V
b) Perfect tuning with complete excitation: polar plot for the fourth mode of model 5V with all masses forced in a 3 rad/s narrow- band sine sweep

amplitude distribution vector $\{F_*\}$ is derived from the 2×1 vector $\{\Gamma_*\}$ with zeros added for the unforced masses. In spite of incomplete excitation, the tuning is seen to be excellent which is often provided by Asher's method.

Fig.42a shows the determinant of the real part of the admittance matrix plotted as a function of frequency for model 5V. The force-amplitude distribution, and the polar plots of the admittance X_i of each mass for perfect tuning of the fourth mode are shown in Fig.42b, for comparison with those of model 5H in Fig.41. Because of the appropriate damping coupling element in model 5V being twice that of model 5H, greater effects of coupling between the third and the fourth modes can be seen on Fig.42b.

Fig.42a shows a false mode crossing at 44,764 rad/s for masses 1,3 and 5 excited. The polar plots of the admittances for a narrow-band sweep around this frequency with the appropriate forces are shown in Fig.43a, which clearly bears no resemblance to a mode. Finally, Fig.43b shows the polar plots of the admittances of each mass for incomplete excitation. The tuning corresponds to the third mode zero-crossing of the determinant at 53,395 rad/s for masses 1,3 and 5 forced. It can be seen that the tuning is good, but not excellent.

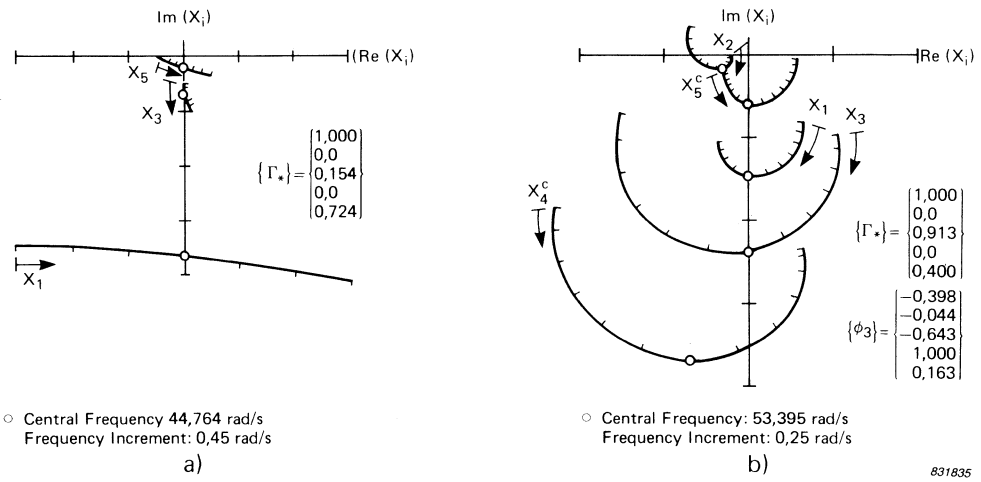

Fig.43. a) Attempted tuning of a false mode: polar plot for model 5V with masses 1,3 and 5 forced in a narrow-band sine sweep. Responses of masses 2 and 4 are far off scale.
b) Good tuning with incomplete excitation: polar plot for the third mode of model 5V with masses 1,3 and 5 forced in a 3 rad/s narrow-band sine sweep

7.3.2. Simulation Studies with FFT-Analyzer and Curve Fitting*

Another interesting study carried out by Hallauer and Gold [31] involves the use of a modern real time Fourier Analyzer and curve fitting techniques in the application of Asher's method. Again an analytical model in the form of a cantilevered plane grid shown in Figs.44a and b was used. It has fifteen degrees of freedom, two of which have nearly identical frequencies. The model contains five masses (moments of inertia are also taken into account), connected by elastic members which may twist about their own axis and bend out of the grid plane. The intersections of the bar centre lines in the grid plane are the node points of the model. The fifteen degrees of freedom are thus one out-of-plane translation and two out-of-plane rotations of each node point as

*The results in this section have been "Reprinted with permission. ©Instrument Society of America 1979. From: Instrumentation in the Aerospace Industry, Vol.25."

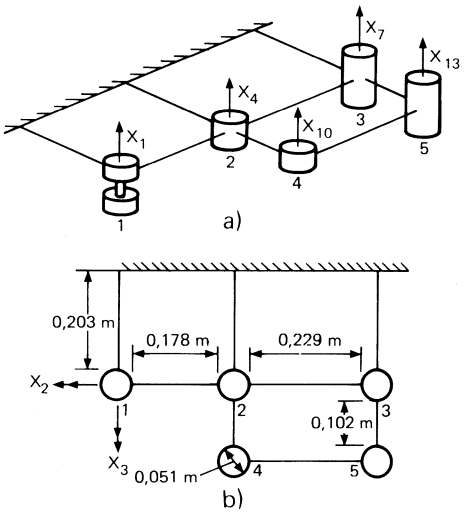

r	3	4
f_{nr}(Hz)	23,745	23,749
$\phi_{1,r}$	1,000	1,000
$\phi_{4,r}$	0,031	−0,274
$\phi_{7,r}$	0,446	−0,444
$\phi_{10,r}$	−0,421	−0,236
$\phi_{13,r}$	−0,151	0,216

T00164GB0

c)

831864

Fig.44. Analytical plane grid model
a) Pictorial view with translational degrees of freedom
b) Plan view with rotational degrees of freedom for mass 1
c) The undamped natural frequencies and the translational mode shape components $\phi_{j,r}$ of the two closely spaced modes

shown in Figs.44a and b for node 1. The numerical solution included only the lowest five modes as they were well separated from the remaining ten. Non-coupling damping was specified and the viscous damping factor was set at $\zeta_r = 0{,}03$ for each mode. The table in Fig.44 shows the undamped natural frequencies and the translational mode shape components $\phi_{j,r}$ of the two closely spaced modes.

Simulated noiseless frequency response function data for the analytical model were stored digitally in the system as if they had been generated experimentally by the Fourier Analyzer with a resolution of 0,048 Hz. The symmetric (5 × 5) frequency response function matrices represented the model's five translational degrees of freedom. The frequency response function curves indicated that there was only a single mode in the neighbourhood of 23,75 Hz. Each complex frequency response function element H(f) was fit by a least-squares algorithm to the basic analytical form (see **section 7.4.3.**):

$$H_{ij}(f) = \sum_{r=1}^{n} \frac{1}{2}\left(\frac{C_{ij_r} e^{j\theta_{ij_r}}}{(\omega_{d_r} - 2\pi f) + j\sigma_r} + \frac{C_{ij_r} e^{-j\theta_{ij_r}}}{(\omega_{d_r} + 2\pi f) - j\sigma_r}\right) \qquad (138)$$

where
C_{ij_r} = amplitude of residue of the r^{th}mode
θ_{ij_r} = phase of residue of the r^{th}mode
ω_{d_r} = damped natural frequency of the r^{th}mode
σ_r = decay rate of the r^{th}mode

The number of terms in the series in eq.(138) can be regarded as the "order" of the fit. For this example the frequency response functions were all fitted in the range 20–30 Hz to first order (n = 1) supplemented with residual functions to account for the "tails" from distant modes.

Using the curve-fit equations the determinants of the real part of the frequency response function matrix were calculated and plotted in the frequency range 23–24 Hz. Fig.45a shows this plot, which indicates a zero tangency at 24,75 Hz. The curve when plotted on finer scales, however, does reveal two zero-crossings exactly at the close natural frequencies, Fig.45b. The zero-crossings are seen to have much gentler slopes.

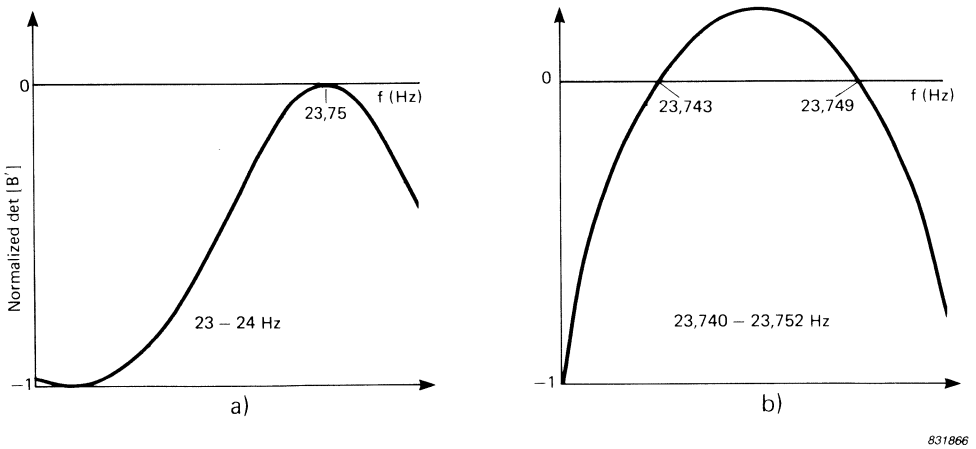

Fig.45. Determinant plots from numerical simulation
a) Frequency range 23–24 Hz
b) Frequency range 23,740–23,749 Hz

The matrices $[B'(f_0)]$ at the natural frequencies f_0 of the two closely spaced modes were calculated to evaluate the 5×1 force amplitude distributions to tune the modes. The polar plots were now drawn by simulating numerically the multiple-shaker tuning sweeps. The mode shapes measured from the polar plots are given in Fig.46a and can be seen to be virtually the same as those of the analytical model in Fig.44. The viscous damping factors calculated were also found to be 0,03 for both modes. Compared to the second and third order fits, the first order fits gave the best results.

The simulated data were now evaluated with a modal analysis package to compare the results with Asher's analysis. The package consisted of a curve-fitting analysis and a modal parameter identification analysis. In this analysis the order n of the curve-fit is equal to the number of dominant modes estimated by the operator to be in the frequency response function data. Thus the first order curve-fit could identify the parameters of only one mode and therefore produced fundamentally incorrect results. Fig.46b shows the modal parameters produced using the best second order curve-fit, which nevertheless vary substantially from the exact parameters in the table of Fig.44. According to Hallauer and Gold, they "were unable to develop a curve-fit of any order from which better estimates of the modal parameters could be obtained. Moreover, using a finer resolution than 0,048 Hz (simulating a zoom transform with real data) could not have improved the results."

r	3	4
f_{nr}(Hz)	23,743	23,749
$\phi_{1,r}$	1,000	1,000
$\phi_{4,r}$	0,031	–0,274
$\phi_{7,r}$	0,446	–0,445
$\phi_{10,r}$	–0,421	–0,236
$\phi_{13,r}$	–0,151	0,217

a)

r	3	4
f_{nr}(Hz)	23,648	23,754
$\phi_{1,r}$	–0,816	1,000
$\phi_{4,r}$	0,249	–0,094
$\phi_{7,r}$	–0,109	0,003
$\phi_{10,r}$	1,000	–0,232
$\phi_{13,r}$	–0,068	0,021

T00166GB0

b)

831865

Fig.46. The undamped natural frequencies and the translational mode shape components $\phi_{j,r}$ of the two closely spaced modes using
a) Asher's method
b) Modal analysis package

7.4. SCOPE FOR FUTURE WORK WITH ASHER'S METHOD

In **Section 7.2.** it was pointed out that difficulties may occur from spurious "test resonance frequencies" not related to the actual modes of vibration. Furthermore problems may also arise if the exciters are not placed judiciously around the structure. This is, however, a practical matter, which is not subject to automatic resolution, and which requires judgement of an experienced engineer.
Classical methods of force appropriation have relied on human iteration and have thus been time consuming. However, with the fast data acquisition and processing techniques available today, one can envision three improvements which can further extend the scope of Asher's method, and help overcome some of the limitations.

7.4.1. Number of Excitation and Response Measurement Points

It was shown previously that for the application of Asher's method to the basic equation

$$\{\bar{U}_*\} = [\bar{B}_*]\{F_*\} = [B'_*]\{F_*\} + j[B''_*]\{F_*\} \tag{139}$$

it was necessary to evaluate $|B'_*|$ as a function of frequency. As determinant operation is only valid for square matrices, the matrix $[B'_*]$ has to be square, implying that the number of excitation points must equal the number of response measurement locations. Invariably the number of response points far exceeds the number of excitation points and the modal amplitudes at many of these points may be of the same order of magnitude as the modal amplitudes at the excitation points. Thus to allow this additional data to be used in the force appropriation algorithm, necessitates relaxation of the requirement that the matrix $[B'_*]$ be square. To do this and yet be able to use Asher's method, Ibáñez [15] suggested plotting the singular values of the real part of the admittance matrix (which equal the eigenvalues of the product $[B'_*]^T[B'_*]$) and the determinant of the matrix product $[B'_*]^T[B'_*]$ as a function of frequency. Note that the matrix $[B'_*]$ can be rectangular in this case, e.g. an $(l \times p)$ complex matrix denoted by $[\tilde{B}_*]$, whose real part is $[\tilde{B}'_*]$, can be obtained by exciting the structure at p number of locations and measuring the response at l number of points. The resonant frequencies are characterized by an extremely sharp peaking of these plotted functions, which are always positive. Each individual singular value peaks only once, as was the case for eigenvalue crossovers. As data from more response points is utilized, one can anticipate reduction in the occurrence of spurious frequencies.

7.4.2. Multiple Exciter Sweeps

From the previous section it can be seen that each of the p columns of the admittance matrix is obtained experimentally from the result of a single exciter sweep with response recorded at l number of locations. Thus $\{\bar{U}_*\} = [\tilde{B}_*]\{F_*\}$

i.e.

$$\begin{Bmatrix} \bar{U}_1 \\ \bar{U}_2 \\ \vdots \\ \bar{U}_l \end{Bmatrix} = \begin{bmatrix} \bar{b}_{11} & \bar{b}_{12} \ldots\ldots \bar{b}_{1p} \\ \bar{b}_{21} & \bar{b}_{22} \ldots\ldots \bar{b}_{2p} \\ \vdots & \vdots \quad\quad \vdots \\ \bar{b}_{l1} & \bar{b}_{l2} \ldots\ldots \bar{b}_{lp} \end{bmatrix} \begin{Bmatrix} F_1 \\ F_2 \\ \vdots \\ F_p \end{Bmatrix} \tag{140}$$

Since the accuracy of the modal parameters depends on how precisely one can measure the admittance matrix, great demands are placed on the excitation to maintain the vibration amplitudes close to operating levels in all areas of interest. Furthermore, for the sake of linearity, the structure must be evenly excited, which is relatively easy for simple structures and individual components. In large structures however, such as aircraft wings, train car bodies, and other large assemblies with numerous joints, vibration energy is quickly dissipated within the structure, producing widely different vibration amplitudes at various locations. Thus by using multipoint excitation, a larger amount of energy can be fed more uniformly to the structure than with single point excitation. Furthermore it allows the use of more and cheaper exciters.

To accomplish this, Ibáñez [15] suggested exciting the structure by q sets of forces (q not necessarily equal to p) and adjoining the results to obtain

$$\begin{bmatrix} \bar{U}_{11} & \bar{U}_{12} & \cdots & \bar{U}_{1q} \\ \bar{U}_{21} & \bar{U}_{22} & \cdots & \bar{U}_{2q} \\ \vdots & \vdots & & \vdots \\ \bar{U}_{l1} & \bar{U}_{l2} & \cdots & \bar{U}_{lq} \end{bmatrix} = \begin{bmatrix} \bar{b}_{11} & \bar{b}_{12} & \cdots & \bar{b}_{1p} \\ \bar{b}_{21} & \bar{b}_{22} & \cdots & \bar{b}_{2p} \\ \vdots & \vdots & & \vdots \\ \bar{b}_{l1} & \bar{b}_{l2} & \cdots & \bar{b}_{lp} \end{bmatrix} \begin{bmatrix} F_{11} & F_{12} & \cdots & F_{1q} \\ F_{21} & F_{22} & \cdots & F_{2q} \\ \vdots & \vdots & & \vdots \\ F_{p1} & F_{p2} & \cdots & F_{pq} \end{bmatrix} \tag{141}$$

i.e. $$[\tilde{U}] = [\tilde{B}_*]\,[\tilde{F}] \tag{142}$$

The matrix $[\tilde{B}_*]$ can then be solved for by the pseudo inversion of $[\tilde{F}]$,

$$[\tilde{B}_*] = [\tilde{U}]\,[\tilde{F}]^{-1} \tag{143}$$

Thus $[\tilde{B}_*]$ and hence $[\tilde{B}'_*]$ can be found by using q sets of multipoint excitation forces. In order to introduce sufficient energy into the system and to excite all the modes, these q sets have to be chosen judiciously so that they are linearly independent. To assist this choice, Ibáñez suggests the use of **a priori** model described in Ref [15] to guide one in determining which forcing is best. One obvious choice would be the use of the **a priori** estimate of the correct force appropriation to isolate each mode, which would ensure not only linear independence, but also the excitation of all the modes. As the matrix $[\tilde{B}'_*]$ is not square, a unique set of appropriated forces will not necessarily be obtained when the solution $[\tilde{B}'_*]\,\{F_*\} = \{0\}$ is evaluated at the resonant frequencies, and therefore a vector average would have to be used.

7.4.3. Wide Band Excitation

The commercial availability of moderately priced two channel real time FFT analyzers has opened the possibilities for the use of impulse and wide band random signals as the source of excitation. Because of the enormous time savings achieved through real time analysis, the dominant technique for modal testing of structures, since the early 1970's has therefore been the use of single-point-excitation, with digital Fourier analysis techniques being employed to determine the frequency response functions (FRF's). Current technical literature abounds with methods and algorithms for the extraction of modal parameters from the measured frequency response functions.

The modal parameter extraction algorithms are based on analytic curve-fitting the measured data in both the time and the frequency domains. While least-squares and collocation methods are used for curve-fitting the impulse response in the time domain, the techniques used in the frequency domain are quadrature peak-picking, Kennedy and Pancu circle-fit, and multiple degree of freedom algorithms. Choice of the most suitable algorithm will invariably depend on the data to be analyzed.

Modal Density: Apart from non-linearities, the dynamic characteristic of the structure that has significant influence on the accuracy of the modal parameters extracted, is the modal density. The term modal density unfortunately, has not been rigorously defined, and has been used loosely in literature to give a subjective judgement of the frequency proximity of adjacent modes. In an effort to quantify this term, Lang [34] suggested using the following definition

$$\text{Average Modal Density} = \frac{\text{Averaged Modal Bandwidth}}{\text{Averaged Natural Frequency Spacing}}$$

Thus the local modal density (that between two adjacent modes) would be given by the average of the bandwidths of those two modes, divided by the difference of their undamped natural frequencies. Similarly the average modal density in any frequency range would be obtained by averaging the bandwidths of the n modes contained in that frequency range, and dividing it by the average of the (n-1) intermode frequency spacings found. (The average intermode spacing is numerically equal to the difference between the highest and the lowest natural frequencies divided by (n-1)).

Using the above definition, Lang in Ref [34] has shown that the precision of modal parameter extraction for modal densities of 0,2 or less depends on the frequency resolution of the analysis system. Thus very accurate results can be achieved in this range because of the "zoom" processing facilities available today. Between 0,2 and 1,0, the accuracy depends on the precision and sophistication of the parameter identification algorithm. For modal densities greater than 1,0, the structure's dynamics defy modal decomposition by signal processing techniques alone, because of the inability to properly identify the number of modes to be extracted from the frequency response functions."Zoom" processing proves unable to separate overlapping modal bandwidths and spatial decomposition becomes mandatory. This was also corroborated by the simulation studies carried out by Hallauer and Gold and described in section 7.3.2. It should be noted that even though noise-free analytical data was used as input in their studies, they were unable to achieve acceptable modal parameters. Also Klosterman [35], in investigating the dynamics of weakly coupled systems, concluded that "close agreement between computed and experimentally measured mode shapes cannot be expected" for such systems. This is because, for weakly coupled subsystems, even small changes in one of the subsystem's properties have an enormous influence on the system modes.

Multiple Input Excitation: Most of the modal analysis software packages available today, estimate experimental mode shapes from using a single column or a single row of the frequency response function matrix, see Ref.[36, 46]. When resonance frequencies are not closely spaced, quite accurate results are obtained by using, for example, the quadrature peak-picking technique. If, however, the frequencies are closely spaced, difficulties arise not only in locating the frequencies at which to identify the modes, but also the mode shapes based on one exciter location may not agree with those based on another exciter location. As pointed out by Craig et al in Ref [36], quadrature peak-picking technique clearly gives erroneous modal vector estimates, and so would circle-fit and multi-degree-of-freedom curve fit techniques. Thus more recently, efforts have been put in to examine the possibilities of combining the information from several rows or columns of the frequency response function matrix to obtain better estimates of the modal vectors. Among the techniques developed are those described in Ref [37] and [38, 39, 40] which obtain the frequency response functions based on several input locations. In other respects multiple inputs may be used to obtain preliminary data, and modal tuning procedures may be employed to refine the modal parameter estimates of closely spaced modes. The use of multiple shakers has the added advantage that they can later be employed to carry out the actual tuned-dwell test based on the results of modal tuning.

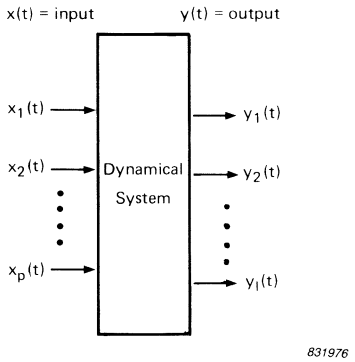

Fig. 47 Dynamical System whose response is measured at l number of points when excited at p number of locations

Consider a dynamical system such as shown in Fig. 47, which is excited at p input locations and whose response is measured at l number of points. Thus the frequency response function matrix to be measured is given by

$$[\tilde{H}(f)] = \begin{bmatrix} H_{11}(f) & H_{12}(f) & \cdots & H_{1p}(f) \\ H_{21}(f) & H_{22}(f) & \cdots & H_{2p}(f) \\ \vdots & \vdots & & \vdots \\ H_{l1}(f) & H_{l2}(f) & \cdots & H_{lp}(f) \end{bmatrix} \quad (144)$$

where $H_{ij}(f)$ is the frequency response function for excitation at point j and response measurement at point i.

For the single-input data acquisition method, the structure is excited sequentially at each of the desired p locations, and the response measured at each of the l locations, by which columns of the frequency response function matrix are obtained successively. (It should be noted that curve-fitting techniques can also be used to generate columns of the FRF matrix corresponding to response locations where no physical input is applied). In practice a dual channel real time FFT analyzer can be used to acquire and process one FRF at a time. However, it would be preferable to record all the acceleration responses in a single excitation run, and post-process the data to obtain the FRF's.

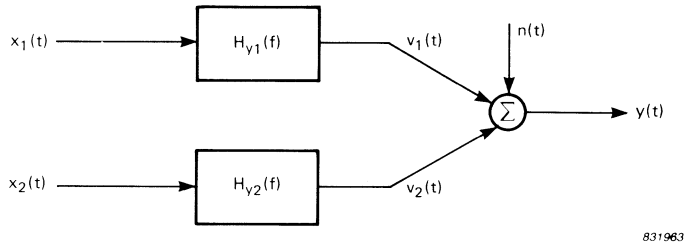

Fig. 48 Dual-Input, Single-Output System

For the multiple-input data acquisition method, the structure is excited with two or more exciters simultaneously. For the sake of simplicity consider a two-input, single output system, such as that shown in Fig. 48 (since generalization to multiple outputs $y_i(t)$ (i = 1,2...l) complicates the notation). The Fourier transformed response Y(f) of such a system is given by

$$Y(f) = H_{y1}(f)\, X_1(f) + H_{y2}(f)\, X_2(f) + N(f) \tag{145}$$

where $X_1(f)$ and $X_2(f)$ are the Fourier transformed inputs at input coordinates 1 and 2. N(f) is noise at the response coordinate, which is not linearly related to the inputs. It can be shown (see Refs [38, 39, 40, 41, 42]), that assuming averaging is employed

$$YX_1^\star = H_{y1} X_1 X_1^\star + H_{y2} X_2 X_1^\star$$

$$YX_2^\star = H_{y1} X_1 X_2^\star + H_{y2} X_2 X_2^\star$$

where * indicates complex conjugation. These equations can be written as

$$\begin{aligned} G_{1y} &= H_{y1} G_{11} + H_{y2} G_{12} \\ G_{2y} &= H_{y1} G_{21} + H_{y2} G_{22} \end{aligned} \tag{146}$$

where the subscripts of the Auto and the Cross Spectra G are according to the conventional definition. Equation (146) can be solved for H_{y1} and H_{y2} i.e.

$$\begin{aligned} H_{y1} &= \frac{G_{1y}G_{22} - G_{2y}G_{12}}{G_{11}G_{22} - |G_{12}|^2} = \left(\frac{G_{1y}}{G_{11}}\right)\left\{\frac{1 - \dfrac{G_{2y}G_{12}}{G_{1y}G_{22}}}{1 - \gamma_{12}^2}\right\} \\ H_{y2} &= \frac{G_{11}G_{2y} - G_{21}G_{1y}}{G_{11}G_{22} - |G_{12}|^2} = \left(\frac{G_{2y}}{G_{22}}\right)\left\{\frac{1 - \dfrac{G_{1y}G_{21}}{G_{2y}G_{11}}}{1 - \gamma_{12}^2}\right\} \end{aligned} \tag{147}$$

provided the ordinary Coherence Function γ_{12}^2 between the inputs $X_1(f)$ and $X_2(f)$ is not equal to unity, i.e.

$$\gamma_{12}^2 = \frac{|G_{12}|^2}{G_{11}\, G_{22}} \neq 1$$

From eqs. (146) and (147) it can be seen that when $G_{12} = G_{21}^{\star} = 0, \gamma_{12}^2 = 0$, and H_{y1} and H_{y2} are given by the single-input expressions

$$H_{y1} = \frac{G_{1y}}{G_{11}}$$

and

$$H_{y2} = \frac{G_{2y}}{G_{22}}$$

As long as the inputs are not fully correlated, eq.(147) can be used in theory to obtain FRFs when two inputs are acting simultaneously. If the Coherence between the inputs is unity, eq.(147) are not valid, and a different analysis is required, see Ref.[41]. The above analysis can be extended to apply to any arbitrary number of inputs and outputs.

Curve-Fitting: Gold and Hallauer in Ref [31] have illustrated, that it is advantageous to apply Asher's method to analytically-synthesized FRF's rather than to the experimentally-obtained FRF's. It can be shown [43], that a frequency response function for input $x_j(t)$ and output $y_i(t)$ can be written as

$$H_{ij}(f) = \frac{Y_i(f)}{X_j(f)} = \sum_{r=1}^{n} \left(\frac{A_{ij_r}}{j2\pi f - s_r} + \frac{A_{ij_r}^{\star}}{j2\pi f - s_r^{\star}} \right) \qquad (148)$$

where $s_r = -\sigma_r + j\omega_{d_r}$
σ_r = decay rate of the r^{th}mode
ω_{d_r} = damped natural frequency of the r^{th}mode
A_{ij_r} = complex residue of the r^{th}mode
and n = order of the curve fit

Eq. (148) can also be written in the form as given by eq. (138).

Although real structures have an infinite number of degrees of freedom, only a finite number of modes can be used to describe the dynamic behaviour of systems. To reduce the number of degrees of freedom, a frequency range of interest between f_a and f_b may be chosen. In this range the number of modes would be finite, which can be employed in the analytically - synthesized FRF. Eq. (148) can now be used to fit the measured FRF in the frequency range of interest, and residual terms can be included to approximate the contributions of modes whose frequencies lie below f_a and above f_b. Eq. (148) is thus modified to

$$H_{ij} = L_{ij} + \sum_{r=r_a}^{r=r_b} \left(\frac{A_{ij_r}}{j\omega - s_r} + \frac{A_{ij_r}^{\star}}{j\omega - s_r^{\star}} \right) + Z_{ij} \qquad (149)$$

where r_a = lower mode index of the frequency range of interest
r_b = upper mode index of the frequency range of interest
$\omega = 2\pi f$
L_{ij} = lower residual term and
Z_{ij} = upper residual term

The lower residual term can be written as

$$L_{ij} = -\frac{Y_{ij}}{\omega^2}$$

where Y_{ij} is called the inertia restraint, and Z_{ij} is called the residual flexibility. Other forms of eq. (149) are given in Ref [43]. Four real constants are associated with each mode that is included in the summation. Thus, if N modes are considered in the frequency range from r_a to r_b, 4N + 2 real constants are required to define H_{ij}. These constants may be obtained by application of a curve-fit algorithm.

There are several advantages in obtaining analytical FRF's by curve fitting experimental FRF's prior to modal tuning, as illustrated by Craig and Chung [42] and Hallauer et al [10, 31]. They are

1) Significant data reduction is achieved.

2) Initial estimates of natural frequencies are provided.

3) It permits interpolation between experimental data points to establish natural frequencies more accurately.

4) Residual functions can be employed so that resonant modes can be tuned.

5) Noisy data are smoothed out.

Modal Tuning: Asher's method of modal tuning can now be applied once the (n×n) FRF matrix $[\bar{H}(f)]$ has either been measured, or synthesized from modal parameters obtained by curve-fitting the measured data over the frequency range of interest. n is the number of degrees of freedom. Thus a relation similar to eq. (124) can be written

$$\underset{(n\times 1)}{\{\bar{Y}\}} = \underset{(n\times n)}{[\bar{H}]}\ \underset{(n\times 1)}{\{\bar{X}\}} \tag{150}$$

where the only difference is that all the quantities are Fourier Transforms. By separating the real and the imaginary parts of the complex FRF matrix we obtain

$$\{\bar{Y}\} = [H']\{\bar{X}\} + j[H'']\{\bar{X}\} \tag{151}$$

where $[H']$ is the real part of $[\bar{H}]$
and $[H'']$ is the imaginary part of $[\bar{H}]$.

If the input $\{\bar{X}\}$ is monophase then $\{\bar{X}\}$ can be assumed to be a real vector at each frequency and the response has real and imaginary parts given by

$$\text{Re}\{\bar{Y}\} = [H']\{\bar{X}\}$$

and (152)

$$\text{Im}\{\bar{Y}\} = [H'']\{\bar{X}\}$$

Using the same reasoning as given in **Section 7.2**, that if f_0 and $\{\overline{X}(f_0)\}$ are chosen to satisfy

$$\text{Re}\{\overline{Y}(f_0)\} = [H'(f_0)]\{\overline{X}(f_0)\} = \{0\} \tag{153}$$

then each f_0 corresponds to an undamped natural frequency and each corresponding $\{\overline{Y}(f_0)\}$ is a principal mode.

For a real structure it is clearly not possible to measure a (n×n) FRF matrix, as n is infinite, and one has to suffice with a (p×p) FRF matrix $[H'_*]$ where $p<n$. Thus a corresponding equation

$$[H'_*(f_*)]\{\overline{X}(f_*)\} = \{0\} \tag{154}$$

has to be solved. For a non-trivial solution it is necessary that

$$\det[H'_*(f_*)] = 0 \tag{155}$$

whose roots should give excellent approximations to the undamped natural frequencies. Once these are identified, the matrix $[H'_*(f_*)]$ can be calculated, for example using eq. (149). The distribution of forces necessary to tune the particular mode can then be obtained from eq. (154). A narrow band frequency sweep about f_* with fixed $\{\overline{X}(f_*)\}$ can be carried out analytically to refine the modal parameter estimates.

Before concluding this section it should be noted, that if the frequency response function data is available in equation form, then Newton's iteration method can be employed to solve the roots of eq. (155) as used by Hallauer et al [10, 31] and Craig et al [36, 42], i.e.

$$f_{i+1} = f_i - D_i\left(\frac{f_i - f_{i-1}}{D_i - D_{i-1}}\right) \tag{156}$$

where $D_i = \det[H'_*(f_i)]$.(If the data is available only at discrete frequencies, two approaches, interpolation and curve-fitting, may be used, as described in Ref [10]).

7.5. MINIMUM COINCIDENT RESPONSE METHOD

It was pointed out earlier, that very often in practice there are far more response measurement locations than excitation positions. Thus the FRF matrix which is measured or synthesized would be given by eq. (144), in which $[\widetilde{H}(f)]$ is a (l×p) matrix, where l the number of response locations is much greater than p the number of excitation positions. Eqs. (150 and 151) would then be modified to

$$\underset{(l\times 1)}{\{\widetilde{Y}\}} = \underset{(l\times p)}{[\widetilde{H}]}\underset{(p\times 1)}{\{\widetilde{X}\}} = [\widetilde{H'}]\{\widetilde{X}\} + j[\widetilde{H''}]\{\widetilde{X}\} \tag{157}$$

where $[\widetilde{H'}]$ is the real part of $[\widetilde{H}]$
and $[\widetilde{H''}]$ is the imaginary part of $[\widetilde{H}]$

If the input $\{\widetilde{X}\}$ is assumed to be real, as in the previous section, then

$$\text{Re}\{\widetilde{Y}\} = \{\widetilde{Y}\}_R = [\widetilde{H'}]\{\widetilde{X}\} \tag{158}$$

As the matrix $[\tilde{H}']$ is not square, Asher's method cannot be applied directly. Nevertheless, to make use of the response data from points which are not excited, Ibáñez suggested the use of the pseudo-inverse as described in Ref [15]. Another technique, however, which makes use of this data for modal tuning is proposed by Ensminger and Turner [44], which is named the "Minimum coincident response method" by Craig et al in Refs [36, 42]. In this technique the sum of the squares of the coincident (inphase, real) displacements is minimized, subject to a normalizing constraint on the quadrature (imaginary) response components. Thus the quantity

$$\epsilon = \{\tilde{Y}\}_R^T \{\tilde{Y}\}_R = \{\tilde{X}\}^T [\tilde{H}']^T [\tilde{H}'] \{\tilde{X}\} \tag{159}$$

which may be termed the error function, is minimized subject to the condition

$$\tilde{Y}_{iI} = [\tilde{H}'']_i \{\tilde{X}\} = 1 \tag{160}$$

where $[\tilde{H}'']_i$ is the i^{th} row of $[\tilde{H}'']$,

and thus $\tilde{Y}_{iI}$ is the quadrature response at the i^{th} point.

Using the method of least squares, Ensminger and Turner in [44] have shown, that the expression for $\{\tilde{X}\}$ which minimizes ϵ for a specific f is given by

$$\{\tilde{X}\} = \frac{1}{[\tilde{H}'']_i \left([\tilde{H}']^T [\tilde{H}']\right)^{-1} [\tilde{H}'']_i^T} \left([H']^T [H']\right)^{-1} [\tilde{H}'']_i^T \tag{161}$$

The procedure employed in [44] uses eq. (161) to evaluate $\{\tilde{X}\}$ at a sequence of discrete values of f, and then eq. (159) to compute the resulting least-squares error $\epsilon(f)$. $\epsilon(f)$ is now plotted as a function of frequency, and the frequencies f_0 corresponding to the local minima of $\epsilon(f)$, are taken as the natural frequency estimates. Eq. (161) is now used to compute $\{\tilde{X}(f_0)\}$ and the mode shape is determined from the quadrature response given by

$$\{\tilde{Y}\} = j[\tilde{H}''(f_0)] \{\tilde{X}(f_0)\} \tag{162}$$

In order to compare the effectiveness of the Standard Asher method and the Minimum Coincident Response Method, in producing modal vector estimates of systems having closely-spaced-modes, Craig et al in Ref.[36] carried out some experiments on a coupled beam model shown in Fig.49a). Frequency response functions were obtained using originally an experimental bandwidth of 10 Hz, which concentrated the spectrum around the lowest pair of closely-spaced-frequency modes. Multi-degree of freedom curve-fit results for eight frequency response functions are presented. Each FRF exhibited two dominant roots in the 118-121 Hz frequency range, and the phase angles of some of the roots were significiantly different than $\pm$ 90°. The "modes" based on having a single shaker at point 1 appeared to be at approximately 119,0 Hz and 119,5 Hz while the "modes" based on having a single shaker at point 6 appeared to be at 118,8 Hz and 120,0 Hz. The "mode" at 119,0 Hz is, however, radically different than the 118,8 Hz "mode".

The multi-degree of freedom curve-fit results were now used to synthesize analytical frequency response functions, which were used as input to the modal tuning algorithms for the Standard Asher and the Minimum Coincident Response method. Although results for several bandwidths are given in Ref.[36] in form of tables, the modal tuning results for bandwidths of 10 Hz and 0,0256 Hz are reproduced here as Figs.49b) and c) and 49d) and e) respectively.

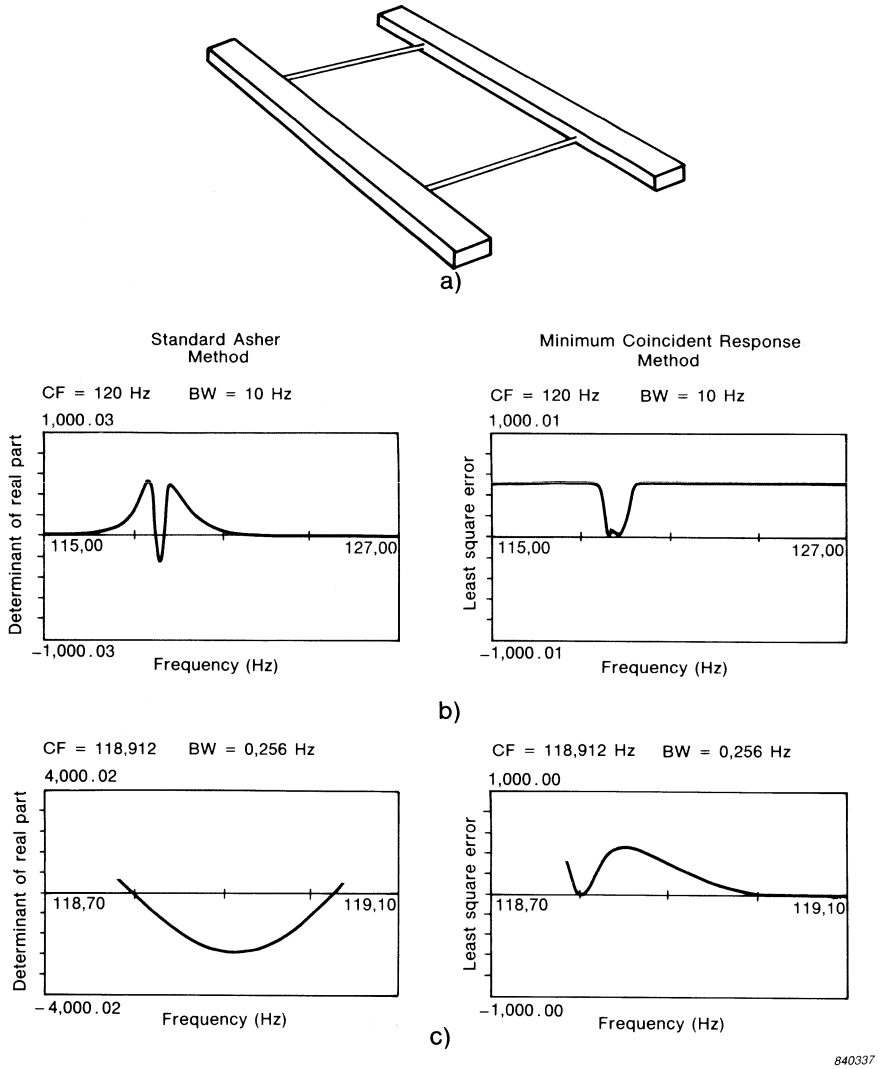

Fig.49. a) Weakly-Coupled Dual Beam Experimental Model
b) Standard Asher Tuning using 10 Hz Analysis Bandwidth
c) Minimum Coincident Response Tuning using 10 Hz Analysis Bandwidth
d) Standard Asher Tuning using 0,256 Hz Analysis Bandwidth
e) Minimum Coincident Response Tuning using 0,256 Hz Analysis Bandwidth

In Craig's results for several bandwidths, two modes at approximately 118,8 Hz and 119,0 Hz are consistently identified by both methods. Phase errors of the identified modes are also reduced for reducing analysis bandwidth. Less phase errors are also apparent for the 118,8 Hz mode than for the 119,0 Hz mode. In Figs.49c) and e) the minimum of $\epsilon(\omega)$ is much sharper for the 118,8 Hz mode than for the mode at 119,0 Hz. Furthermore, the agreement between the Standard Asher and the Minimum Coincident Response Method is better for the 118,8 Hz mode than for the second mode. The tuned modes do not exhibit the symmetrical antisymmetric behaviour, which was expected on account of the apparent symmetry of the structure. The explanation for this discrepancy offered by Craig, is the mode sensitivity of weakly coupled systems.

7.6. CONCLUSIONS

On the basis of research carried out in Ref [36], Craig et al concluded that "Standard Asher tuning and Minimum Coincident Response tuning, both provide rational means for employing multiple rows or columns of the FRF matrix to improve modal vector estimates." In Ref.[42] he used a simple two-degree of freedom analytical model as well as the above described model to investigate the frequency separation capabilities of both these methods. Based on the application of both tuning procedures to analytically-formulated FRF's and to experimentally-acquired FRF's, Craig states "it appears that the Standard Asher Method may be able to separate modes in situations where the Minimum Coincident Response method breaks down."

The latter method was also applied by Ensminger and Turner to synthesized frequency response function data, obtained from the ground vibration test at Boeing, of the 747 Carrier Aircraft Modification (CAM) airplane (Space Shuttle Orbiter). They concluded that this "approach was found to provide more consistent results" than Asher's method, which was also applied to the same synthesized FRF's.

It is thus evident that further research is required on the application of tuning procedures for the testing of complex structures. In view of the above, it is worth bearing in mind, that there exists no ideal modal test to date, and that many a sophisticated mathematical algorithm may fail when applied to real hardware, with measurement errors, noise and non-linearity effects—emphasising the indispensibility of an experienced engineer with a critical eye. It is perhaps easy to appreciate why modal testing has become more of an art than a science.

8. REFERENCES

[1] KENNEDY, C.C. and PANCU, C.D.P. "Use of Vectors in Vibration Measurement and Analysis", *J. Aeronautical Sciences,* Vol. 14, No. 11, 1947, pp. 603-625.

[2] STAHLE, C.V. Jr., "Phase Separation Technique for Ground Vibration Testing," *Aerospace Engineering,* July 1962

[3] LEWIS, R.D. and WRISLEY, D.L. "A System for the Excitation of Pure Natural Modes of Complex Structures.", *J. Aeronaut Sci,* 17 (11), pp 705-722 (1950)

[4] TRAILL-NASH, R.W. "On the Excitation of Pure Natural Modes in Aircraft Resonance Testing," *J. Aeronaut. Sci,* 125 (12), pp 775-778 (Dec 1958)

[5] HAWKINS, F.J. "GRAMPA-An Automatic Technique for Exciting the Principal Modes of Vibration of Complex Structures," *Royal Aircraft Establishment, Farnborough, Technical Report* No 65142, England (1965)

[6] TAYLOR, G.A. GAUKROGER, D.R. and SKINGLE, C.W. "MAMA—A Semi-Automatic Technique for Exciting the Principal Modes of Vibration of Complex Structures," *Royal Aircraft Establishment, Farnborough, Technical Report* No 67211, England (Aug 1967)

[7] ASHER, G.W. "A Method of Normal Mode Excitation Utilizing Admittance Measurements", *Proc. National Specialists' Meeting on Dynamics and Aeroelasticity, Ft. Worth, Inst. of Aeronautical Sciences.,* 1958, pp. 69-76

[8] BISHOP, R.E.D. and GLADWELL, G.M.L., "An Investigation into the Theory of Resonance Testing", *Phil. Trans. of the Royal Society of London, Series A, Vol. 255, Mathematical and Physical Sciences,* 1963, pp. 241-280

[9] CRAIG, R.R. and SU, Y.W.T., "On Multiple Shaker Resonance Testing", *AIAA Journal,* Vol. 12, No. 7, 1974, pp. 924-931

[10] HALLAUER, W.L. Jr., and STAFFORD, J.F., "On the Distribution of Shaker Forces in Multiple-Shaker Modal Testing", *The Shock and Vibration Bulletin, Bull.* 48, Part 1, 1978, pp. 49-63

[11] SMITH, S., STROUD, R.C., HAMMA, G.A., HALLAUER, W.L. and YEE, R.C., "MODALAB-A Computerized Data Acquisition and Analysis System for Structural Dynamic Testing", *Proc. of the 21st International Instrumentation Symposium, Vol. 12, Philadelphia, Instrument Society of America,* 1975, pp. 183-189

[12] STROUD, R.C., SMITH, S. and HAMMA, G.A., "MODALAB-A New System for Structural Dynamic Testing", *The Shock and Vibration Bulletin, Bulletin 46, Part 5,* 1976, pp. 153-175

[13] HAMMA, G.A., SMITH, S. and STROUD, R.C., "An Evaluation of Excitation and Analysis Methods for Modal Testing", *SAE Paper No. 760872, Aerospace Engineering and Manufacturing Meeting,* San Diego, 1976

[14] SMITH, S. and WOODS, A.A. Jr., "A Multiple Driver Admittance Technique for Vibration Testing of Complex Structures," *Shock Vib. Bull., U. S. Naval Res. Lab., Proc. 42,* Part 3, pp 15-23 (Jan 1972)

[15] IBÁÑEZ, P., "Force Appropriation by Extended Asher's Method", *SAE Paper No. 760873, Aerospace Engineering and Manufacturing Meeting,* San Diego, 1976

[16] DECK, A., "Automatic Appropriation of Excitation at Ground Vibration Tests of Airplanes", *Communication presented at the Euromech 22 Congress "Dynamics of Mechanics"* New Castle (15-16 Sept. 1970)

[17] BISHOP, R.E.D. and JOHNSON, D.C. "The Mechanics of Vibration", *Cambridge University Press*

[18] MEIROVITCH, L. "Elements of Vibration Analysis", *Mc.Graw-Hill*

[19] MEIROVITCH L. "Analytical Methods In Vibration, *The Macmillan Company*

[20] KIMBAL, A.L. and LOVELL, D.E. "Internal Friction in Solids, *Physics Review* 30 (2nd ser.) pp 948-959 (1927)

[21] THOMSON, W.T., "Theory of Vibration with Applications (2nd Ed.)", *George Allen and Unwin Ltd.*

[22] FRAZER, R.A., DUNCAN, W.F. and COLLAR, A.R. "Elementary Matrices", *Cambridge University Press*

[23] FRAEIJS DE VEUBEKE, B.M. "A variational approach to pure mode excitation based on characteristic phase lag theory." *AGARD Report 39,* April 1956

[24] BISHOP, R.E.D., GLADWELL, G.M.L. and MICHAELSON, S. "The Matrix Analysis of Vibration", *Cambridge University Press,* 1965

[25] MOROSOW, G. and AYRE, R.S., "Force Apportioning for Modal Vibration Testing Using Incomplete Excitation," *Shock Vib. Bull., U. S. Naval Res. Lab., Proc. 48,* Part 1, pp 39-48 (1978)

[26] RAY, J.D. and BERT, C.W. "The Use of Lissajous Figures in Vibration Testing" *Shock Vib. Bull, Vol 44*, Part 5, pp 117-127, Aug. 1974

[27] BLACKMAN, P.F. "The Pole-Zero Approach to System Analysis", *Rowse Muir Publications Ltd.*

[28] DE VRIES, G. -"Beitrag zur Bestimmung der Schwingungseigenschaften von Flugzeugen im Standversuch unter Besonderer Berücksichtigung eines neuen Verfahrens zur Phasenmessung.," *Z W B, Forschungs Bericht,* No. 1882, 1942, p. 115

[29] SALYER, R. A., JUNG E. J. Jr., HUGGINS, S.L., and STEPHENS, B.L., "An Automatic Data System for Vibration Modal Tuning and Evaluation," *NASA Tech. Note TN D*-7945 (Apr 1975).

[30] BUDD, R.W., "A New Approach to Modal Vibration Testing of Complex Aerospace Structures," *Inst. Environ. Sciences, Proc.,* 15, pp 14-20 (1969)

[31] GOLD, R.R. and HALLAUER, W.L.Jr., "Modal Testing with Asher's Method Using a Fourier Analyzer and Curve Fitting," *Proc. 25th International Instrumentation Symposium, The Instrument Society of America,* May 7-10, 1979, pp. 185-192

[32] BROWN, D., CARBON, G. and RAMSEY, K., "Survey of Excitation Techniques Applicable to the Testing of Automotive Structures", *SAE Paper No. 770029, International Automotive Engineering Congress and Exposition,* Detroit, 1977

[33] HALLAUER, W.L. Jr., WEISSHAAR, T.A., and SHOSTAK, A.G., "A Simple Method for Designing Structural Models with Closely Spaced Modes of Vibration", *Journal of Sound and Vibration,* Vol. 61, No. 2, November 1978

[34] LANG, G.F., "Modal Density - a Limiting Factor in Analysis" *S/V Sound and Vibration*, March 1983

[35] KLOSTERMAN, A.L. "Modal Surveys of Weakly Coupled Systems", *SAE Paper No. 760876*, Nov. 1976

[36] CRAIG, R.R.Jr., CHUNG, Y.T.and BLAIR, M. "Modal Vector Estimation For Closely-Spaced-Frequency Modes", *Report No. CAR 82-1, Center for Aeronautical Research, Bureau of Engineering Research,* The University of Texas at Austin, Feb. 1982

[37] RICHARDSON, M.and KNISKERN, J. "Identifying Modes of Large Structures from Multiple Input and Response Measurements", *SAE Paper No. 760875,* Nov. 1976

[38] ALLEMANG, R. J. "Investigation of Some Multiple Input/Output Frequency Response Function Experimental Modal Analysis Techniques", *Ph. D. Thesis,* University of Cincinnati, 1980

[39] ALLEMANG, R.J. ROST, R.W. and BROWN, D.L. "Dual Input Estimation of Frequency Response Functions for Experimental Modal Analysis of Aircraft Structures", *IMAC Conference Orlando* FA 1982

[40] CARBON, G.D. BROWN, D.L. and ALLEMANG, R.J. "Application of Dual Input Excitation Techniques to the Modal Testing of Commercial Aircraft", *IMAC Conference Orlando* FA 1982

[41] BENDAT, J.S. and PIERSOL, A.G. "Engineering Applications of Correlation and Spectral Analysis", Chapter 8 *John Wiley & Sons,* 1980

[42] CRAIG, R.R.Jr and CHUNG, Y.T. "Modal Analysis Using a Fourier Analyzer, Curve-Fitting, and Modal Tuning", *Report No. CAR 81-1, Center for Aeronautical Research, Bureau of Engineering Research,* University of Texas at Austin, Oct. 1981

[43] BROWN, D.L., ALLEMANG, R.J., ZIMMERMAN, R. and MERGEAY, M., "Parameter Estimation Techniques for Modal Analysis", *SAE Paper* No. 790221 (Mar 1979).

[44] ENSMINGER, R.R. and TURNER, M.J., "Structural Parameter, Identification from Measured Vibration Data", *AIAA/ASME/ASCE/AHS 20thSDM Conference* April 1979, pp. 410-416

[45] HERLUFSEN, H. "Dual Channel FFT Analysis", *Brüel & Kjær Technical Review* Nos.1 and 2, 1984

[46] BRÜEL & KJÆR, Instruction Manual, Modal 3.0 (SMS 3001 A) Modal Analysis

9. RELATED LITERATURE

ANDERSON, D

"Multi-point Excitation Techniques",
Environmental Engineering, Dec. 1971

ANGELINI, J.J. and DARRAS, B.,

"Determination of Eigenmodes of the RF8 Airplane Starting from a Ground Vibration Test with Non-Appropriated Excitation",
ONERA NT1/1984RY, (1973) (In French)

BÉATRIX, C.

"La Détermination Expérimentale des Caractéristiques Vibratoires des Structures,"(Experimental Determination of the Vibratory Characteristics of Structures),
ONERA Technical Note No. 212, (1973)

BONNEAU, E

"Détermination des Caractéristiques Vibratoires D'une Structure a L'aide de L'expression de la Puissance Complexe Fournie." (Determination of the Vibration Characteristics of a Structure from the Expression of the Complex Power Supplied),
La Recherche Aerospatiale, No. 130, May-June 1969

COUPRY, G.

"Measure des Amortissements Génèralises Non Diagonaux d'une Structure lors d'une Essai au sol de Vibration,"(Measurement of Non-Diagonal Generalized Damping Ratios During Ground Vibration Tests),
La Recherche Aerospatiale No. 4, July-August, 1977

CHU, F.H., VOORHEES, C., METZGER, W.W., and WILDING, R.,

"Spacecraft Modal Testing Using Systematic Multi-Shakers Sine-Dwell Testing Techniques",
Shock Vib. Bull., U. S. Naval Res. Lab., Proc., 51, Part 2, pp 41-58 (May 1981)

DAT, R.,

"Determination of the Natural Modes of a Structure from a Vibration Test with Arbitrary Excitation,"
RAE Library Translation No. 1741, 1973

EWINS, D.J.,

"State-of-the-Art Assessment of Mobility Measurements - A Summary of European Results,"
Shock Vib. Bull., U. S. Naval Res. Lab., Proc. 51, part 1, pp 15-35 (May 1981)

EWINS, D.J.,

"Whys and Wherefores of Modal Testing,"
J. Soc. Environ. Engrs., 18 (3), pp 3-15 (1979)

EWINS, D.J.
"Measurement and Application of Mechanical Impedance Data"
Part 1—Introduction and Ground Rules,"
Journal of the Society of Env. Eng., Dec. 1975
Part 2—Measurement Techniques,
Journal of the Society of Env. Eng., March 1976
Part 3—Interpretation and Application of Measured Data,
Journal of the Society of Env. Eng., June 1976

FERRANTE, M., STAHLE, C.V., and BRESKMAN, D.G.,
"Single-Point Random and Multi-Shaker Sine Spacedraft Modal Testing",
Shock Vib. Bull., U. S. Naval Res. Lab., Proc. 50, Part 2, pp 191-198 (1980)

FRAEIJS DE VEUBEKE, B.M.,
"Déphasage caractéristiques et vibrations forcées d'une système amorti",
Académie Royale de Belguique. Bulletin de la Classe des Sciences, Series 5, 34, 624-641, 1948

GAUKROGER, D.R. and COPLEY, J.C.,
"Methods for Determining Undamped Normal Modes and Transfer Functions from Receptance Measurements",
Royal Aircraft Establishment, Farnborough, Technical Report No 79071, England (June 1979)

GAUKROGER, D.R., SKINGLE, C.W. and HERON, K.H.
"Numerical Analysis of Vector Response Loci",
Jounal of Sound and Vibration (1973) 29(3), pp 341-353

HALLAUER, W.L. Jr.
"A Method For Experimental Modal Separation",
NASA Report N77-23539, Feb. 1976—May 1977

HALLAUER, W.L. Jr.
"A Study of Multi-Shaker Modal Survey Testing",
NASA Report N79-10447, Feb. 1976—Sep. 1978

HALLAUER, W.L. Jr.
"Active Damping of Modal Vibration by Force Apportioning",
NASA Report N80-28372, Jun. 1978—Jun. 1980

HALLAUER, W.L. Jr. and FRANCK, A.,
"On Determining the Number of Dominant Modes in Sinusoidal Structural Response",
Shock Vib. Bull., US Naval Res. Lab., Proc. 49, Part 2, pp 19-33 (Sept 1979)

HAWKINS, F.J. and MOUSLEY, R.F.
"Resonance Tests on A Beagle B206 Series Aircraft",
Royal Aircraft Establishment, Farnborough, Technical Report No 3589, England

HERON, K.H., GAUKROGER, D.R. and SKINGLE, C.W.
"The Processing of Response Data to obtain Modal Frequencies and Damping Ratios",
Royal Aircraft Establishment, Farnborough, Technical Report No 74027, England

IBÁÑEZ, P., "Review of Analytical and Experimental Techniques for Improving Structural Dynamic Models", *Welding Res. Council, Bull.* 249 (June 1979)

IBÁÑEZ, P., "Methods for the Identification of Dynamic Parameters of Mathematical Structural Models from Experimental Data", *Nuclear Engineering and Design* 27 (1974), pp 209-219

LEPPERT, E.L., LEE, S.H., DAY, F.D., CHAPMAN, P.C., and WADA, B.K., "Comparison of Modal Test Results: Multipoint Sine Versus Single Point Random", *SAE Paper* No. 760879 (1976)

PENDERED, J.W. "Theoretical Investigation into the Effects of Close Natural Frequencies in Resonance Testing", *Journal Mechanical Engineering Science* Vol. 7 No 4, 1965

RADES, M., "On Modal Analysis of Structures with Non-Proportional Damping", *Rev. Roum. Sci. Tech. - Méc. Appl.,* 26 (4), pp 605-622 (July-Aug.1981)

RADES, M., "Methods for the Analysis of Structural Frequency Response Measurement Data", *Shock Vib. Dig.,* 8 (2), pp 73-88 (Feb. 1976)

RADES, M., "Analysis Techniques of Experimental Frequency Response Data," *Shock Vib. Dig.,* 11 (2), pp 15-24 (Feb 1979)

RADES M., "Paramter Identification of a Structure with Combined Coulomb and Hysteretic Damping", *Rev. Roum. Sci. Techn—Méc. Appl., Tome 27,* No 2, pp 299-308, Bucarest, 1982

RAMSEY, K.A., "Effective Measurements for Structural Dynamics Testing, Part I", *Sound and Vibration, Vol.9, No. 11,* November 1975, pp. 24-35

RAMSEY, K.A., "Effective Measurements for Structural Dynamics Testing, Part II", *Sound and Vibration, Vol. 10, No. 4,* April 1976, pp. 18-31

RICHARDSON, M. "Modal Analysis Using Digital Test Systems", *Seminar on Understanding Digital Control and Analysis in Vibration Test Systems, published by the Shock and Vibration Information Center, Naval Research Laboratory, Washington D. C.,* May 1975, pp. 43-64

STAHLE, C.V. and FORLIFER, W.R.,
"Ground Vibration Testing of Complex Structures",
Proc. of AIA-AFOSR Flight Flutter Testing Symposium, May 1958

TRAILL-NASH, R.W., LONG G., and BAILEY, C.M.
"Experimental Determination of the Complete Dynamical Properties of a Two-Degree-of-Freedom Model having nearly Coincident Natural Frequencies",
Journal Mechanical Engineering Science Vol.9, No. 5, 1967

PIAZZOLI, G.,
"New Methods for Ground Tests of Aeronautical structures",
Aeroelastic Problems in Aircraft Design, Lecture Series, Von Karman Inst. Fluid Dyn. (May 7-11, 1979)

WALGRAVE, S.C. and EHLBECK, J.M.
"Understanding Modal Analysis",
SAE Technical Paper 780695

APPENDICES

APPENDIX A

Definitions and Operating Rules for Determinants and Matrices

Finite degrees of freedom systems are described analytically in terms of linear algebraic equations. Since manipulation of these equations for systems having more than three degrees of freedom can become lengthy and cumbersome, some form of algebraic shorthand becomes necessary. This is conveniently achieved using matrix notation which furthermore makes the mathematics more tractable. The intention of this appendix, however, is **not** to expound on the theories of Determinants and Matrices, but rather to give just the very necessary definitions and operating procedures, such that the understanding of the main text can be facilitated when followed step by step.

Determinants

A determinant is an array of elements or numbers written between vertical bars. For example a second order determinant is defined as

$$|A| = \begin{vmatrix} a_{11} & a_{12} \\ a_{21} & a_{22} \end{vmatrix} = a_{11}a_{22} - a_{12}a_{21} \qquad \text{(A1)}$$

where a_{11}, a_{12}, a_{21}, a_{22} are called the elements. The elements in a horizontal line are said to form a row, and the elements in a vertical line are said to form a column. The first suffix of the element identifies the row while the second identifies the column. Thus a_{21} implies the element in the second row and the first column.

In expanding a determinant of order 3 or greater, it is necessary to define what is called a Minor M_{ij} and a Cofactor C_{ij} of the element a_{ij}.

Minors

The minor M_{ij} of the element a_{ij} is defined as the sub-determinant formed by deleting the i^{th} row and the j^{th} column of the original determinant.

Consider the determinant

$$|A| = \begin{vmatrix} a_{11} & a_{12} & a_{13} \\ a_{21} & a_{22} & a_{23} \\ a_{31} & a_{32} & a_{33} \end{vmatrix} \qquad \text{(A2)}$$

The minor M_{21} of a_{21} is thus given by

$$M_{21} = \begin{vmatrix} a_{11} & a_{12} & a_{13} \\ a_{21} & a_{22} & a_{23} \\ a_{31} & a_{32} & a_{33} \end{vmatrix} = \begin{vmatrix} a_{12} & a_{13} \\ a_{32} & a_{33} \end{vmatrix} = (a_{12}\,a_{33} - a_{13}\,a_{32}) \qquad \text{(A3)}$$

Cofactors
The cofactor C_{ij} of the element a_{ij} is defined by

$$C_{ij} = (-1)^{i+j} M_{ij} \tag{A4}$$

Thus the cofactor C_{21} of the element a_{21} (using eq. (A3)) is given by

$$C_{21} = (-1)^{2+1} M_{21} = (-1)(a_{12}\, a_{33} - a_{13}\, a_{32}) \tag{A5}$$

Expansion of a Determinant
The determinant of eq. (A2) can be expanded as the sum of the products of the element and its cofactor, either along any row or along any column, for example,

$$\begin{vmatrix} a_{11} & a_{12} & a_{13} \\ a_{21} & a_{22} & a_{23} \\ a_{31} & a_{32} & a_{33} \end{vmatrix} = a_{21}\, C_{21} + a_{22}\, C_{22} + a_{23}\, C_{23} \tag{A6}$$

$$= a_{21}\,(-1)^{2+1} M_{21} + a_{22}\,(-1)^{2+2} M_{22} + a_{23}\,(-1)^{2+3} M_{23}$$

$$= a_{21}\,(-1) \begin{vmatrix} a_{12} & a_{13} \\ a_{32} & a_{33} \end{vmatrix} + a_{22}(1) \begin{vmatrix} a_{11} & a_{13} \\ a_{31} & a_{33} \end{vmatrix} + a_{23}(-1) \begin{vmatrix} a_{11} & a_{12} \\ a_{31} & a_{32} \end{vmatrix}$$

$$= -a_{21}\,(a_{12}a_{33} - a_{13}a_{32}) + a_{22}\,(a_{11}a_{33} - a_{13}a_{31}) - a_{23}\,(a_{11}a_{32} - a_{12}a_{31}) \tag{A7}$$

In this example the determinant is said to be expanded along its second row.

Matrices
An array of elements arranged in m rows and n columns is called an m × n matrix, and usually enclosed in square brackets. For example

$$[A] = \begin{bmatrix} a_{11} & a_{12} & a_{13} & a_{14} \\ a_{21} & a_{22} & a_{23} & a_{24} \\ a_{31} & a_{32} & a_{33} & a_{34} \end{bmatrix} \tag{A8}$$

is a 3 × 4 matrix. It is thus like a determinant, but with one essential difference. Whilst a determinant has a single numerical value, arrived at by a process of reduction, a matrix may not be reduced in this way, but remains an array of elements or numbers.

Row Matrix
A row matrix is one in which m = 1 and is written either between square or normal brackets, for example

$$[A] = (a_{11}\ a_{12}\ a_{13}) \tag{A9}$$

Column Matrix
A column matrix (often called a vector) is one in which n = 1 and is written between curly brackets, for example

$$\{A\} = \begin{Bmatrix} a_{11} \\ a_{12} \\ a_{13} \end{Bmatrix} \tag{A10}$$

Square Matrix
A square matrix is one in which the number of rows is equal to the number of columns. It is referred to as an (n × n) matrix or a matrix of order n.

Symmetric Matrix
A square matrix is said to be symmetrical if the elements about the principal diagonal in the upper right half are identical to those in the lower left half i.e. $a_{ij} = a_{ji}$. For example

$$\begin{bmatrix} 1 & -3 & 4 \\ -3 & 2 & -5 \\ 4 & -5 & 7 \end{bmatrix} \tag{A11}$$

Singular Matrix
If the determinant of a matrix is zero, the matrix is said to be singular.

Zero (Null) Matrix
A zero or null matrix denoted by [0] in one in which all the elements are zero,

$$[0] = \begin{bmatrix} 0 & 0 & 0 \\ 0 & 0 & 0 \end{bmatrix} \tag{A12}$$

Unit (Identity) Matrix
A unit or identity matrix denoted by [I] is a square matrix in which all the elements in the principal diagonal (top left to bottom right) are unity, and the remainder are all zero.

$$[I] = \begin{bmatrix} 1 & 0 & 0 \\ 0 & 1 & 0 \\ 0 & 0 & 1 \end{bmatrix} \tag{A13}$$

Diagonal Matrix
A square matrix having elements a_{ii} along the principal diagonal with all other elements equal to zero is a diagonal matrix designated by $\lceil A \rfloor$

$$\lceil A \rfloor = \begin{bmatrix} a_{11} & 0 & 0 \\ 0 & a_{22} & 0 \\ 0 & 0 & a_{33} \end{bmatrix} \tag{A14}$$

Transposed Matrix

The transpose $[A]^T$ of a matrix [A] is one in which the rows and columns of [A] are interchanged. For example, if

$$[A] = \begin{bmatrix} 4 & 3 & -7 \\ 5 & -6 & 2 \end{bmatrix} \qquad [A]^T = \begin{bmatrix} 4 & 5 \\ 3 & -6 \\ -7 & 2 \end{bmatrix} \tag{A15}$$

Thus a column matrix when transposed becomes a row matrix,

$$\{A\} = \begin{Bmatrix} 6 \\ 3 \\ -2 \end{Bmatrix} \qquad \{A\}^T = (6 \quad 3 \quad -2) \tag{A16}$$

It should be noted that a symmetric matrix is equal to its transpose, see eq. (A11).

Adjoint Matrix

An adjoint (adjugate) of a matrix [A] is the transpose of the matrix of the cofactors of [A]. Thus, if the cofactor matrix [C] of [A] is

$$[C] = \begin{bmatrix} C_{11} & C_{12} & C_{13} \\ C_{21} & C_{22} & C_{23} \\ C_{31} & C_{32} & C_{33} \end{bmatrix} \tag{A17}$$

the adjoint of [A] is designated by $[\hat{A}]$ and is given by

$$\text{adj } [A] = [\hat{A}] = [C]^T = \begin{bmatrix} C_{11} & C_{21} & C_{31} \\ C_{12} & C_{22} & C_{32} \\ C_{13} & C_{23} & C_{33} \end{bmatrix} \tag{A18}$$

Inverse Matrix

The inverse (reciprocal) matrix $[A]^{-1}$ of the matrix [A] is defined such that

$$[A]^{-1}[A] = [A][A]^{-1} = [I] \tag{A19}$$

It is evaluated from $[A]^{-1} = \dfrac{[\hat{A}]}{|A|}$

Rules for Matrix Operations

Addition

Two matrices may be added, if they have the same number of rows and columns. For example

$$\begin{bmatrix} 3 & -4 & 2 \\ -1 & 5 & 4 \end{bmatrix} + \begin{bmatrix} 6 & 2 & -3 \\ 4 & -1 & -5 \end{bmatrix} = \begin{bmatrix} 9 & -2 & -1 \\ 3 & 4 & -1 \end{bmatrix} \tag{A20}$$

Multiplication by a Constant k

The multiplication of matrix [A] by a constant k involves multiplication of each element by k. Thus

$$k \begin{bmatrix} a_{11} & a_{12} & a_{13} \\ a_{21} & a_{22} & a_{23} \end{bmatrix} = \begin{bmatrix} ka_{11} & ka_{12} & ka_{13} \\ ka_{21} & ka_{22} & ka_{23} \end{bmatrix} \tag{A21}$$

Multiplication of Matrices

If [A] is an (m × n) matrix and [B] is an (r × p) matrix, the product [A][B] (in this order) is defined only when r = n and the product [C] is a (m × p) matrix, see Fig.(A1). The matrices in this case are called **conformable.**

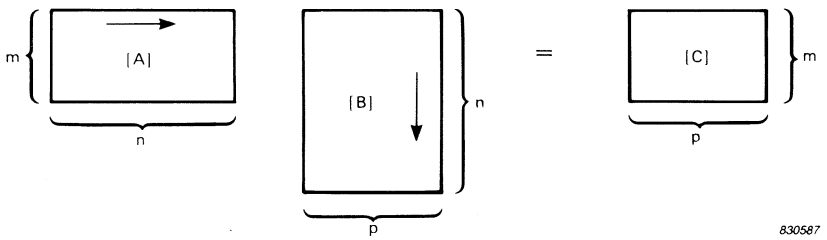

Fig.A1. Matrix Multiplication [A][B] = [C]

For calculation of the elements of the product matrix, the arrangement shown in Fig.A2 is very useful. In this example a (3 × 3) matrix [A] is post-multiplied by a (3 × 2) matrix [B].

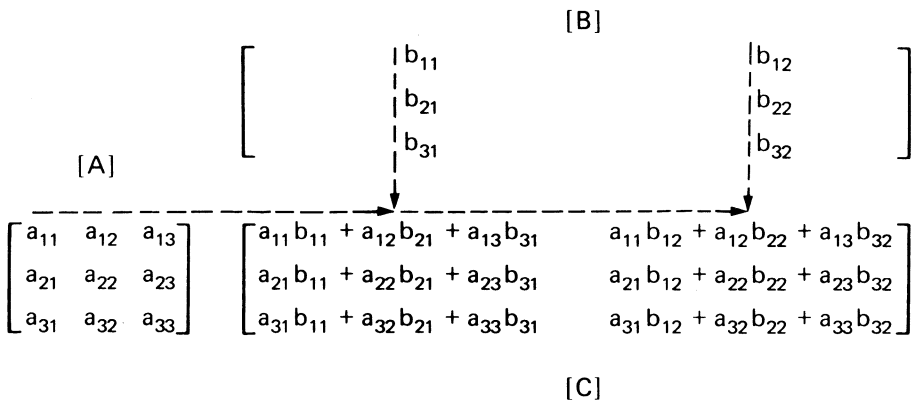

Fig.A2. Matrix Arrangement for calculation of the elements of the product matrix

It can be seen that the element c_{ij} of the product matrix occupies the intersection of the row of the first matrix and the column of the second matrix which are used for computing c_{ij}. The element c_{ij} of the product matrix is calculated from the expression

$$c_{ij} = a_{i1}\, b_{1j} + a_{i2}\, b_{2j} + \text{———} + a_{in}\, b_{nj} = \sum_{k=1}^{n} a_{ik}\, b_{kj} \qquad \text{(A22)}$$

when an (m × n) matrix [A] is post-multiplied by an (n × p) matrix [B]. It should be noted that matrix multiplication is not commutative, i.e. even if [A][B] and [B][A] are defined, $[A][B] \neq [B][A]$ in general. Thus the order of multiplication of matrices must be strictly observed. Therefore to be precise, for the product [A][B], matrix [B] is said to be **pre-multiplied** by matrix [A], and matrix [A] is said to be **post-multiplied** by matrix [B].

The arrangement shown in Fig.A2 can easily be extended to product of three or more matrices as shown in Fig.A3. As can be seen, three matrices are multiplied together. The product of two matrices [B][C] is first obtained, which is then pre-multiplied by matrix [A].

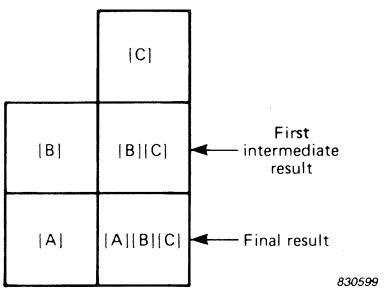

Fig.A3. Matrix Arrangement for product of three or more matrices

Transpose of Matrix Products

When two matrices [A] and [B] are conformable when multiplied in the order [A][B], the transpose of their product is given by $[B]^T[A]^T$, i.e. if

$$[A]\,[B] = [P] \qquad \text{(A23)}$$

then $$[P]^T = \left([A]\,[B]\right)^T = [B]^T[A]^T$$

This transposition rule can be extended to any number of matrices, i.e. if

$$[A]\,[B]\,[C] = [P]\,[C] = [Q] \qquad \text{(A24)}$$

then $$[Q]^T = [C]^T[P]^T = [C]^T[B]^T[A]^T$$

Furthermore, the product of a matrix with its own transpose gives a symmetric matrix. If

$$[A]^T[A] = [P] \tag{A25}$$

then

$$[P]^T = \left([A]^T[A]\right)^T = [A]^T\left([A]^T\right)^T = [A]^T[A] = [P] \tag{A26}$$

Since $[P]^T = [P]$, matrix [P] the product of $[A]^T[A]$ must be symmetric.

For example,

$$\begin{bmatrix} 2 & 4 & 3 \\ -1 & 2 & -5 \end{bmatrix} \begin{bmatrix} 2 & -1 \\ 4 & 2 \\ 3 & -5 \end{bmatrix} = \begin{bmatrix} 29 & -9 \\ -9 & 30 \end{bmatrix}$$

The result of eq. (A25) can be further extended to show that if [A] is a symmetric matrix, $[B]^T[A][B]$ is also a symmetric matrix. This is illustrated as follows,

$$[B]^T[A][B] = [B]^T[P] = [Q]$$

then

$$[Q]^T = [P]^T\left([B]^T\right)^T = [P]^T[B] = [B]^T[A]^T[B] \tag{A27}$$

Since [A] is a symmetric matrix, i.e. $[A] = [A]^T$, eq. (A27) reduces to

$$[Q]^T = [B]^T[A]^T[B] = [B]^T[A][B] = [Q] \tag{A28}$$

Since $[Q]^T = [Q]$, matrix [Q] which is the product $[B]^T[A][B]$ must be symmetric.

Partitioned Matrices

A matrix may be partitioned into sub-matrices as shown

$$\left[\begin{array}{ccc|c} 3 & -2 & 5 \\ 1 & 4 & 0 \\ 0 & 3 & -2 \\ \hline 2 & -1 & 4 \end{array}\right] = \left[\begin{array}{c|c} [A] & [B] \\ \hline [C] & [D] \end{array}\right]$$

where the sub-matrices are

$$[A] = \begin{bmatrix} 3 & -2 \\ 1 & 4 \\ 0 & 3 \end{bmatrix} \quad \{B\} = \begin{Bmatrix} 5 \\ 0 \\ -2 \end{Bmatrix}$$

$$[C] = \begin{pmatrix} 2 & -1 \end{pmatrix} \quad [D] = (4)$$

The normal rules of matrix algebra also apply to partitioned matrices, where the submatrices can be treated as elements. For example,

$$\left[\begin{array}{c|c} [A] & [B] \\ \hline [C] & [D] \end{array}\right] \left\{\begin{array}{c} \{x\} \\ \hline \{y\} \end{array}\right\} = \left[\begin{array}{c} [A]\{x\} + [B]\{y\} \\ \hline [C]\{x\} + [D]\{y\} \end{array}\right] \tag{A29}$$

$$\left[\begin{array}{c|c} [A] & [B] \\ \hline [C] & [D] \end{array}\right] \left[\begin{array}{c|c} [E] & [F] \\ \hline [G] & [H] \end{array}\right] = \left[\begin{array}{c|c} [A][E] + [B][G] & [A][F] + [B][H] \\ \hline [C][E] + [D][G] & [C][F] + [D][H] \end{array}\right] \tag{A30}$$

APPENDIX B

Inversion of a (3 × 3) Matrix

Consider a set of simultaneous linear algebraic equations given by

$$\begin{aligned} a_{11}x_1 + a_{12}x_2 + \ldots + a_{1n}x_n &= y_1 \\ a_{21}x_1 + a_{22}x_2 + \ldots + a_{2n}x_n &= y_2 \\ \ldots\ldots\ldots\ldots\ldots\ldots\ldots\ldots\ldots\ldots &\quad \ldots \\ a_{n1}x_1 + a_{n2}x_2 + \ldots + a_{nn}x_n &\quad y_n \end{aligned} \tag{B1}$$

This set of equations can be written in matrix form as

$$\begin{bmatrix} a_{11} & a_{12} & \ldots & a_{1n} \\ a_{21} & a_{22} & \ldots & a_{2n} \\ \ldots\ldots\ldots\ldots\ldots\ldots & & & \\ a_{n1} & a_{n2} & \ldots & a_{nn} \end{bmatrix} \begin{Bmatrix} x_1 \\ x_2 \\ \ldots \\ x_n \end{Bmatrix} = \begin{Bmatrix} y_1 \\ y_2 \\ \ldots \\ y_n \end{Bmatrix} \tag{B2}$$

Thus

$$[A]\{x\} = \{y\} \tag{B3}$$

where [A] is the square matrix and $\{x\}$ and $\{y\}$ are column matrices. To solve the above set of equations requires determination of a matrix [R] which is such that

$$[A][R] = [R][A] = [I] \tag{B4}$$

where

$$[I] = \begin{bmatrix} 1 & 0 & 0 & \ldots\ldots & 0 \\ 0 & 1 & 0 & \ldots\ldots & 0 \\ 0 & 0 & 1 & \ldots\ldots & 0 \\ \ldots\ldots\ldots\ldots\ldots\ldots\ldots\ldots & & & & \\ 0 & 0 & 0 & \ldots\ldots & 1 \end{bmatrix}$$

is called the **Unit** or **Identity** matrix.

The matrix [R] is called the **inverse** of [A] and is denoted by $[A]^{-1}$. If this matrix [R] can be found, eq. (B3) can be premultiplied on both sides to give

$$[R][A]\{x\} = [R]\{y\}$$

This reduces to

$$\{x\} = [R]\{y\} = [A]^{-1}\{y\} \tag{B5}$$

since

$$[R][A]\{x\} = [I]\{x\} = \{x\}$$

Denoting the elements of [R] by r_{ij} eq. (B5) can be written as

$$\begin{Bmatrix} x_1 \\ x_2 \\ .. \\ x_n \end{Bmatrix} = \begin{bmatrix} r_{11} & r_{12} & \cdots & r_{1n} \\ r_{21} & r_{22} & \cdots & r_{2n} \\ \cdots & \cdots & \cdots & \cdots \\ r_{n1} & r_{n2} & \cdots & r_{nn} \end{bmatrix} \begin{Bmatrix} y_1 \\ y_2 \\ .. \\ y_n \end{Bmatrix} \tag{B6}$$

giving the n relations

$$\begin{aligned} x_1 &= r_{11}\, y_1 + r_{12}\, y_2 + \ldots + r_{1n}\, y_n \\ x_2 &= r_{21}\, y_1 + r_{22}\, y_2 + \ldots + r_{2n}\, y_n \\ &\cdots\cdots\cdots\cdots\cdots\cdots\cdots \\ x_n &= r_{n1}\, y_1 + r_{n2}\, y_2 + \ldots + r_{nn}\, y_n \end{aligned} \tag{B7}$$

which is the solution of eq. (B1).

The matrix [R] which is the inverse of matrix [A] is given by the formula

$$[R] = [A]^{-1} = \frac{[\hat{A}]}{|A|} \tag{B8}$$

where $[\hat{A}]$ is defined as the adjoint of [A] and $|A|$ is the determinant of [A]. To calculate these, consider a (3 × 3) matrix [A] given by

$$[A] = \begin{bmatrix} a_{11} & a_{12} & a_{13} \\ a_{21} & a_{22} & a_{23} \\ a_{31} & a_{32} & a_{33} \end{bmatrix} \tag{B9}$$

The determinant of [A] can be expanded, for example, along the first row as

$$|A| = a_{11} C_{11} + a_{12} C_{12} + a_{13} C_{13} \tag{B10}$$

where the cofactors $C_{ij} = (-1)^{i+j} M_{ij}$ are given by

$$C_{11} = (-1)^{1+1} M_{11} \qquad C_{12} = (-1)^{1+2} M_{12} \qquad \text{and } C_{13} = (-1)^{1+3} M_{13} \tag{B11}$$

Substituting eq. (B11) in eq. (B10) yields

$$|A| = a_{11}(+1)\begin{vmatrix} a_{22} & a_{23} \\ a_{32} & a_{33} \end{vmatrix} + a_{12}(-1)\begin{vmatrix} a_{21} & a_{23} \\ a_{31} & a_{33} \end{vmatrix} + a_{13}(+1)\begin{vmatrix} a_{21} & a_{22} \\ a_{31} & a_{32} \end{vmatrix} \tag{B12}$$

i.e.

$$|A| = a_{11}\,(a_{22}a_{33} - a_{23}a_{32}) - a_{12}\,(a_{21}a_{33} - a_{23}a_{31}) + a_{13}\,(a_{21}a_{32} - a_{22}a_{31}) \tag{B13}$$

To determine $[\hat{A}]$ the adjoint of [A], we need to calculate the remaining of the cofactors C_{21} C_{22} C_{23} C_{31} C_{32} and C_{33} and write the cofactor matrix [C] i.e. the matrix whose elements are the cofactors of [A],

$$[C] = \begin{bmatrix} C_{11} & C_{12} & C_{13} \\ C_{21} & C_{22} & C_{23} \\ C_{31} & C_{32} & C_{33} \end{bmatrix} \tag{B14}$$

By transposing the cofactor matrix, the adjoint of matrix [A] is obtained, i.e.

$$[\hat{A}] = [C]^T = \begin{bmatrix} C_{11} & C_{21} & C_{31} \\ C_{12} & C_{22} & C_{32} \\ C_{13} & C_{23} & C_{33} \end{bmatrix} \tag{B15}$$

Substitution of eqs. (B13) and (B15) in eq. (B8) gives $[A]^{-1}$ and thus the solution of the set of eqs. (B1). If $|A| = 0$ the elements of $[A]^{-1}$ approach infinity (or are indeterminate at best), and the inverse matrix $[A]^{-1}$ does not exist and the matrix [A] is said to be **singular**.

Consider a numerical example of three linear algebraic equations

$$\begin{aligned} x_1 \quad +4x_2 \quad\quad &= y_1 \\ -2x_1 \quad +2x_2 \quad +x_3 &= y_2 \\ 3x_1 \quad\quad +x_2 \quad\quad &= y_3 \end{aligned}$$

which can be written in matrix form $[A]\{x\} = \{y\}$ as

$$\begin{bmatrix} 1 & 4 & 0 \\ -2 & 2 & 1 \\ 3 & 1 & 0 \end{bmatrix} \begin{Bmatrix} x_1 \\ x_2 \\ x_3 \end{Bmatrix} = \begin{Bmatrix} y_1 \\ y_2 \\ y_3 \end{Bmatrix}$$

Using eq. (B12) we get

$$|A| = 1\,(+1)\begin{vmatrix} 2 & 1 \\ 1 & 0 \end{vmatrix} + 4\,(-1)\begin{vmatrix} -2 & 1 \\ 3 & 0 \end{vmatrix} + 0\,(+1)\begin{vmatrix} -2 & 2 \\ 3 & 1 \end{vmatrix}$$

Thus

$$|A| = 1\,(-1) \;\; +4\,(+3) \;\; +0\,(-8) = 11$$

where the cofactors can be seen to be $C_{11} = (-1)$; $C_{12} = (+3)$ and $C_{13} = (-8)$

To determine [C] the matrix whose elements are the cofactors of [A], C_{21} C_{22} C_{23}, C_{31} C_{32} and C_{33} have to be calculated and are found to be

$$[C] = \begin{bmatrix} C_{11} & C_{12} & C_{13} \\ C_{21} & C_{22} & C_{23} \\ C_{31} & C_{32} & C_{33} \end{bmatrix} = \begin{bmatrix} -1 & 3 & -8 \\ 0 & 0 & 11 \\ 4 & -1 & 10 \end{bmatrix}$$

Thus the adjoint of [A] obtained by transposing the matrix [C] is given by

$$[\hat{A}] = [C]^T = \begin{bmatrix} -1 & 0 & 4 \\ 3 & 0 & -1 \\ -8 & 11 & 10 \end{bmatrix}$$

and

$$[A]^{-1} = \frac{[\hat{A}]}{|A|} = \begin{bmatrix} -1/11 & 0 & 4/11 \\ 3/11 & 0 & -1/11 \\ -8/11 & 1 & 10/11 \end{bmatrix}$$

Since $\{x\} = [A]^{-1}\{y\}$ according to eq. (B5), we can write

$$\begin{Bmatrix} x_1 \\ x_2 \\ x_3 \end{Bmatrix} = \begin{bmatrix} -1/11 & 0 & 4/11 \\ 3/11 & 0 & -1/11 \\ -8/11 & 1 & 10/11 \end{bmatrix} \begin{Bmatrix} y_1 \\ y_2 \\ y_3 \end{Bmatrix}$$

which gives

$$\begin{aligned} x_1 &= -1/11\, y_1 & & & +4/11\, y_3 \\ x_2 &= 3/11\, y_1 & & & -1/11\, y_3 \\ x_3 &= -8/11\, y_1 & +y_2 & & +10/11\, y_3 \end{aligned}$$

Inversion of a (2 × 2) Matrix

Most of the examples used in the main text make use of a (2 × 2) matrix. Therefore its inversion, which is widely used, will be outlined in the following. Consider a (2 × 2) matrix [A] given by

$$[A] = \begin{bmatrix} a_{11} & a_{12} \\ a_{21} & a_{22} \end{bmatrix} \tag{B16}$$

The cofactors are given by

$C_{11} = (-1)^{1+1} M_{11}$ $\quad C_{12} = (-1)^{1+2} M_{12}$ $\quad C_{21} = (-1)^{2+1} M_{21}$ $\quad$ and $C_{22} = (-1)^{2+2} M_{22}$

where $M_{11} = a_{22}$ $\quad M_{12} = a_{21}$ $\quad M_{21} = a_{12}$ $\quad$ and $M_{22} = a_{11}$

Thus the cofactor matrix is given by

$$[C] = \begin{bmatrix} a_{22} & -a_{21} \\ -a_{12} & a_{11} \end{bmatrix} \tag{B17}$$

The adjoint of matrix [A] is given by

$$[\hat{A}] = [C]^T = \begin{bmatrix} a_{22} & -a_{12} \\ -a_{21} & a_{11} \end{bmatrix} \tag{B18}$$

Thus

$$[A]^{-1} = \frac{[\hat{A}]}{|A|} = 1/(a_{11}a_{22} - a_{12}a_{21}) \begin{bmatrix} a_{22} & -a_{12} \\ -a_{21} & a_{11} \end{bmatrix} \tag{B19}$$

APPENDIX C

Complex Frequency Solution for Free Damped Vibration

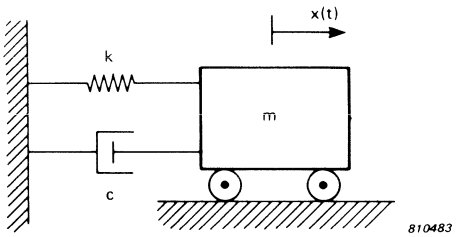

Fig.C1. Single degree of freedom system with viscous damping

In this appendix, the basic ideas of a complex frequency form of solution, for a single degree of freedom system with viscous damping, shown in Fig.C1, are introduced [18, 21, 27]. In the main text it was shown, that the steady state solution to eq.(2) for **forced vibration** of such a system was given by $x = Xe^{j\omega t}$. In the case of **free damped vibration**, for which the equation of motion is given by

$$m\ddot{x} + c\dot{x} + kx = 0 \qquad \text{(C1)}$$

the above solution can be extended to a more general type of the form

$$x = X\, e^{st} \qquad \text{(C2)}$$

where $s = (\sigma + j\omega)$ is known as the complex frequency.

Before solving eq.(C1) it is important to examine the variable s. Since s is complex it is best illustrated in the Argand plane, or the **complex frequency** plane, where the real

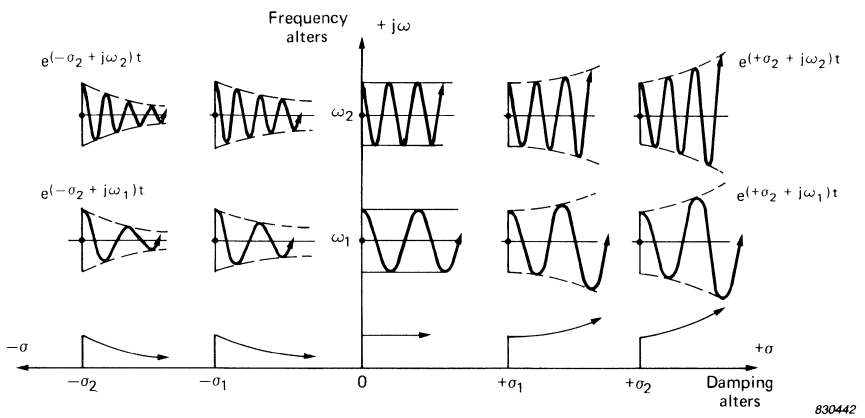

Fig.C2. Oscillations corresponding to points in the complex plane

axis represents σ, the decay rate (amount of damping), and the imaginary axis represents $j\omega$, the frequency, see Fig.C2. Every point in this plane defines a particular form of oscillation. Thus values of s which are purely imaginary, giving solutions of the form $x = Xe^{j\omega t}$, describe constant magnitude oscillations, whereas values of s which are purely real, giving solutions of the form $x = Xe^{\sigma t}$, describe **non-oscillatory** motion. For positive σ the magnitude increases exponentially with time and for negative σ it decreases exponentially with time, see Fig.C2. Values of s which are complex, thus lying anywhere in the plane (giving solutions of the form $x = Xe^{(\sigma+j\omega)t}$), describe **oscillatory** motion increasing or decreasing exponentially with time depending on the sign of σ.

Roots of the Characteristic Equation

To solve eq.(C1), the anticipated solution (C2) is inserted in (C1), leading to the algebraic equation

$$s^2 \frac{m}{k} + s \frac{c}{k} + 1 = 0 \qquad \text{(C3)}$$

which is known as the characteristic equation of the system. In the absence of damping the natural frequency of the system is given by $\omega_0 = \sqrt{k/m}$ which may be substituted in eq.(C3) to yield

$$\left(\frac{s}{\omega_0}\right)^2 + \frac{c}{\sqrt{km}}\left(\frac{s}{\omega_0}\right) + 1 = 0 \qquad \text{(C4)}$$

or

$$\left(\frac{s}{\omega_0}\right)^2 + 2\zeta\left(\frac{s}{\omega_0}\right) + 1 = 0 \qquad \text{(C5)}$$

where $\zeta = \frac{c}{c_c} = \frac{1}{2} \frac{c}{\sqrt{km}}$ is the damping ratio.

Since eq. (C5) is a quadratic, the two roots of the equation are given by

$$\left(\frac{s_{1,2}}{\omega_0}\right) = -\zeta \pm \sqrt{\zeta^2 - 1} \qquad \text{(C6)}$$

and the values of s obtained, thus define two forms of oscillation in the complex plane. Obviously the nature of the roots s_1 and s_2 depends on the value of ζ. The effect of the variation of ζ on the roots can be illustrated in the complex plane (s plane) in the form of a diagram representing the locus of roots plotted as a function of the parameter ζ, see Fig.C3. From eq.(C6) it can be seen, that for $\zeta = 0$ the roots are given by $s_{1,2} = \pm j\omega_0$, which lie on the imaginary axis, corresponding to undamped oscillations at the natural frequency of the system.

For $0 < \zeta < 1$ or $c < 2\sqrt{km}$ which is known as the **underdamped** case, the roots are given by

$$\left(\frac{s_{1,2}}{\omega_0}\right) = -\zeta \pm j\sqrt{1 - \zeta^2} \qquad \text{(C7)}$$

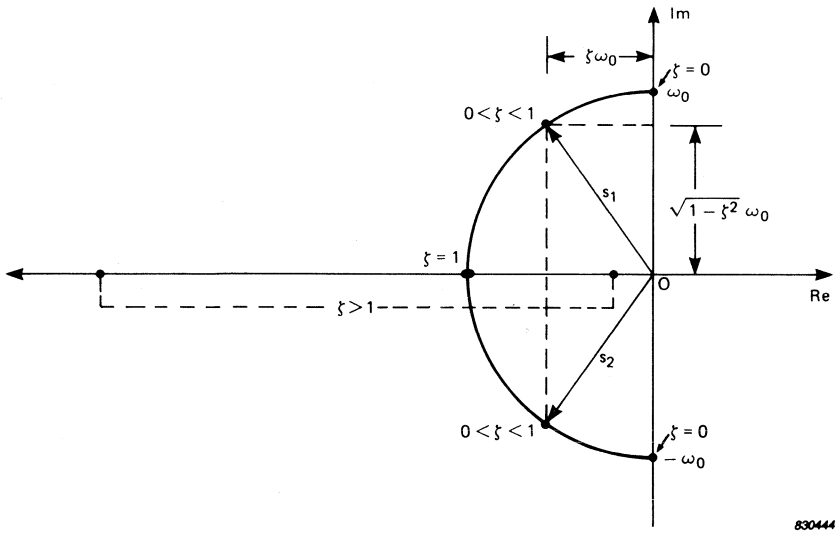

Fig.C3. Locus of roots as the damping ratio ζ is varied

Thus s_1 and s_2 are always complex conjugate pairs, located symmetrically with respect to the real axis. As the values of (s/ω_0) are complex, the magnitude

$$\left|\frac{s}{\omega_0}\right| = \sqrt{\zeta^2 + 1 - \zeta^2} = 1 \qquad \text{(C8)}$$

indicating that the locus of the roots is a circle of radius ω_0, centred at the origin, see Fig.C3. Furthermore, when the complex conjugate pairs of the roots are associated with each other, they can be interpretated as a real oscillation, for example

$$e^{(-\sigma + j\omega)t} + e^{(-\sigma - j\omega)t} = 2\, e^{-\sigma t} \cos \omega t \qquad \text{(C9)}$$

As ζ approaches unity, ($c \rightarrow 2\sqrt{km}$) the two roots approach the point $-\omega_0$ on the real axis, which is known as the **critically damped** case.

For $\zeta > 1$, or $c > 2\sqrt{km}$, known as the **overdamped** case, the roots are given by

$$\left(\frac{s_{1,2}}{\omega_0}\right) = -\zeta \pm \sqrt{\zeta^2 - 1} \qquad \text{(C10)}$$

which lie on the negative real axis. As $\zeta \rightarrow \infty$, $s_1 \rightarrow 0$ and $s_2 \rightarrow -\infty$.

Time Response

To obtain the time response of free vibration for given initial conditions, eq.(C6) is substituted in eq.(C2) to give

$$x(t) = X_1\, e^{s_1 t} + X_2\, e^{s_2 t} \qquad \text{(C11)}$$

For the overdamped case $\zeta > 1$, the solution is given by

$$x(t) = X_1 e^{\left(-\zeta + \sqrt{\zeta^2 - 1}\right)\omega_0 t} + X_2 e^{\left(-\zeta - \sqrt{\zeta^2 - 1}\right)\omega_0 t}$$

$$\text{i.e.} \quad x(t) = \left\{ X_1 e^{\left(\sqrt{\zeta^2 - 1}\right)\omega_0 t} + X_2 e^{\left(-\sqrt{\zeta^2 - 1}\right)\omega_0 t} \right\} e^{-\zeta\omega_0 t} \qquad \text{(C12)}$$

which describes aperiodic motion decaying exponentially with time. X_1 and X_2 are determined from the initial displacement and velocity which in turn govern the shape of the decaying curve, see Fig.C4.

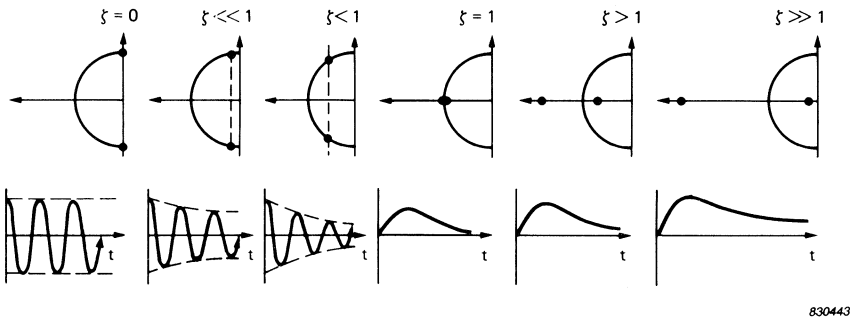

Fig.C4. Positions of the roots in the complex plane for various values of ζ and the corresponding time histories

For the critically damped case $\zeta = 1$, eq.(C5) has a double root $s_1 = s_2 = -\omega_0$ and the solution is given by

$$x(t) = (X_1 + tX_2)\, e^{-\omega_0 t} \qquad \text{(C13)}$$

The response again represents aperiodic motion decaying exponentially with time. However, a critically damped system approaches the equilibrium position the fastest for given initial conditions.

For the underdamped case $0 < \zeta < 1$ the solution is given by

$$x(t) = \left\{ X_1 e^{\left(j\sqrt{1 - \zeta^2}\right)\omega_0 t} + X_2 e^{\left(-j\sqrt{1 - \zeta^2}\right)\omega_0 t} \right\} e^{-\zeta\omega_0 t}$$

$$\text{i.e.} \quad x(t) = \left\{ X_1 e^{j\omega_d t} + X_2 e^{-j\omega_d t} \right\} e^{-\zeta\omega_0 t} \qquad \text{(C14)}$$

where $\omega_d = \omega_0 \sqrt{1 - \zeta^2}$ is called the frequency of damped free vibration. Eq.(C14) represents exponentially decaying oscillatory motion with constant frequency ω_d.

Fig.C4 illustrates the position of the roots in the complex plane for various amounts of damping, and the general form of the corresponding time histories. For large values of ζ the response is dominated by a slowly decaying exponential component corresponding to the solution close to the origin.

APPENDIX D

Two Channel Exciter System

To illustrate the principles behind multiple shaker excitation and the Kennedy and Pancu technique, a simple system shown in Fig.D1 is ideal for demonstration purposes. The Exciter Control Type 1047 feeds the high frequency signals (fixed and variable) to the Multiplier Type 5748 which generates a sine and a cosine signal. The cosine signal is fed to the two Power Amplifiers Type 2706, while the sine signal is fed to the X input of a two channel oscilloscope. Since the power amplifiers do not have a high output impedance, a 22 Ohm resistance is connected in series between each power amplifier and the shaker Type 4809. Thus the **output current** from the power amplifiers (and

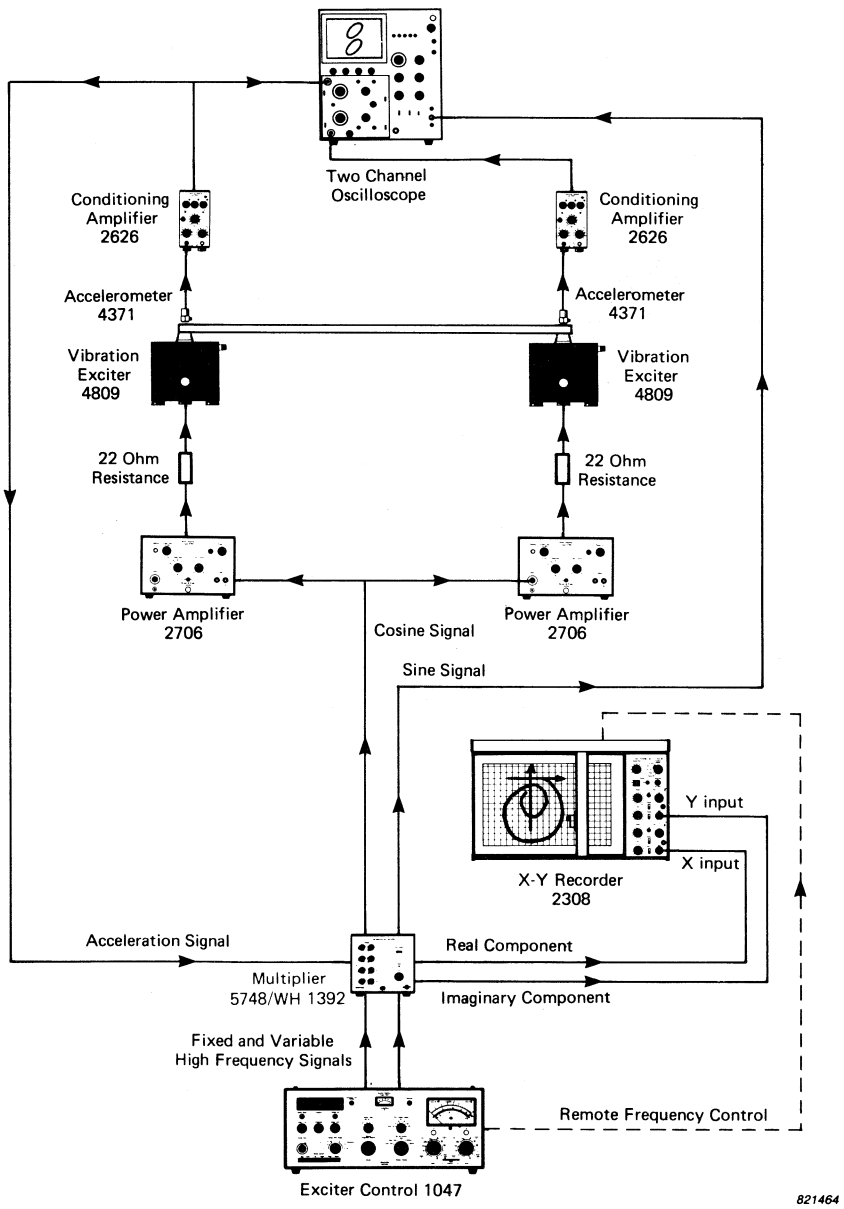

Fig.D1. Two Channel Shaker System

hence the force output from the shakers) are proportional to the **input voltage** to the power amplifiers. This avoids the need for having a servo-loop control for each shaker for constant force level excitation, since the force output from the shakers can now be independently adjusted via the gain control of its associated power amplifier.

On the measuring side, the signals from the two accelerometers mounted on the beam, are fed via their Conditioning Amplifiers Type 2626 to the two Y inputs of the oscilloscope, for obtaining the Lissajous figures. One of the accelerometer signals to be analyzed is fed to the Multiplier, where it is multiplied by the sine and the cosine signals, see Fig.D2. It can be seen that the product of the cosine signal and the acceleration signal gives one component with twice the frequency, and another DC component proportional to the **real part** ($^1/_2 \cos \theta$) of the acceleration signal. Similarly, the product of the sine signal gives one component with twice the frequency, and another DC component proportional to the **imaginary part** ($^1/_2 \sin \theta$) of the acceleration signal. The Multiplier has two built-in low-pass filters to remove the second harmonic of the fundamental frequency, which additionally, in the bargain, gets rid of the high frequency noise which may be present on account of background vibration. The two DC signals, proportional to the real and imaginary components of the acceleration signal, are now fed to the X-Y Recorder Type 2308, where a Nyquist plot can be obtained for the Kennedy and Pancu technique, as the frequency is scanned. If the real and imaginary components are desired as a function of frequency, the X axis of the X-Y Recorder can be synchronized to the frequency sweep of the Exciter Control Type 1047 as shown by the dashed line in Fig.D1. If the total amplitude as a function of frequency is required, the output from the relevant Conditioning Amplifier is fed to the Y input of the X-Y Recorder.

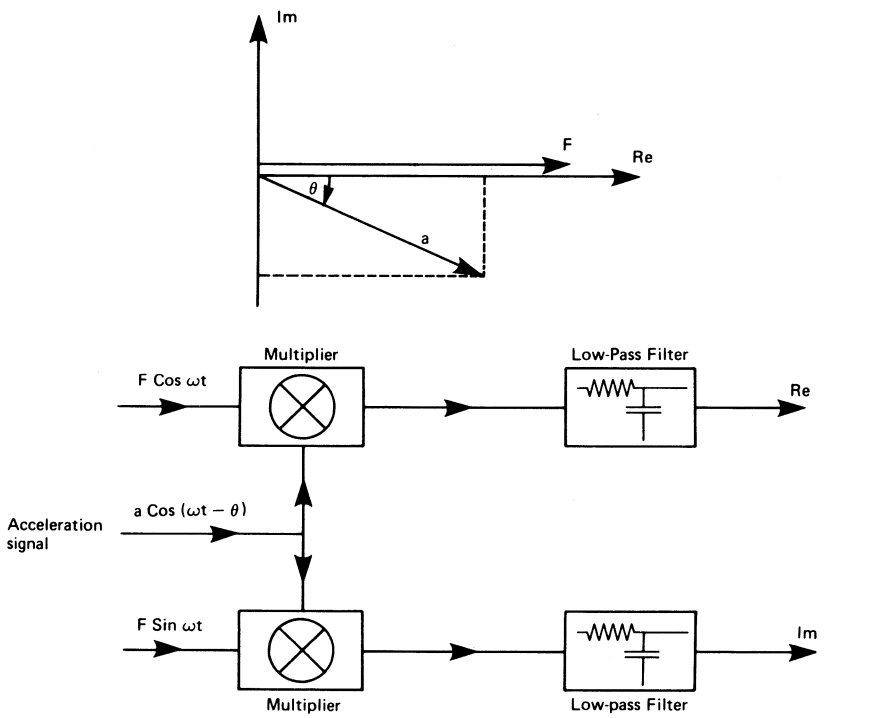

$$F \cos \omega t \quad a \cos (\omega t - \theta) = Fa \left\{ \frac{1}{2} \cos (2\omega t - \theta) + \frac{1}{2} \cos \theta \right\}$$

$$F \sin \omega t \quad a \cos (\omega t - \theta) = Fa \left\{ \frac{1}{2} \sin (2\omega t - \theta) + \frac{1}{2} \sin \theta \right\}$$

821460

Fig.D2. Principle of Operation of Multiplier Type 5748

APPENDIX E

Complex Admittance Matrix

The equations of motion for a linear, n degree of freedom system, with linear damping and excited by a set of mono-phase forces was given by eq.(119) as

$$[m]\{\ddot{\bar{u}}\} + [c(\omega)]\{\dot{\bar{u}}\} + [k]\{\bar{u}\} = \{F\}\, e^{j\omega t} \tag{E1}$$

where $[c(\omega)] = [c] + 1/\omega[d]$ encompasses any combination of the standard viscous and hysteretic types of damping given by [c] and [d] matrices respectively, and $\{\bar{u}\}$ represents the complex displacement.

Substituting the trial solution

$$\{\bar{u}\} = \{\bar{U}\}\, e^{j\omega t} \tag{E2}$$

in eq.(E1) yields

$$-\omega^2[m]\{\bar{U}\} + j\omega[c(\omega)]\{\bar{U}\} + [k]\{\bar{U}\} = \{F\} \tag{E3}$$

i.e.

$$[[k] - \omega^2[m] + j\omega[c(\omega)]]\{\bar{U}\} = \{F\} \tag{E4}$$

Eq.(E4) may be written as

$$[\bar{A}]\{\bar{U}\} = \{F\} \tag{E5}$$

where the elements $\bar{a}_{ij}$ of the matrix $[\bar{A}]$ are complex quantities.

Thus

$$\{\bar{U}\} = [\bar{A}]^{-1}\{F\} = \frac{[\hat{\bar{A}}]}{|\bar{A}|}\{F\} \tag{E6}$$

Consider now a two degree of freedom system for which eq.(E5) can be written as

$$\begin{bmatrix} \bar{a}_{11} & \bar{a}_{12} \\ \bar{a}_{21} & \bar{a}_{22} \end{bmatrix} \begin{Bmatrix} \bar{U}_1 \\ \bar{U}_2 \end{Bmatrix} = \begin{Bmatrix} F_1 \\ F_2 \end{Bmatrix} \tag{E7}$$

From eq.(B18) we can find $[\hat{\bar{A}}]$, thus

$$\begin{Bmatrix} \bar{U}_1 \\ \bar{U}_2 \end{Bmatrix} = [\bar{A}]^{-1}\begin{Bmatrix} F_1 \\ F_2 \end{Bmatrix} = \frac{[\hat{\bar{A}}]}{|\bar{A}|}\begin{Bmatrix} F_1 \\ F_2 \end{Bmatrix} = 1/(\bar{a}_{11}\,\bar{a}_{22} - \bar{a}_{12}\,\bar{a}_{21})\begin{bmatrix} \bar{a}_{22} & -\bar{a}_{12} \\ -\bar{a}_{21} & \bar{a}_{11} \end{bmatrix}\begin{Bmatrix} F_1 \\ F_2 \end{Bmatrix} \tag{E8}$$

Eq.(E8) can be written as

$$\begin{Bmatrix} \bar{U}_1 \\ \bar{U}_2 \end{Bmatrix} = \begin{bmatrix} \bar{b}_{11} & \bar{b}_{12} \\ \bar{b}_{21} & \bar{b}_{22} \end{bmatrix} \begin{Bmatrix} F_1 \\ F_2 \end{Bmatrix} \tag{E9}$$

where the matrix $[\bar{B}]$ is called the complex admittance matrix, and its complex elements having units of m/N are given by

$$\bar{b}_{11} = \frac{\bar{a}_{22}}{(\bar{a}_{11}\bar{a}_{22} - \bar{a}_{12}\bar{a}_{21})}; \qquad \bar{b}_{12} = \frac{-\bar{a}_{12}}{(\bar{a}_{11}\bar{a}_{22} - \bar{a}_{12}\bar{a}_{21})};$$

$$\bar{b}_{21} = \frac{-\bar{a}_{21}}{(\bar{a}_{11}\bar{a}_{22} - \bar{a}_{12}\bar{a}_{21})}; \qquad \bar{b}_{22} = \frac{\bar{a}_{11}}{(\bar{a}_{11}\bar{a}_{22} - \bar{a}_{12}\bar{a}_{21})}.$$

Eq.(E9) can be written in its expanded form as

$$\bar{U}_1 = \bar{b}_{11} F_1 + \bar{b}_{12} F_2 \tag{E10}$$

$$\bar{U}_2 = \bar{b}_{21} F_1 + \bar{b}_{22} F_2 \tag{E11}$$

When the system is excited by a single force F_1, (which acts at point 1) and $F_2 = 0$, it can be seen from eq.(E10), that $\bar{b}_{11}$ represents the complex displacement at point 1 per unit of force. From eq.(E11) it can be seen that $\bar{b}_{21}$ represents the complex displacement at point 2 per unit of force, due to excitation at point 1 by F_1.

Similarly, by exciting the system at point 2 by F_2, and setting $F_1 = 0$, we obtain $\bar{b}_{12}$ and $\bar{b}_{22}$, which are the complex displacements at points 1 and 2 respectively. Thus the elements $\bar{b}_{ij}$ ($i = 1 \ldots n$) of the columns of the matrix $[\bar{B}]$, represent the complex displacements at the points $i = 1 \ldots n$ per unit of force when the structure is excited at point j.

Brüel & Kjær DK-2850 NÆRUM, DENMARK · Telephone: + 45 2 80 05 00 · TELEX: 37316 bruka